Study on Bond Degradation of Reinforced Concrete Members with Induced Cracks due to Rebar Corrosion

March 2023

SYLL AMADOU SAKHIR

Study on Bond Degradation of Reinforced Concrete Members with Induced Cracks due to Rebar Corrosion

Graduate School of Science and Technology
Degree Programs in Systems and Information Engineering
University of Tsukuba

March 2023

SYLL AMADOU SAKHIR

ABSTRACT

During their lifetime, reinforced concrete (RC) structures are subjected to aggressive environmental conditions such as chloride ingress and concrete carbonation. These harsh conditions may corrode the embedded reinforcing steel bars. The corrosion propagation affects more than the cross-sectional area of the rebar. The volume of steel also increases due to expansive corrosion products, leading to the cracking, delamination, and spalling of concrete. Corrosion attacks are expected on many buildings and bridges in tectonically active coastal areas. As a result, more excellent knowledge of structural performance degradation is required to address the rising concern for better assessing damaged structures. Consequently, research focusing on the structural behavior of corroded RC structures has received increasing attention. The researchers demonstrated that the bond is more vulnerable to corrosion. Consequently, the bond capacity of corroded structures may be a crucial consideration when evaluating the deterioration. However, the bond mechanisms between rebar and concrete are quite complex due to many influential factors. The perplexity may increase when the impact of corrosion on the bond is also investigated. Although researchers have extensively studied this subject, several knowledge gaps remain. The proposed models for bond strength degradation due to rebar corrosion are dispersed in the literature. Accordingly, a need to better understand the visual damage impacts (corrosion-related cracks) on the structural behavior of deteriorated structures to propose a practical model capable of predicting the residual performance in such structures. To address this, the main objective of this study is to investigate the performance degradation of RC structures due to corrosion-related cracks, with a particular focus on the bond between concrete and rebars. Chapter 1 includes an introductory part that comprehensively summarizes the covered topics. The original features and context are also presented. The following is a brief description of each chapter in the thesis.

Chapter 2: Systematic literature review

To begin, Chapter 2 systematically reviewed the literature to explore experimental methods, outcomes, and trends on this topic. Key factors that affect bond strength degradation, including concrete cover, concrete strength, and stirrups, have been documented. However, a general model is still unavailable due to discrepancies caused by differences in testing methods to evaluate the effect of corrosion on bond strength. Furthermore, researchers attempted to clarify

the degradation mechanism of bond strength affected by corrosion. As a result, new alternatives have been proposed to build a practical model to assess the bond strength deterioration of corroded structures.

Chapter 3: Bond strength degradation in concrete cracked by electrical-induced corrosion

Chapter 3 aims to increase the knowledge about the bond behavior in RC structures cracked by corrosion. Specifically, the link between bond degradation and corrosion-related crack is investigated. Two types of bond test specimens with rebar subjected to electrical-induced corrosion are designed to fail either in side-split (S1 series) or single-split (S2 series). Moreover, the effect of stirrup on bond degradation was also assessed.

The pull-out result showed that the rebar corrosion does not severely affect the residual bond strength when the specimen is not cracked by corrosion. This is the case of the S1 series in which the specimens were corroded without cracks observation prior to loading.

On the others hand, the test result of the S2 series showed that the residual bond strength ratio decreases with the increase in crack width. This demonstrates that the corrosion-related crack is primarily responsible for bond strength degradation and could be considered the primary variable.

Furthermore, a comparison of the residual bond strength ratio in specimens S2 without and with a stirrup shows that the bond degradation in specimens without a stirrup is more severe than those with stirrups. Conclusively, significant bond deterioration begins only when the corrosion of the stirrup is very high. However, some stirrup legs are fractured at the pitting points or almost consumed by uniform corrosion in extreme situations.

Chapter 4: Bond strength degradation in concrete cracked by expansion agent filled pipe

The corrosion of rebar changes the surface properties of the steel, and the rebar shape and cracks the surrounding concrete. This phenomenon altogether affects the bond strength of the corroded specimen. However, the combination of these effects leads to difficulties in analyzing the processes at a fundamental level and negates the overall accuracy of the bond strength degradation prediction. This chapter proposed a novel method to simulate cracking due to volumetric expansion by expansion agent filled pipe (EAFP) to overcome the limitation related to electrical corrosion techniques and discretely assess bond strength deterioration. The alternative approach proposed here focuses on the single effect of crack width on the bond mechanism through interlocking ribs. While ignoring the ambiguity related to corrosion product or rate, the crack width could quantify the exclusive corrosion on bond strength. The first part of this chapter thoroughly describes the novel method to induce crack and confirms the induced

surface and internal crack using various specimens. In the second part, the newly proposed method is used to examine the effect of crack pattern and width on bond degradation. Moreover, the effect of the stirrup on bond strength loss in the cracked specimen is investigated.

EAFP was able to simulate cracks due to the rebar expansion related to corrosion in RC beams. This technique makes it easier to target crack width due to increased induced crack width over elapsed time from filling the aluminum pipe with an expansion agent. Furthermore, the transversal cut of the cracked RC beams shows that internal side-splitting crack patterns mainly occur.

Two series of cracked bond test specimens considering the pattern of the induced cracks using EAFP (single or side crack) were tested. It was seen that the bond strength exponentially decreased with the increase of induced crack width in both types of specimens. We concluded that cracking without rust fundamentally causes bond degradation in specimens with corrosion-related cracks. Additionally, the bond strength degradation is more severe in specimens with a side-splitting crack than with a single-splitting crack.

In Series S2, the bond strength degradation of the specimen without stirrup appears to be more severe than that of the specimen with stirrup. This is due to the crucial role of the stirrup in providing additional confinement. First, the stirrups can effectively limit crack propagation due to EAFP. Furthermore, stirrups help to maintain the bearing between the steel bar and the concrete. However, the bond strength degradation is not significant because of the big diameter of stirrup, leading to a fully confined specimen. A systematic understanding of how the reduction in confinement provided by the stirrup contributes to bond strength deterioration is needed to build a formula for predicting bond strength degradation.

Chapter 5: bond strength prediction in concrete cracked by EAFP simulating rebar corrosion

Findings in Chapters 3 et 4 indicated that induced crack width and stirrup diameter reduction due to corrosion are essential parameters for evaluating bond strength deterioration. Therefore, Chapter 5 proposes an empirical prediction for bond strength degradation in cracked concrete. The combined effects of concrete cracking and cross-sectional reduction of stirrups on bond strength are considered. EAFP is adopted to simulate concrete cracking and focus on induced cracks without rust accumulation or change in rebar profile. In addition, rebars with different diameters are used as stirrups to illustrate the reduction in rebar cross-section due to corrosion. The test result reflects the crucial role of the stirrup on the bond strength degradation mechanism due to induced cracks. The bond strength degradation rate is considerably fast in specimens without stirrups. However, bond strength degradation is limited in specimens with

stirrup, respectively, to the stirrup ratio increase. Moreover, the stirrup can also restrict the opening of cracks induced by EAFP, leading to a more ductile failure mode.

The bond strength degradation in specimens cracked by electrical-induced corrosion or EAFP was compared to investigate the effect of corroded rebar shape. The main difference between these two specimens is the rust presence and rebar profile change due to corrosion. The result shows no significant difference in bond strength degradation. Conclusively. The residual bond strength ratio can be estimated by considering the single effect of cracking, ignoring the rust presence or rebar profile change. It is also confirmed that a direct relationship between bearing and crack width can ignore ambiguity related to the accumulation of corrosion products.

Finally, an empirical model has been proposed to assess the bond strength degradation considering the induced crack width and the stirrup ratio. Comparisons with previous data of corroded specimens show that the proposed model can give reasonable estimations. An empirical model has been proposed to assess the bond strength degradation in specimens cracked by EAFP. The proposed degradation prediction is mainly based on induced crack width. The formula also reflects the critical role of the stirrup in limiting bond strength degradation. Comparisons with previous data of corroded specimens show that the proposed model can give reasonable estimations.

Chapter 6: structural performance of RC beams cracked by expansion agent filled pipe

To investigate the performance degradation of cracked concrete RC structures, previous studies mainly adopted accelerated corrosion techniques where it can be challenging to control the widths or patterns of the cracks. To address the drawbacks related to this technique, the RC beams tested in this study are cracked using EAFP, which allows us to easily control the cracking in a short time and focus on the single fundamental effect of crack. In the previous chapter, it is confirmed that the bond strength is affected by corrosion-induced cracking. This bond strength degradation is more critical than the sectional loss of corroded rebar. During loading, cracks on RC members highly depend on the bond strength between concrete and rebar. The final part of this thesis focuses on the seismic performance of damaged RC beams. Experiments were carried out to demonstrate the influence of corrosion related cracks on the structural response of cracked RC beams. To achieve this goal, different damage levels (crack width) are simulated in ten RC beam specimens by inducing cracks using an EAFP. Then, antisymmetrical static loading tests of the damaged beam are carried out to grasp the mechanical performance of the damaged beam. Furthermore, the effects of induced crack on the seismic behavior, such as shear capacity, stiffness, energy dissipation are described.

The test results showed that bond strength degradation due to induced cracks change the failure mode of the specimen under antisymmetrical loading. The correlation between the maximum lateral force of specimens and induced crack width was not clear enough. As a result, it is considered that the beam capacity degradation due to induced crack cannot be merely evaluated with the crack width as the main parameter. Furthermore, it is shown that significant modifications of service behavior were observed due to the bond strength degradations, namely: loss of initial stiffness and reduction of energy dissipation until 1/50 rad loading.

Chapter 7 Conclusion and future suggestions

Chapter 7 describes the conclusions drawn from this study and highlight the future research.

CONTENTS

LIST OF TABLES

LIST OF FIGURES

1 INTRODUCTION

1.1 Background

Concrete is currently one of the most widely used structural materials. Many reinforced concrete (RC) structures were constructed during the economic growth that followed World War II. Many are approaching the end of their intended service life due to time-dependent deterioration. Therefore, it is essential to evaluate existing structures since an efficient maintenance and repair approach requires predicting the structural behavior and remaining service life of decaying structures.

The reinforcing steel bar (rebar) corrosion is considered the most common and severe cause of RC structure degradation. In recent years, the RC structures durability has been a major concern, particularly for structures under aggressive environments. Figure 1.1 overviews the consequences of corrosion on the RC structures. Advanced corrosion can cause various damage to RC structures, including loss of effective concrete section due to concrete cracking and cover spalling, loss of rebar tensile performance due to reduced cross-section, and deterioration of bond strength between corroded rebar and concrete. Corrosion directly reduces cross-sectional rebar area and produces rust that expands in volume. Localized or pitting corrosion comes from chloride ingress. It often concentrates at a point or in a limited rebar area, whereas uniform corrosion is related to carbonation. The reduction in rebar cross-section and pitting deteriorates the strength and ductility of corroded rebar. The rust volumetric expansion causes cover concrete cracking which leads to cover delamination and spalling. As a result, the bond strength between concrete and rebar is seriously affected by the concrete cover cracking and rebar cross-section loss. At the structural level, bond strength degradation can affect the structural performance of RC structures, such as failure mode, stiffness, strength, and deformation capacity.

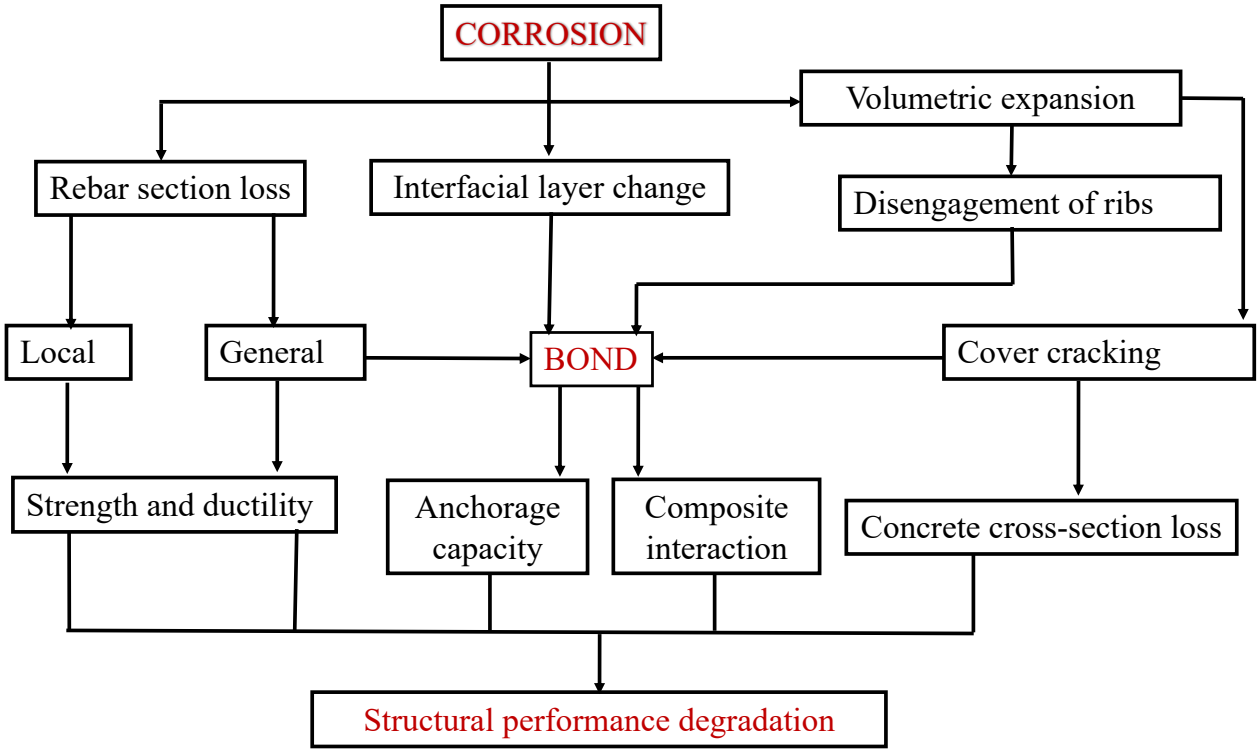

Figure 1.1 Corrosion effect on RC structural performance

*Reproduced from Cairns et al.[1]

Numerous countries with a high risk of earthquakes, including Japan, have major populated cities along coastal areas. Thus, RC structures are vulnerable to corrosion and seismic effects in these regions. Although RC structures collapse due to corrosion is rare, In 2018, the Polcevera Viaduct in Genoa, which had been in use for over half a century, collapsed due to a combination of corrosion and fatigue effects [2]. Another example is the collapse of a building in Surfside (Miami) in 2021; preliminary analyses suggest that its causes could have been the differential settlement of the foundation, the corrosion of reinforcement and concrete cracking, and long-term waterproofing problems [3]. In recent years, structural behavior of corroded RC structures has received increasing attention. However, the observed seismic behavior of corroded RC beams has not been given enough consideration. Under seismic reversed loading circumstances, flexural and shear strengths of RC beams degrade more severely than under monotonic loading.

The bond between concrete and rebar is an essential property of RC structures. It enables the transfer of force from the rebar to concrete and ensures the composite action of the RC members [4]. Furthermore, the researchers demonstrated that the bond strength is more vulnerable to corrosion. Auyeung et al. [5] confirmed that the bond strength degradation of an unconfined concrete specimen with corroded rebar is much more critical than the cross-section loss.

According to their findings, a diameter reduction of 2% could result in a bond loss of 80%. The investigation by Li and Zheng [6] also reveals that the structural degradation of the bond varies more than the loss in stiffness and strength. Consequently, the bond capacity of corroded structures may be a crucial consideration when evaluating the deterioration. However, the bond mechanisms between rebar and concrete are quite complex due to many influential factors. The perplexity may increase when the impact of corrosion on the bond is also investigated. Although researchers have extensively studied this subject, several knowledge gaps remain. In addition, the proposed models for bond strength degradation due to rebar corrosion are dispersed in the literature.

In practice, engineers document the deterioration found during inspections to propose an accurate evaluation of the performance of deteriorated RC structures and reduce the safety risks and maintenance costs of these damaged structures. Today, the acquisition of excellent visual records of structures (*e.g.,* cracks) is possible thanks to the remarkable progress of automated monitoring surveys (inspection drones). Furthermore, it is necessary to determine the parameters that influence the structural behavior of severely deteriorated structures by assessing the material properties and detailing the cover cracking. Models are required to analyze a deteriorated structure behavior and estimate its residual performance. However, a practical unified model for general use is yet unavailable. Accordingly, a need to better understand the visual damage impacts (corrosion related cracks) on the structural behavior of deteriorated structures to propose a practical model capable of predicting the residual performance in such structures.

1.2 Aim and scope

This thesis aims to expand our understanding of the structural degradation behavior of corroded RC members, with a particular focus on the degradation of the bond strength between rebars and concrete. To provide a practical assessment method, the presented research focus on the induced cracks width that is considered the visual and easy measurable damages due to corrosion of the rebars. The primary areas of interest are as follows:

i. Bond strength degradation in reinforced concrete with corroded rebars.

ii. Methods to induce corrosion related crack with expansion agent filled pipe (EAFP).

iii. Effect of stirrups cross-section reduction (confinement deterioration) on bond strength degradation in concrete cracked by EAFP.

iv. Seismic performance of RC beams with bond strength deterioration due to cracks induced by EAFP.

The influence of corrosion-related cracks on the behavior of RC structures was investigated in detail. First, a comprehensive experimental program was conducted to evaluate the effect of induced cracks on the bond strength degradation. Furthermore, a practical formula to predict bond deterioration due to induced cracks is proposed. Finally, the impact of bond strength deterioration on the RC beam performance is thoroughly investigated using cracked beams under cyclic antisymmetrical loading. The interrelated effects corrosion-induced cracks width, bond strength degradation and seismic performance of cracked beams is experimentally examined in this thesis. This field of interest is illustrated in Figure 1.2.

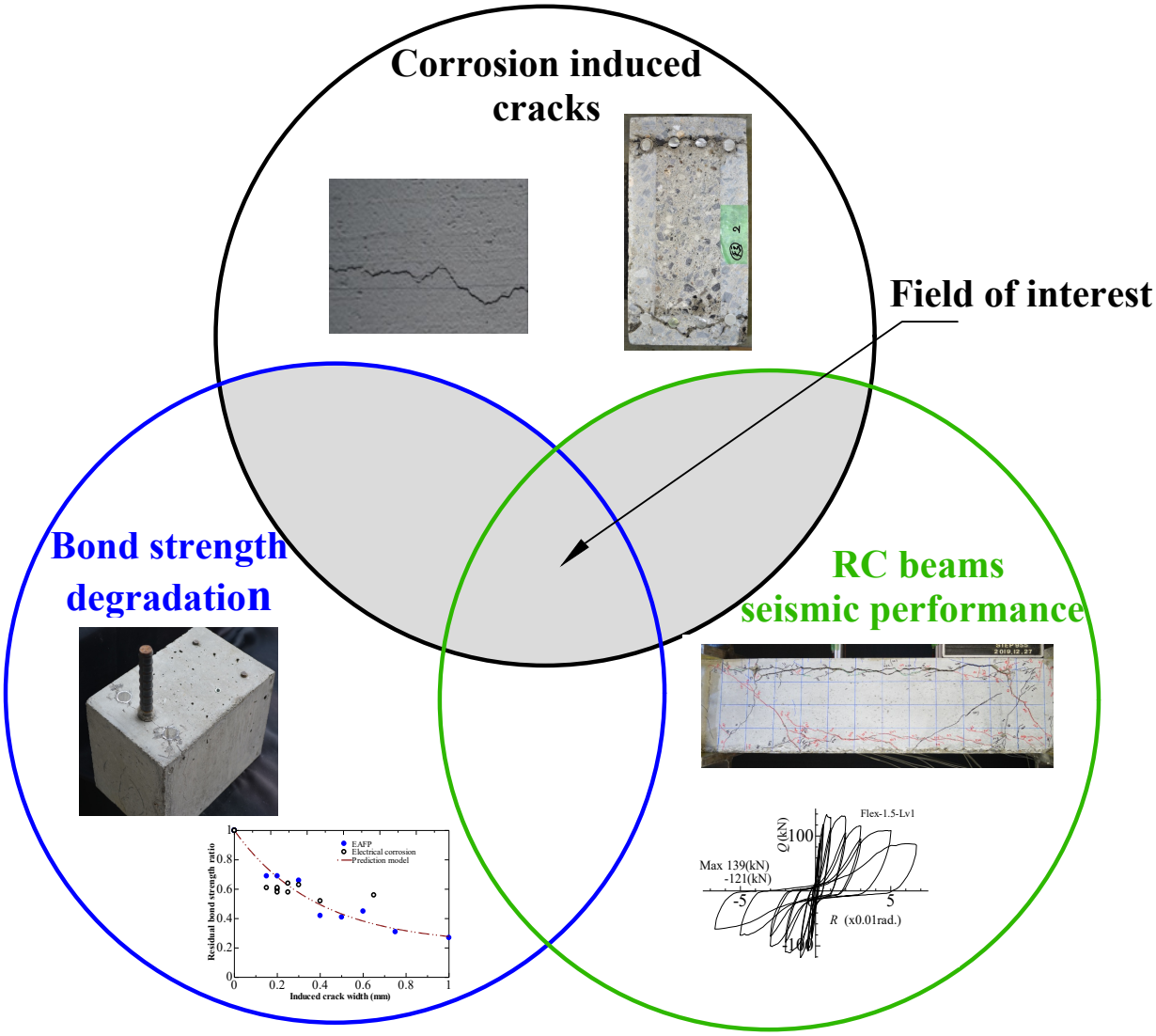

Figure 1.2 Field of research

The findings and knowledge of this study will be useful in analyzing existing damaged structures for engineers and researchers. Little study has been done of the degradation of bond strength due to corrosion-related cracks. This thesis expands on previous research by examining the impact of stirrup cross-section reduction on bond strength degradation. The most important outcome of this research is the proposal of a prediction dependent on the crack width and stirrup ratio for bond strength degradation. Furthermore, the cyclic antisymmetrical bending test provides a better knowledge of seismic behavior on RC beam with induced cracks.

1.3 Original Features

The effects of induced cracks on the bond strength of deformed bars are investigated through experiments. I use a novel method to simulate cracking due to volumetric expansion using an expansion agent filled pipe (EAFP) to overcome limitations related to electrical corrosion

techniques and discretely assess bond strength deterioration. It consists of inserting an aluminum pipe into the concrete and then filling it with an expansion agent to simulate the volumetric expansion of the bar due to corrosion. EAFP is particularly useful for controlling induced crack and focusing on its fundamental influence on bond strength deterioration.

It is claimed that no other studies exist that demonstrate the influence of stirrups cross-section reduction on bond strength degradation due to cover cracking; hence the pull-out tests conducted to explore this phenomenon are novel.

The EAFP method is also used to induce cracks in different RC beams. First, the crack beams are transversally cut to observe the internal cracking pattern. Furthermore, the cracked RC beams are subjected to cyclic antisymmetrical static loading to assess the effect of crack-related bond strength deterioration on the structural performance.

1.4 Outline of the thesis

The Figure 1.3 shows the organization of the thesis. It is divided into seven chapters. *Chapter 1* includes an introductory part that comprehensively summarizes the covered topics. The original features and context are also presented.

Chapter 2 begins to identify the most common methods, outcomes, and trends on the effect of corrosion on bond strength through a systematic literature review.

Chapter 3 aims to increase the knowledge about the bond behavior in cracked RC structures due to corrosion. Specifically, the link between bond strength degradation and corrosion-related crack width and pattern visual inspection data is investigated using electrical induced corrosion techniques. I create two specimens with corroded rebars designed to fail either in side-split (leading to delamination) or single-split (leading to spalling) when subjected to a pull-out test. Moreover, the effect of stirrup on bond strength degradation is also assessed.

In *Chapter 4*, first the novel method to induce crack is thoroughly described and tested in various specimens to observe the surface and internal crack. Then the newly proposed method is used to examine the effect of crack pattern and width on the bond strength degradation. Moreover, the effect of stirrup on bond loss in a cracked specimen is investigated.

Chapter 5 aims to propose an empirical prediction for bond strength degradation in cracked concrete. The combined effects of concrete cracking and cross-sectional reduction of stirrups on bond strength are considered. EAFP is adopted to simulate concrete cracking and focus on induced cracks without rust accumulation or change in rebar profile. In addition, rebars with

different diameters are used as stirrups to illustrate the reduction in rebar cross-section due to corrosion.

Chapter 6 aims to contribute to this growing area of research by exploring the effect of bond deterioration on the structural capacity (shear and flexural) of deteriorated RC beams. To achieve this goal, different damage levels (crack width) are simulated in the specimens by inducing cracks using an EAFP. Then, an anti-symmetrical static loading of the damaged beam are carried out to grasp the mechanical performance of the damaged beam. The conclusions and suggestions for future research are given in *Chapter 7*.

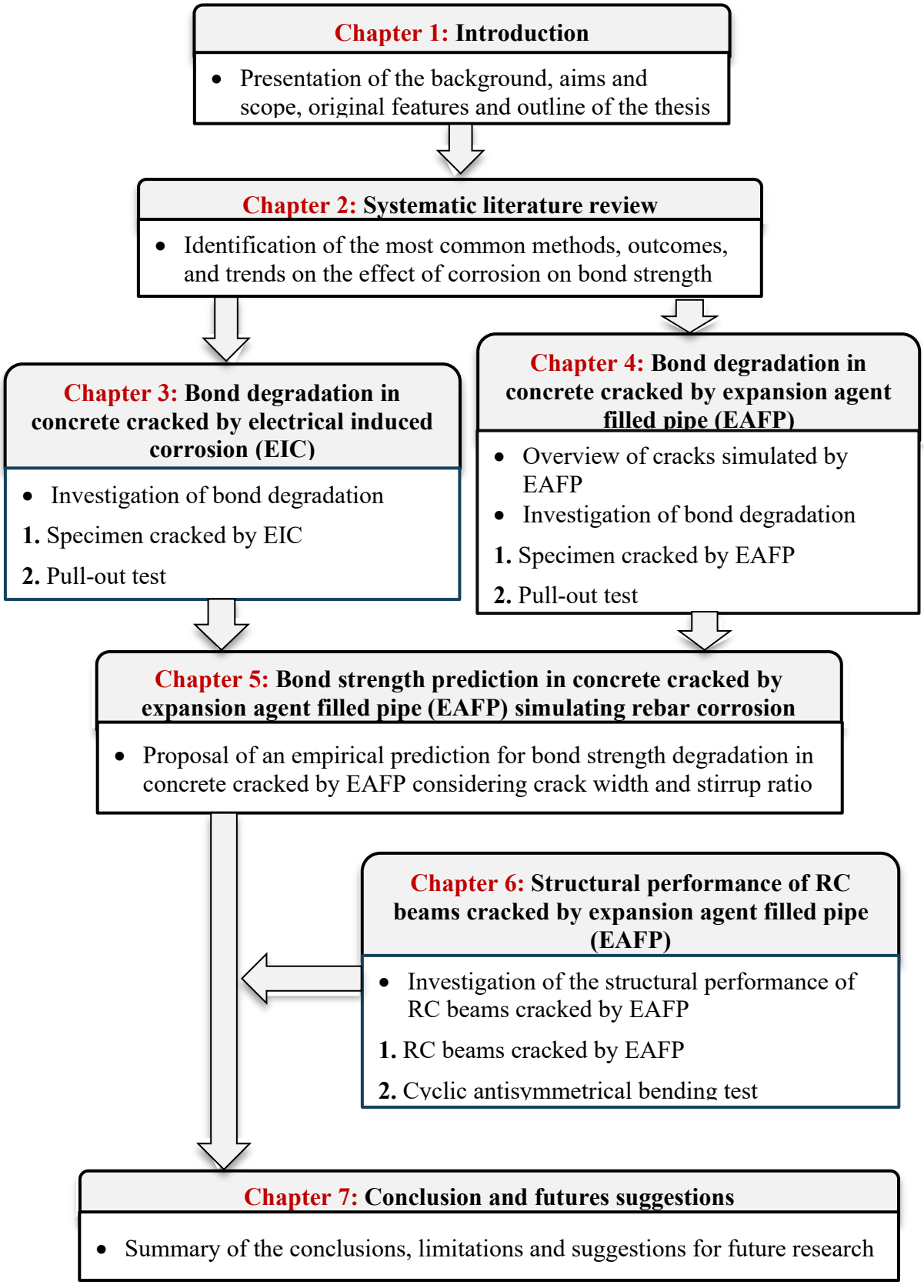

Figure 1.3 Organization of the thesis

2 SYSTEMATIC LITERATURE REVIEW

2.1 Introduction

Some authors have also published review articles on this topic due to the rapid growth of the literature [7–9]. Lundgren [7] (2007) systematically described the effect of corrosion on the bond strength between reinforcement and concrete. Finite element analyses provided a basic understanding of the different cases. The FEM results are then compared with studies of experimental work to provide an overview of the influence of the rebar type, the presence of stirrups, and the confinement of concrete. Mancini and Tondolo [8] reviewed studies on corrosion-related bond strength degradation in RC members. The effects of bond length combined with various methods of the bond test were summarized in the study. In 2019, Lin et al. [9] reviewed the latest research on the bond deterioration of corroded rebars under cyclic or monotonic loads. The review described the most influential factors affecting corrosion-related bond degradation. Furthermore, various proposed models are compared to assess the bond behavior (bond strength and stress-slip curve). They highlighted that the degradation models are mainly based on specific test results and are not yet generalized.

This chapter aims to identify the most common methods, outcomes, and trends on the effect of corrosion on bond strength through a systematic literature review. This chapter includes seven sections structured as follows. Subsection 2.2 presents the methodology for conducting the systematic review of the literature. Subsection 2.3 summarizes the experimental methods used to determine the bond strength in corroded specimens. Subsection 2.4 analyzes the influential factors that affect bond strength degradation due to corrosion. Subsection 2.5 examines empirical models to assess bond degradation. The challenge and new trends are reviewed in Subsection 2.6. Finally, the conclusion and limitations of this study are presented in Subsection 2.7.

2.2 Research Methodology

According to Palmatier et al. [10], a systematic review can help researchers to analyze the status of their field of study to reach clear conclusions. In the literature, several approaches and methods to adequately perform a systematic review are described in detail [11–14]. This study follows the guidelines described by Denyer and Tranfield [11]. The evaluation was carried out

in five steps: (1) selection of objectives; (2) selection of databases; (3) identification of keywords; (4) selection of compatible papers; and (5) extraction of data. This approach has been chosen to make the process transparent and replicable. However, this thesis identifies methods, issues, and trends in corrosion-related bond strength deterioration. The methodology used to collect, analyze, and report the data is detailed in this thesis.

2.2.1 Search Strategy

Figure 2.1 summarizes the research methodology. The literature search was conducted using the "Web of Science" database due to its reputation for high-quality indexing publications in civil engineering [15]. In the Web of Science search, the research criteria were "title and keywords." The search link can be found in [16]. To filter the literature, I formulated the query using the combination of keywords "Bond", "concrete," and "corro*." The first search resulted in 218 articles. The number of articles was reduced to 175 after eliminating manuscripts that had not been peer-reviewed (letters, conference abstracts, and patents). The articles were then reduced to 139, including only those related to civil engineering, construction, or building applications. Finally, the title and abstract of the manuscript were manually selected to assess the relevant articles. In this step, the articles were selected if they included an experimental protocol and a bond strength assessment. Finally, 84 articles were considered in this review.

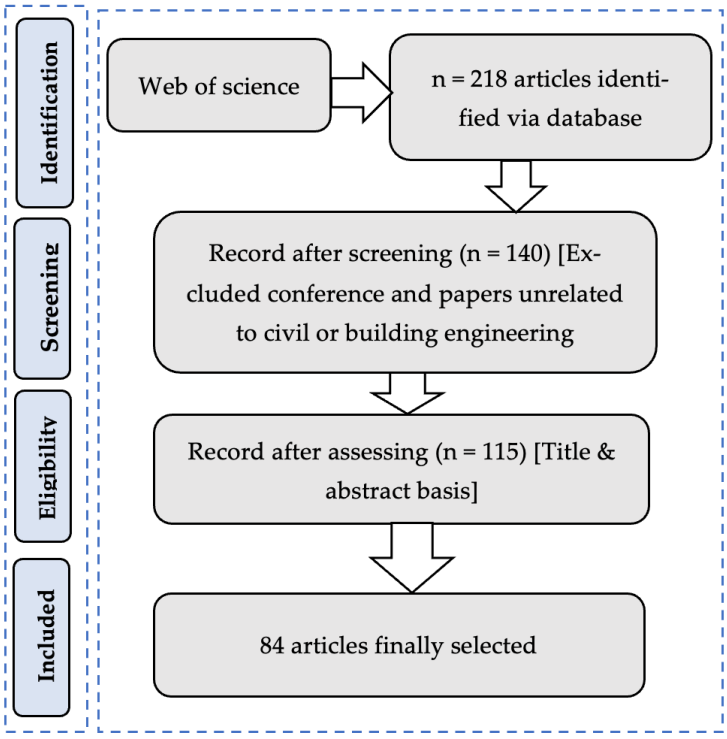

Figure 2.1: Research methodology

2.2.2 Search Result

The study included 84 published articles from 1990 to 2022 (April). Scientific attention to empirical evaluation of bond strength in corroded reinforced structures has continuously grown over the past few years. Figure 2.2 shows that from 1990 to 2013, studies on this topic did not exceed four articles per year. From 2014, the number of publications increased, reaching six articles published in 2016 and 2017. However, the most significant increase was in 2021, when twelve works were published.

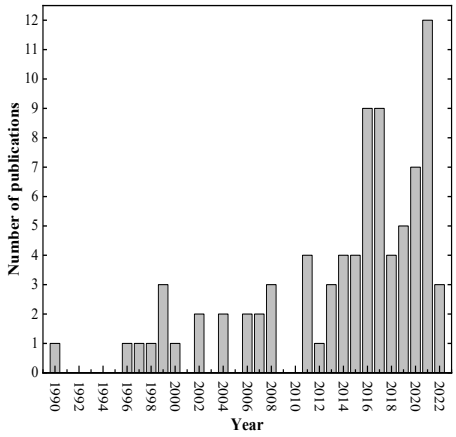

Figure 2.2 Time distribution of publications

Figure 2.3 shows the sources of the selected publications. The journal "Construction and Building Materials" (22 articles) was the most prolific. Only four journals published more than four articles on the topic. Among them, "Materials and Structures" published eight articles, "Magazine of Concrete Research" published six articles, followed by "Cement and Concrete Research" and "ACI Structural Journal" with five articles each. Moreover, four articles were published in "Engineering Structures," and one to three articles were published in the remaining nineteen journals. It is interesting to note that most journals have a sectorial scope on construction materials. Only two journals ("Metals" and "Applied Sciences") have a broad focus and publish articles unrelated to the field of civil engineering or building and construction.

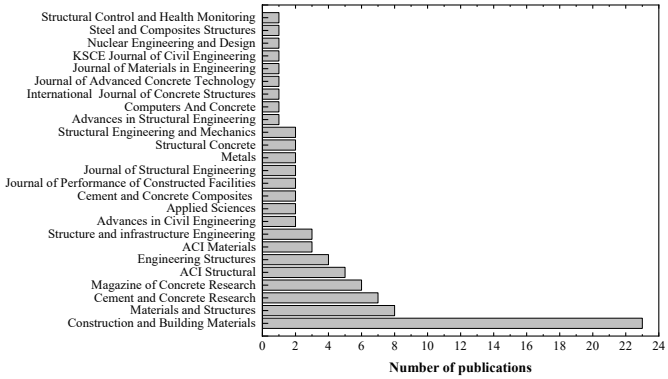

Figure 2.3 Distribution of articles by year of publication

Furthermore, Figure 2.4 shows the geographical distribution of the authors of the selected articles. In terms of publications, China is the most influential (35%), followed by the United States (11%) and Canada (9%). These three countries have published up to half of the total publications. Although geographical distribution cannot provide a solid conclusion, this could help researchers develop collaboration, create joint venture studies, and exchange innovative technologies and ideas.

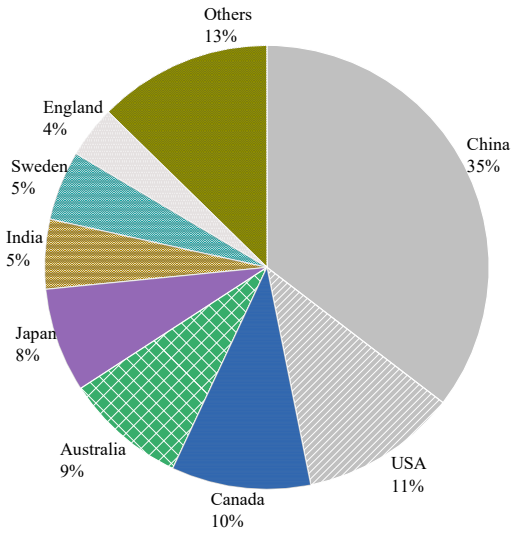

Figure 2.4 Geographical distribution of publications.

2.3 Test Specimens and Bond Test Methods

2.3.1 Corroded Bond Specimens

2.3.1.1 Specimens from Decommissioned Structures

The most prominent and realistic conditions are obtained when using naturally deteriorated specimens to investigate the influence of corrosion. The authors [17–20] studied the effect of corrosion on the end anchorage by performing a four-point bending test on decommissioned edge beams from Stallbacka (Sweden). However, testing specimens from a decommissioned structure can be challenging because the influential factors are likely uncontrollable. Thus, the data can only be informative. In a recent article, Lundgren et al. [21] suggested an approach for selecting and designing bond tests using specimens from decommissioned structures.

2.3.1.2 Accelerated Corrosion Method

Natural corrosion is a relatively slow phenomenon. To reproduce this phenomenon in the laboratory, accelerated corrosion methods are commonly used, including dry-wet cycles, salt spray tests, and accelerated electrical corrosion. The electric accelerated corrosion test is

frequently used to study the bond performance of corroded RC because of its benefits. (short time, controllable current density, and portable test equipment) [22]. The approach is primarily electrochemical, with rebar as the anode and stainless steel or copper plate as the cathode. The corrosion of the rebar is then accelerated by applying a direct current. To ensure the normal conduct of the electric accelerated corrosion test, approximately 5% sodium chloride is often added to fresh concrete. The specimen is either immersed in a salt solution or wrapped with a humidified sponge, as illustrated in Figure 2.5.

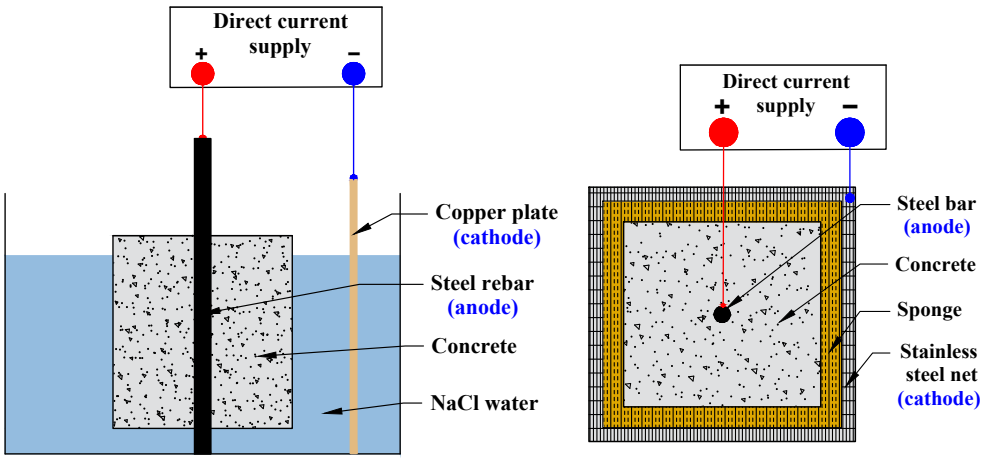

Figure 2.5 Accelerated electrical method

2.3.2 Experimental Bond Test Setup

2.3.2.1 Pull-Out Test

The researchers used the pull-out test to measure the bond strength because of its simplicity and high replicability. It consists of applying a tensile force to pull-out steel bars embedded in the concrete, as shown in Figure 2.6. A short bond length (mostly five times the diameter of the rebar) is generally adopted to focus on the local bond behavior. Depending on the position of the main tested rebar, the pull-out test can be referred to as central or eccentric. However, in the pull-out test, the rebar is in tension, and the concrete is in compression, which does not reflect the actual situation in the structure. To overcome this drawback, Auyeung et al. [5] used a modified version of the concentric pull-out test. They set two aligned rebars with different embedding lengths. One end of the longer rebar is fixed, and the shorter embedding length is pulled out to determine the bond strength (Figure 2.7).

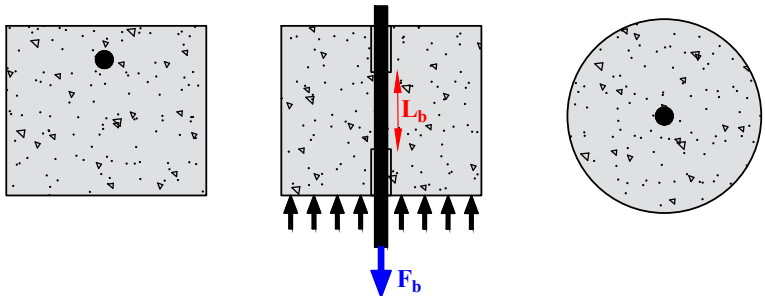

Figure 2.6 Pull-out test

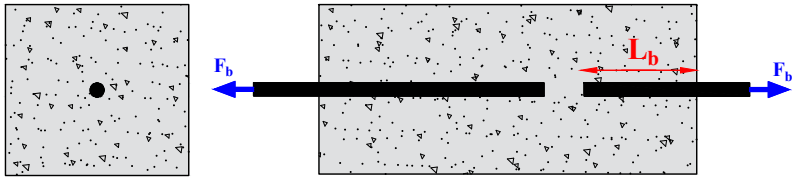

Figure 2.7 Pull-out test modified by Auyeung

2.3.2.2 Beam Test

Some authors also evaluated the bond behavior using a beam in four-point bending to replicate the actual stress in RC beams [19,23–26]. Bond performance is measured using the steel bars arranged in the tension area, as shown in Figure 2.8. Mangat and Elgarf [27] used another variant of a hinged beam. Compared to the pull-out test, the beam test is more realistic, including the bending moment and shear in the RC member [28]. In addition, the bond is investigated while both the concrete and the rebar are under tension. However, the beam test is generally less widely used due to its complex operation, high cost, and relatively low replicability. Therefore, Chana [29] designed a beam end specimen with parallel bars cast around the four corners. As a result, the bond strength can be tested for both top and bottom cast conditions. (Figure 2.9).

Furthermore, Hanjari et al. [30] further simplified the beam test. As shown in Figure 2.10, only the supported part of the beam end was selected, and the reaction force of the part was simulated, which reduced the test cost and improved the repeatability.

The presence of corrosion increases the uncertainties, leading to a greater scattering of the bond strength. Each test method features some characteristics of bond behavior. Therefore, a unified standard for the bond test cannot be identified because any test cannot fully describe the bond behavior.

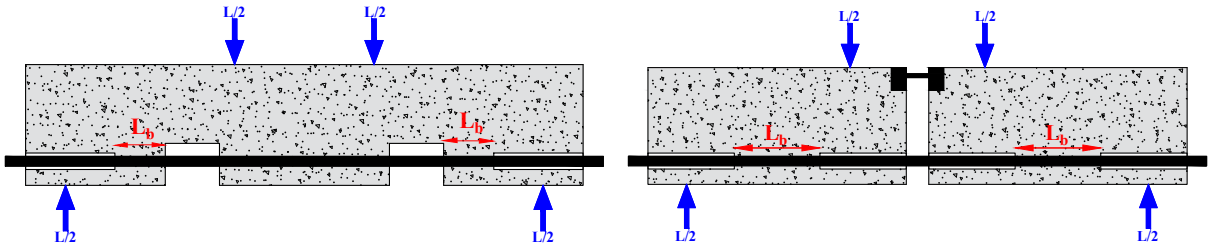

With a pocket With a hinge

Figure 2.8 Beam test

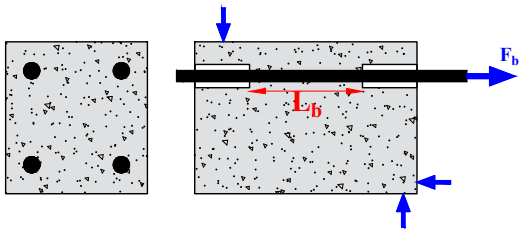

Figure 2.9 Beam end test proposed by Chana [29]

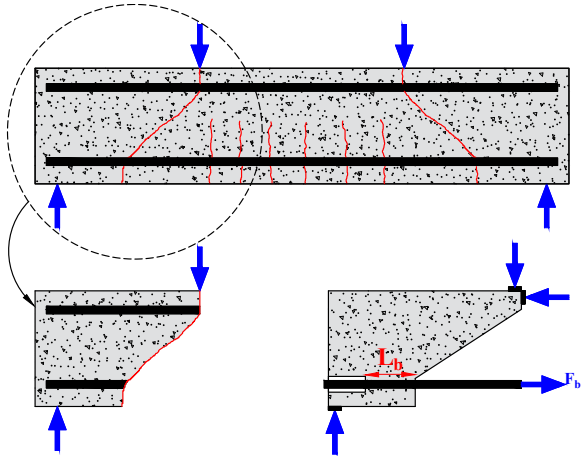

Figure 2.10 Modified Beam test by Hanjari et al.

2.4 Bond Strength Deterioration Due to Corrosion

2.4.1 Corrosion of the Main Rebar

Several investigations have examined the impact of longitudinal rebar corrosion on bond strength [31–36]. The findings point to a general trend of bond strength deterioration owing to corrosion. Figure 2.11 shows the bond strength ratio of corroded rebar to non-corroded rebar at various degrees of corrosion. Three stages characterize the degradation trend. In stage 1 (low levels of corrosion), the production of expansive corrosion products could improve confinement to the rebar, increasing the bond strength. Expansive materials can crack the concrete cover as corrosion develops, rapidly decreasing bond strength (stage 2). In stage 3 (high levels of

corrosion), the bond strength did not alter with increasing mass loss, asymptotically approaching a limit. Significant rib deterioration would result in friction-type behavior comparable to plain bars [37–40]. As a result, the bond strength slowly decreases in stage 3.

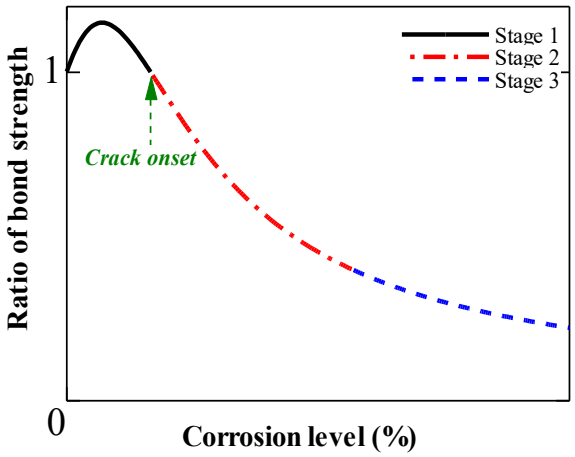

Figure 2.11 Degradation of bond strength with corrosion level

2.4.2 Essential Factors Affecting the Bond Strength of Corroded Specimens

The selected articles revealed that several factors affect the bond strength deterioration, including the type of corrosion (uniform/ pitting, due to chloride or carbonation; wet or dry environment); the amount of stirrup; the position of the main bar; concrete cover; bar diameter and concrete strength. However, this review included only three factors (concrete strength, concrete cover-to-rebar diameter ratio, and stirrup). These factors were selected because they are considered to have the most significant influence. Moreover, the selected influencing factors are rather clearly definable.

2.4.2.1 Influence of Concrete Strength

The bond performance of sound RC elements is proportional to the strength of the concrete. Increased concrete strength leads to increased bond strength. Yalciner et al. [41,42] investigated the effect of concrete strength on bond loss due to corrosion. They conducted a pull-out test on unconfined specimens with two different concrete strengths (23 MPa and 51 MPa). The results summarized in Figure 2.12 demonstrated that corroded specimens with higher concrete strength showed a more substantial bond strength degradation. This is probably because the brittleness of the corroded specimens caused an abrupt loss of bond strength. Corrosion products do not diffuse rapidly into concrete pores because of the excellent resistance to permeability in high-strength concrete. Therefore, the accumulation of expansive products around the rebar leads to

more significant induced crack widths, leading to a more severe deterioration of the bond strength [43,44].

Figure 2.13 shows the results of Zhou et al. [45,46]. They examined the effect of concrete strength on bond degradation using two different concrete mixes (20.7 MPa and 44.4 MPa) in specimens with stirrups. In contrast, they discovered that the compressive strength of the concrete did not affect the bond degradation trend. They emphasized that mixing different failure modes can complicate the observation of the concrete strength effect.

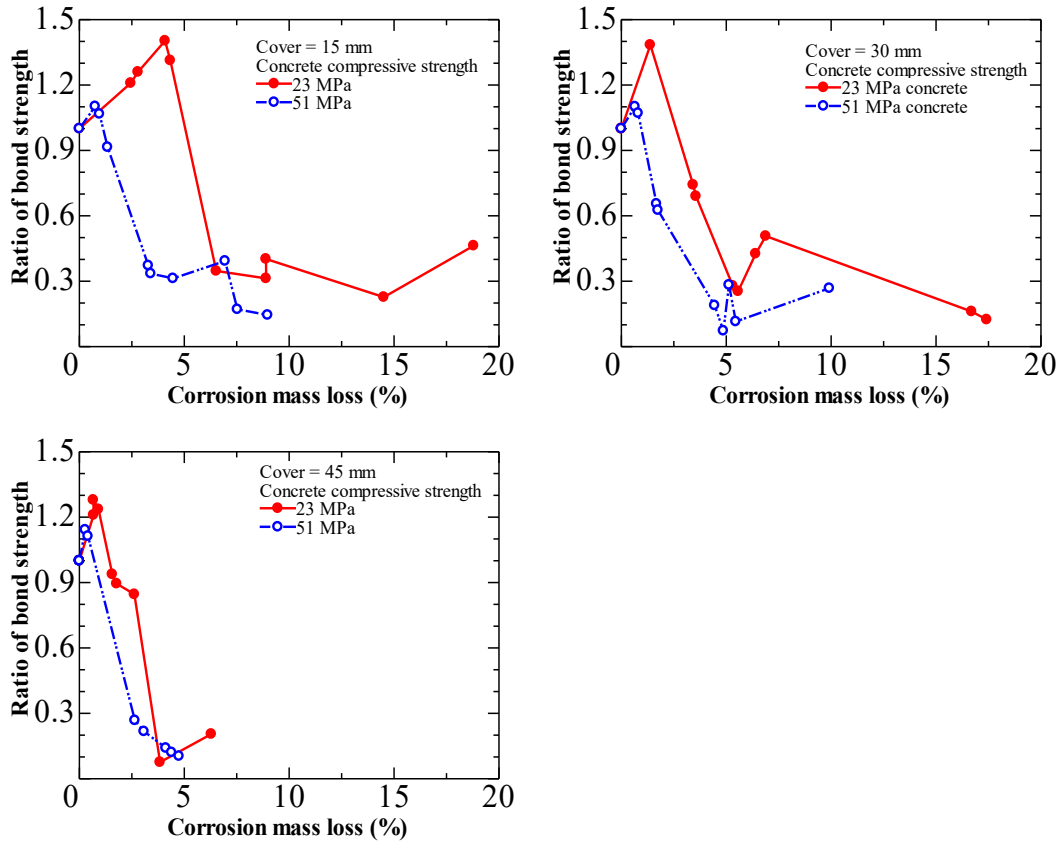

Figure 2.12 Influence of concrete strength on bond deterioration from Yalciner et al.

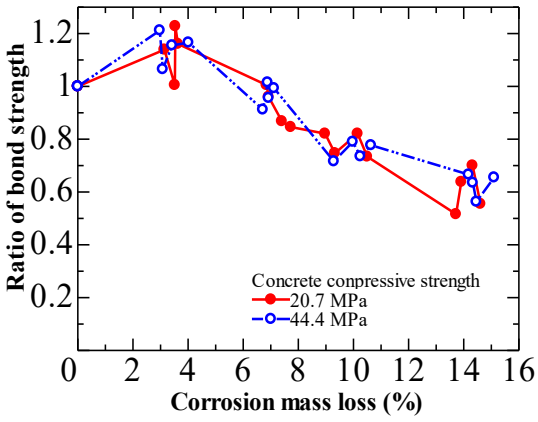

Figure 2.13 Influence of concrete strength on bond deterioration from Zhou et al.

2.4.2.2 Influence of the Cover-to-Rebar Diameter Ratio c/d

The concrete cover thickness c to steel bar diameter d (c/d) ratio is frequently regarded as a crucial element influencing bond strength. The bond strength was observed to increase as c/d increased. However, this increase is limited; for example, the bond strength will remain stable when c/d ≥ 3 in the specimen without stirrups [47]. Al-Sulaimani et al. [32] performed a pull-out using corroded specimens where three cover-to-diameter ratios (c/d) ratios of 3.75, 5.36, and 7.5 were adopted over 20, 14, and 10-mm bars, respectively. Data showed that 4% of corrosion is needed to start cracking for a c/d ratio of 7; however, about 1% is necessary to crack specimens with a c/d ratio of 3. They suggested that the ratio of cover-to-diameter (c/d) could be considered a significant factor that expresses corrosion protection.

Furthermore, Al-Sulaimani et al. [32] showed that bond deterioration is more severe in specimens with a smaller c/d, as shown in Figure 2.14. The results of Amleh et al. [33] shown in Figure 2.14 are consistent with those of Al-Sulaimni et al. concrete can still transfer stress across cracks. As a result of the residual confinement, the specimens with a more significant concrete cover demonstrated stronger bond strength.

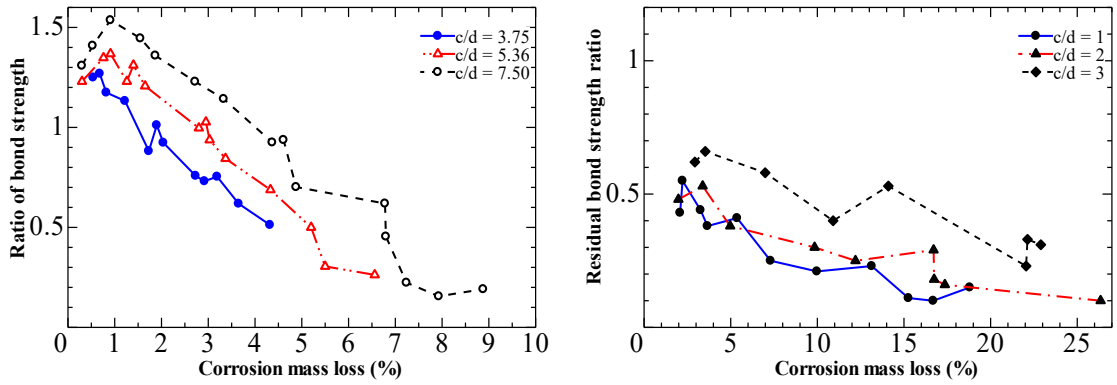

Al-Sulaimani et al. [32] Amleh et al. [33]

Figure 2.14 Influence of the cover-to-diameter ratio on bond deterioration

2.4.2.3 Influence of Stirrups

The influence of stirrups on the deterioration of the bond as a result of corrosion is twofold. Studies showed that the stirrup could increase concrete confinement, limiting the width of cracks due to corrosion [48–52], as illustrated in Figure 2.15. Second, several authors investigated the effect of stirrup corrosion on bond degradation. Fang et al. [39,40] performed a centric pull-out test on corroded specimens with and without stirrups. They discovered that a moderate corrosion rate (about 4%) had no significant influence on bond strength. However, bond degradation was observed when the degree of corrosion was greater than 6%. Zhou et al. [53] focused on the effect of corroded stirrups on the bond performance of reinforced concrete.

They concluded that the bond strength improved when the degree of stirrup corrosion was less than 10%. However, bond degradation was observed when the degree of stirrup corrosion reached 15%. These findings are likely related to the corroded stirrup that produces hoop stress that acts inside and outside. This stress can crack the cover and add more confinement to the core concrete where the tested rebar is located [54–56]. As a result, the bond strength can increase.

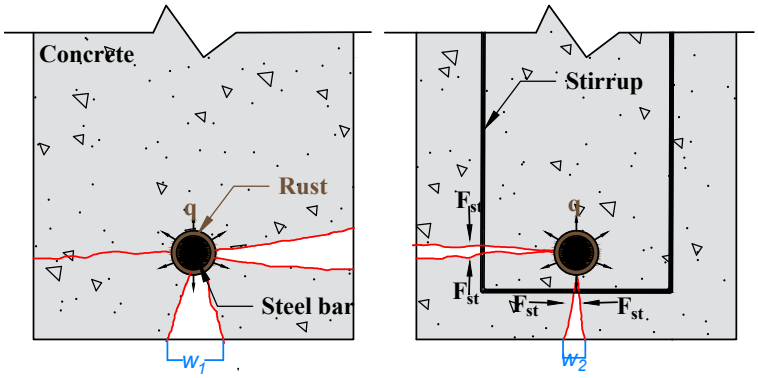

Figure 2.15 Effect of stirrups on corrosion-induced cover cracking

2.5 Prediction of Bond Strength Deterioration Due to Corrosion

Researchers have used different techniques to derive models to predict corrosion-related bond strength degradation. Most models are based on specific experimental results and consider different parameters. Furthermore, Wang et al. [57,58] and Bhargava et al. [59,60] used a thick-walled cylinder approach to propose a theoretical model, further validated by experimental results. Other authors also collected data from previous studies to propose bond degradation models using statistical analysis [61,62] or deep learning [63–66]. The major limitation of these models is that they are based on assumptions regarding the value of essential input factors that are not consistently measurable. In addition, the models go through a sequence of complicated integration and derivation techniques. In reference [67], an extensive database of experimental studies on corrosion-related bond degradation is available.

The following subsections present some empirical models. The proposed model can be divided into two main categories: a model based on corrosion mass loss and a model based on induced crack width.

2.5.1 Models Based on Corrosion Mass Loss

The suggested models [5,43,68–71] agree with the experimental data for which they were calibrated. Figure 2.16 indicates little agreement among the suggested models despite some degradation trend similarities.

The same degradation trends are observed in almost all proposed empirical models. Due to the limited amount of test data used for validation, each model claimed to be able to evaluate bond loss with reasonable accuracy. However, the models are characterized by their dispersion of the bond loss level. The scatter can be attributed to the specimen design or uncertainty related to the complex corrosion process.

However, it is found that this model, where mass loss is the main parameter, is likely challenging to implement. The mass loss of corroded rebar is not easily measurable in real situations. Therefore, to implement these models, engineers would first need a model to correlate the measurements of surface crack widths with the "hidden" internal corrosion. However, many uncertainties associated with each model can seriously weaken its effectiveness and accuracy.

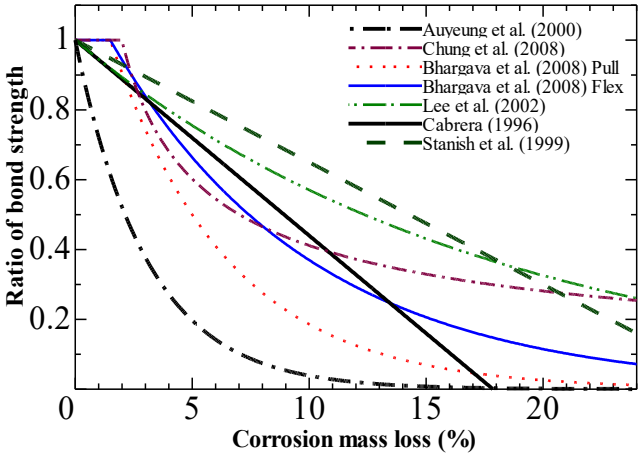

Figure 2.16 Comparisons of model predictions based on mass loss

2.5.2 Models Based on Induced Crack Width

Corrosion-induced surface cracking is easily measurable in actual structures and is convenient for practical use. Law et al. [72–74] investigated the effect of concrete cracking on bond deterioration. They claimed that bond strength correlates with induced crack widths rather than corrosion level. Furthermore, they underlined that the maximum crack width showed a stronger relationship than the average. In addition, the study by the same authors has highlighted the influence of the cover-to-diameter ratio on deterioration [72]. Their test data were better fitted

with a linear or logarithmic function because corrosion has little influence on cracking when a certain crack width is reached.

Lin et al. [75] made significant contributions by examining the relationship between surface crack widths and bond degradation. They used accelerated corrosion and eccentric pull-out experiments to examine the effects of various factors, such as bond length, concrete cover, corrosion level, and stirrup spacing. They proposed a mathematical model to assess bond loss using the surface crack width as the main parameter, as expressed in Eq. (2-1).

$$\tau_u(w_{ave}, w_{stave}) = \tau_u(0) D_{st}(1.0 - 0.9e^{-20p_{st}}(1.0 - e^{-1.73w_{ave}e^{-56.6p_{st}}})) \quad (2\text{-}1)$$

Where w_{ave} is the average longitudinal crack width; pst is the stirrup index, $p_{st} = A_{st}/CS_{st}$; A_{st} is the cross-sectional area of the stirrup; S_{st} is the stirrup spacing, and C is the concrete cover. D_{st} is a function of the average lateral crack width w_{stave}.

$$D_{st} = 1 - 0.68\left(\frac{w_{stave}d_{st}}{-0.29C_{st} + 1.58d_{st}} + 1 - \left(1 - \frac{\theta}{d_{st}}(7.53 + 9.32\frac{C_{st}}{d_{st}})10^{-3}\right)^2\right) \quad (2\text{-}2)$$

Where C_{st} is the concrete cover of stirrups; d_{st} is the stirrup diameter; θ is the pit concentration factor.

The fib model [76] provides a simplified relationship between corrosion-induced crack width and bond deterioration. Figure 2.17 compares experimental data from the literature [72–75,77–79] with the simplified correlation of the fib model [76].

Figure 2.16 indicates a strong correlation between induced crack widths and bond deterioration in unconfined specimens. Furthermore, fib model code estimations for specimens without stirrups are well predicted. The data scatter is higher for specimens with stirrups. The fib model fails to predict the increase in bond strength caused by stirrups, resulting in an overestimation.

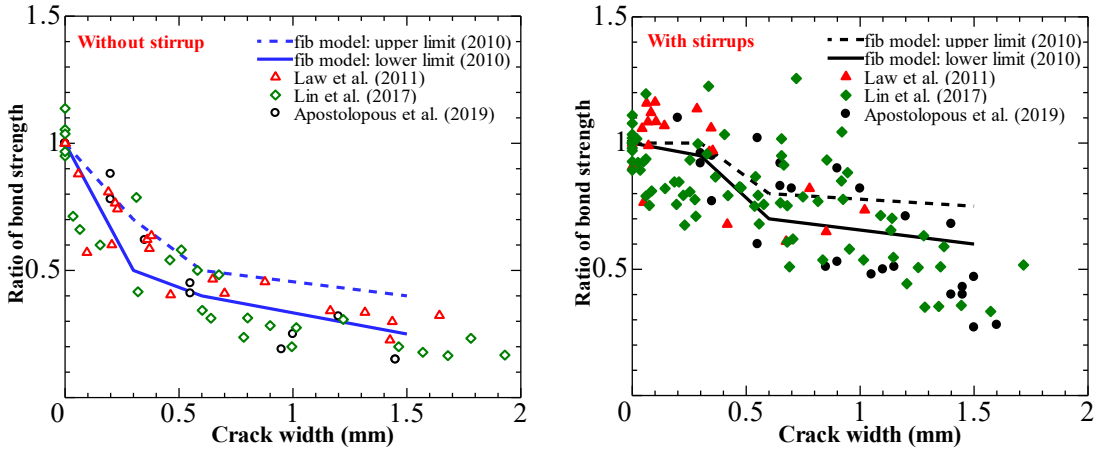

Specimens without stirrups Specimens with stirrups

Figure 2.17 Comparisons of fib model with test results in the literature

2.6 Challenges and New Trends

The corrosion of rebar leads to a reduction in the steel cross-section, change in the concrete-rebar interfacial layer, and cracking of the concrete. These damages entirely affect the bond strength of the corroded specimen. However, these effects lead to difficulties in analyzing the processes at the fundamental level and negate the overall accuracy of the proposed models. Furthermore, a literature review showed that a unified model for general validity is not yet available. The discrepancies found in the data were mainly attributed to specimen variability, experimental machine setup, corrosion rate, or corrosion type (uniform or non-uniform). The following subsection summarizes the previous work to address this challenge. In addition, new alternatives for practical models are introduced.

2.6.1 Influence of the Corrosion Rate

Generally, researchers have widely adopted an accelerated corrosion setup with different current densities to replicate the natural corrosion effect relatively quickly. However, the densities of the accelerated corrosion current can be thousands of times higher than those measured under natural conditions [1,80]. Some authors focused on the influence of the induced current density on bond deterioration. Increased current density has been shown to worsen bond deterioration [81,82]. Furthermore, Alonso et al. [83] concluded that current density reduces the effect of oxide formation on cracking, perhaps due to the production of oxides with a lower volumetric expansion ratio. Furthermore, Corronelli [84] pointed out that material degradation due to electrical current can worsen bond degradation when applying a high current density level.

On the other hand, researchers investigated the bond deterioration of corroded specimens extracted from decommissioned RC bridges [17–20]. Tahershamsi et al. [18] examined the bond degradation due to corrosion-induced crack widths of 32-year-old naturally corroded RC girders. They found more significant crack widths for given levels of corrosion than previous researchers using accelerated corrosion. Figure 2.18 shows that the reduction in bond strength in the naturally corroded specimen was less significant than the results of artificial corrosion. They attributed the disparity to the difference between natural and accelerated corrosion and the cumulative effects of freeze-thaw and corrosion. In conclusion, they stated that estimating bond deterioration using accelerated corrosion would be safe.

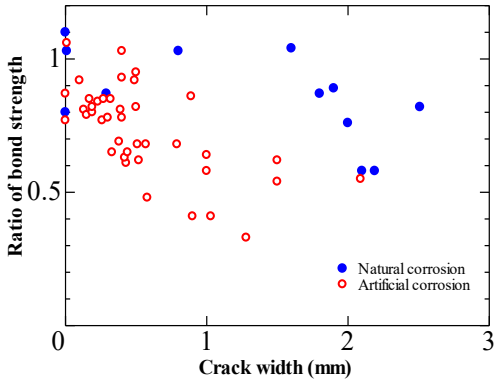

Figure 2.18 Influence of corrosion rate on bond strength deterioration

Although a universally accepted current density limit does not yet exist, El Maaddawy and Soudki [85] recommended that current densities less than 200 μA/cm^2 are preferable for more realistic data in accelerated tests.

2.6.2 Non-Uniformly Corroded Steel Bar

Previous investigations on the effect of corrosion on the bond strength of RC specimens were conducted by accelerated corrosion using impressed currents. As a result, the tested rebars were uniformly corroded. In this way, only mechanical interlocking and friction contributed to the bond strength of the corroded specimens. However, the natural corrosion of steel is typically non-uniform around the surface of the rebar [24]. Therefore, the interfaces of the corroded and non-corroded sections contribute to the bond. To address this, studies [86–88] focused on the influence of the rebar's non-uniform corrosion on the bond strength's deterioration. Fu et al. [87] adopted two corrosion modes for corroded RC specimens to induce non-uniform and uniform corrosion. Figure 2.19 shows that the bond strength degradation was generally more severe in non-uniformly corroded specimens than in the case of uniform corrosion. Deterioration becomes more noticeable as the corrosion level increases. This is likely related to the stress concentration within the interface.

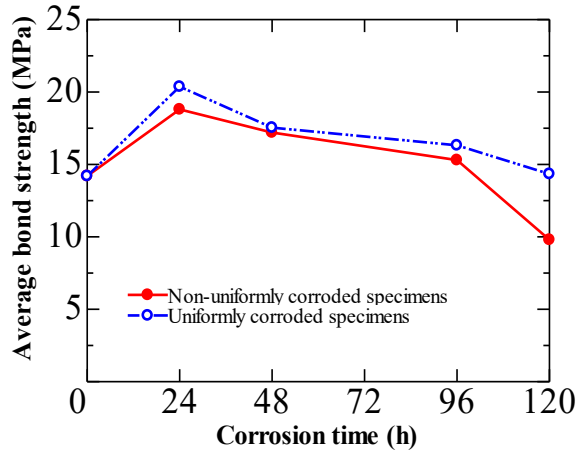

Figure 2.19 Influence of corrosion type on bond strength

2.6.3 Damage Identification of Bond in Corroded Specimens

Many factors affect the bond between rebar and concrete, leading to a complicated interaction. Recently, researchers have attempted to clarify damage using acoustic emission [89], ultrasonic technology [90], or digital image correlation (DIC) [91,92]. Ouglova et al. [92] used DIC to examine the beginning of bond failure in corroded specimens. They found that the increase in corrosion level slows the beginning of bond failure. Furthermore, the average bond stress at the start of the slippage is smaller than the bond strength during the pull-out test. Avadh et al. [91] used corroded specimens with a window to observe the rebar and concrete interface during the uniaxial tension test. The corroded rebars were cast in new concrete to eliminate the hindrance caused by the corrosion-induced cracks. They performed a DIC to examine the influence of rib height reduction and rust's presence on bond failure. Figure 2.20 shows the change in strain distribution with loading adopted from Avadh et al. [86]. The onset and progression of diagonal cracks are observed in uncorroded specimens and specimens with degrees of corrosion up to 12% (Specimens UC-00, C-06, and C-12). Furthermore, failure-cracking observations revealed that the increased corrosion led to faster debonding between the rebar and the concrete. Diagonal cracks were not observed in specimens with higher degrees of corrosion despite having ribs (Specimens C-15 and C-20).

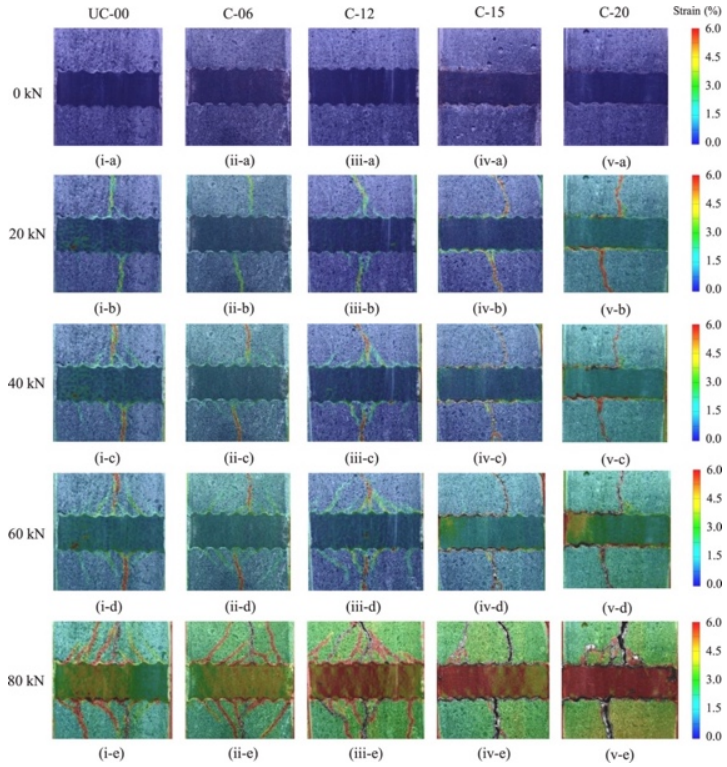

Figure 2.20 Change in strain distribution with loading [87]

2.6.4 Clarification of the Effect of Corrosion on Bond

In the recent literature, researchers [93–95] attempted to investigate the separate effect of corrosion-induced cracks, corroded rebar shape, and rust around the rebar on the bond properties of RC members. The results of Yang et al. [93] contribute to understanding the isolated effect of different corrosion damage on bond degradation. The first group included uncorroded specimens, and the specimens were subjected to accelerated corrosion in the second group. The specimens in the third and fourth groups were obtained by recasting the artificially corroded rebar into new concrete. The corroded rebars were cleaned for the third group (without rust) and intact for the fourth group (with rust). The authors concluded that corrosion-induced cracks were the primary cause of bond degradation.

Furthermore, its effect was more significant than the variations in the rebar profile or accumulation of rust at the interface. Jiradilok et al. [96,97] confirm Yang et al.'s [93] point that corrosion cracks have a dominant effect on bond behavior. Furthermore, they stated that the commonly used experimental method could not capture several factors due to corrosion. However, only the effect of surface cracking could be observed in the final result.

On the other hand, Mak et al. [94] changed the sealing condition of diverse specimens to vary the flow of rust through the concrete voids. They successfully separated the level of corrosion

and the expansive effect that cracks the concrete. Their results showed it is challenging to correlate bond deterioration and rebar corrosion directly. Therefore, the width of the concrete cracks could be a better indicator than the corrosion level to assess the bond strength degradation.

2.6.5 Trend: Toward a Direct Crack-Based Model

Novel methods have been proposed to simulate cracking due to corrosion to overcome limitations related to electrical corrosion techniques. Crack width is used as a parameter to assess bond deterioration discretely. This alternative approach is based on previous findings demonstrating that the bond mechanism through interlocking ribs predominates over friction after cracking. Furthermore, it is assumed that a direct relationship between interlock reduction and crack width ignores the ambiguity related to corrosion product accumulation.

2.6.5.1 Cracking Induced by a Splitting Load

Desnerck et al. [98] conducted a pull-out test on cracked specimens to focus on the more fundamental effect of the induced cracks. Before loading, the specimens were subjected to a split cylinder test to induce cracks. Two-line loads are applied to the specimen on opposite sides and along the concrete cylinder's axis until the concrete's first cracking. At this point, the specimen is unloaded. Their results showed that the bond strength degradation for double-cracked specimens was 65% higher than for single-cracked specimens. Furthermore, the effect of crack inclination on the rib pattern is negligible. Mousavi et al. [99] also adopted the same method to induce cracks. Although research has shown an interesting result, this method is not easily replicable.

2.7 Summary

The systematic review of the literature conducted in this thesis found that issues related to bond strength degradation due to corrosion have received significant attention in recent years. Furthermore, this review presents a general overview of the effect of corrosion on the bond strength between concrete and rebar. The following summaries can be drawn:

i. The following variables are most frequently used in the literature to build models that predict the bond strength of corroded RC elements: corrosion mass loss, corrosion-induced crack width, stirrup quantity, and ratio of cover to bar diameter c/d.

ii. The confinement provided by stirrups and concrete cover is essential to limit the deterioration of the bond due to corrosion. However, the influence of the concrete strength on bond deterioration remains unclear.

iii. Most available bond strength degradation models based on corrosion mass loss do not adequately account for the contributing factors. Moreover, they are inadequate for practical use. Models using surface crack width as the governing parameter perform better; however, they can still be improved.

iv. Most data were obtained using different current densities with various bond test setups on artificially corroded specimens. Therefore, a general model is still unavailable due to discrepancies caused by differences in testing methods to evaluate the effect of corrosion on bond strength.

v. In recent literature, the authors effortlessly attempted to clarify the mechanism of bond strength degradation due to corrosion. As a result, new alternatives have been proposed to build a practical model to assess the deterioration of the bond strength in corroded structures. Indeed, researchers should harmonize their efforts between different research programs to achieve consistent results in this field.

3 BOND STRENGTH DEGRADATION IN CONCRETE CRACKED BY ELECTRICAL INDUCED CORROSION (EIC)

3.1 Introduction

In the Chapter 2, the systematic literature review shows that the most studies related to bond strength degradation due to corrosion focused on the relationship between corrosion level (steel mass loss). However, little study has investigated the effect of cracking on bond strength degradation, a parameter that can easily be measured on the real RC structures. The rebar corrosion produces iron oxides with a greater volume than the sound rebar. This expansion induces tensile hoop strains in the surrounding concrete, which eventually causes the concrete cover to crack. Thus, the confinement capacity is lost due to cracks development. As a result, the bond strength degradation may be proportional to crack width. Moreover, stirrup presence can somewhat compensate confinement loss and bond degradation.

During structures inspection, engineers thoroughly documented the cracking conditions. However, numerous studies have shown that the pattern of corrosion-induced cracking depends on the design of concrete sections. Corrosion can develop cracks in the plane of the rebar, and cracks may be inclined or horizontal depending on the cover thickness. An inclined crack may develop when the concrete cover thickness is relatively small. A horizontal crack may appear for large cover thicknesses. However, no study investigates the effect of crack patterns on bond strength degradation. Therefore, this chapter investigates the effect of crack width and pattern due to corrosion.

This chapter aims to increase the knowledge about the bond strength in cracked RC structures. Specifically, the link between bond strength degradation and corrosion-related crack width and pattern visual inspection data is investigated. I created two corroded specimens designed to fail either in side-split (leading to delamination) or single-split (leading to spalling) when subjected to a pull-out test. Moreover, the effect of stirrup on bond strength degradation was also assessed.

3.2 Crack pattern due to rebar corrosion

Numerous studies have shown that the pattern of corrosion-induced cracking depends on the geometric situations and configurations of concrete sections. Corrosion can develop cracks in the plane of the rebar and depending on the thickness of the cover. These cracks may be inclined or horizontal. When the thickness of the concrete cover is less than 25.4 mm, an inclined crack may develop. In contrast, a horizontal crack may appear for cover thicknesses of 31.8 mm or more [100].

Assuming that concrete with embedded rebars is a thick-walled cylinder and corrosion products distribute uniformly around the rebars, Bazant [101] indicated that the corrosion-related cracking occurs essentially in two distinct modes. As illustrated in Figure 3.1, cover thickness (C) and rebar spacing (S) strongly affects the cracking mechanisms. If the spacing S is higher than six times the rebar diameter (D) or the cover thickness (C) is relatively small, two diagonal cracks spread from the rebar to the concrete surface at a 45-degree angle, resulting in cover spalling. If the cover thickness (C) is more than (S-D)/2, the two cracks spread separately to adjacent rebars. As a result, cracks parallel to the surface of the concrete are induced, leading to cover delamination.

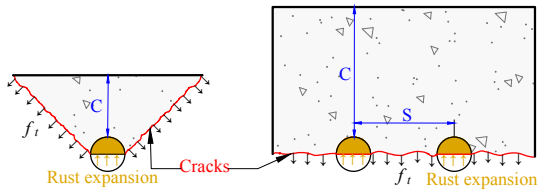

Figure 3.1 Cracking mode after Bažant

As shown in Figure 3.2, Tsutsumi et al. [102] established a similar criterion for the internal crack patterns of single rebar specimens, using the elastic theory that accounts for stress concentration. Cracks propagate diagonally to the surface of the concrete if the value of k, which is determined by the ratio of cover-to-bar diameter (C/D), is less than three. A vertical crack in the concrete cover and two horizontal cracks appear if k is greater than three.

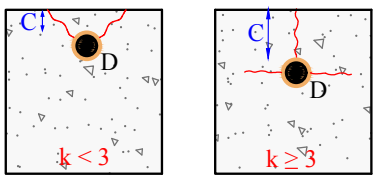

$$k = \frac{2C + D}{D}$$

Figure 3.2 Pattern of internal cracks (Tsutsumi criterion)

Engineers frequently find extensive cracking due to corrosion while inspecting deteriorated structures. The pattern of corrosion-related cracks may vary depending on the location of the rebar of RC member, which in turn affects the bond strength. Therefore, to appropriately model the damage, the crack pattern in specimens should closely match the circumstances prevalent in corroded RC members. I focus on two types of crack patterns in this work: "side-splitting" and "single splitting." Figure 3.3 illustrates the types of cracks considered in this chapter.

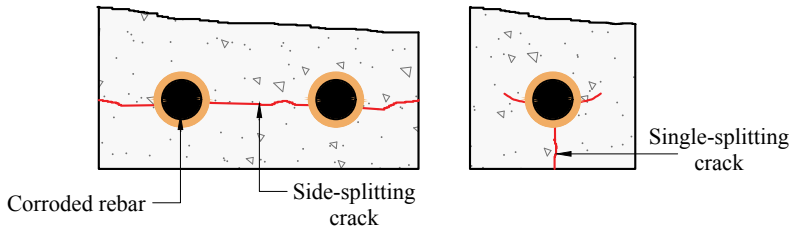

Figure 3.3 Crack pattern considered in this work

3.3 Experimental Program Outline

3.3.1 Materials

The general characteristics of all materials used in this study are described herein. Concrete with a nominal strength of 13.5 MPa and a target compressive strength of 18 MPa was ordered from a local concrete factory.

3.3.1.1 Concrete

A local concrete factory provided the ready-mixed concrete with 18 MPa as the target compressive strength. The concrete was composed of 248 kg/m3 of ordinary Portland cement, a water-cement ratio of 78.5%, and an aggregate of maximum size of 20 mm. The proportion of the concrete mixture used is shown in Table 1. The mechanical properties of the concrete were measured using Ø 100 x 200 mm cylinder specimens following JIS A 1108 and JIS A 1113. The compressive and splitting tensile strengths at the age of pull-out test were, on average, 24.2 MPa and 2.17 MPa, respectively.

Table 3.1 Concrete mixture proportion

Water-cement ratio (%)	**Unit weight (kg/m^3)**				
	Cement	**Water**	**Fine aggregate**	**Coarse aggregate**	**Water reducing agent**
78.5	248	195	930	840	2.48

3.3.1.2 Steel rebar

Figure 3.4 shows the rebar used in this study. The main tested rebar is a deformed bar (D19) with a nominal diameter of 19.1 mm, according to JIS G 3112. The rib height and spacing are 1.2 mm and 13.4 mm, respectively. Stirrups are D6 rebars with a diameter of 6.35 mm. Tensile tests under JIS Z 2241 were performed on three representative specimens of each type of rebar, and the average results are summarized in Table 3.2. Figure 3.5 shows the stress-strain relationship of the steel rebar.

Figure 3.4 Used steel rebar

Table 3.2 Mechanical properties of rebar

Designation by JIS G 3112	Nominal diameter (mm)	Yield strength (MPa)	Tensile strength (MPa)	Elastic modulus (GPa)
D6	6.35	456*	554	201
D19	19.1	366	535	195

*0.2% offset strength

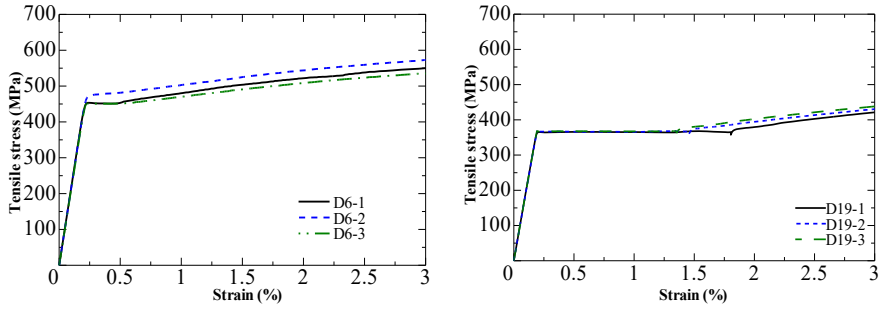

Figure 3.5 Stress-strain relationship of the steel rebar

3.3.2 Pull-out specimen

Table 3.3 summarizes the details of the experimental program. The specimens were divided according to the possible crack pattern: a single bar for Series S1 and three adjacent rebars in Series S2. Moreover, the effect of stirrup was investigated in S2.

Table 3.3 List of pull-out specimens

Series	S1	S2	
Stirrup diameter (mm)	No	No	6.35
Splitting mode	Single	Side	
Electrical Corrosion time (days)	No-corroded reference		
	3-7-14		

3.3.2.1 Specimens design

Figure 3.6 shows the specimen details. The dimensions of the specimen are 260×260×101.6 mm for S1 Series and 260×170×170 mm for S2 Series. The concrete was cast with the main longitudinal D19 rebar horizontally positioned at the bottom of the framework. A small concrete cover of 28.5 (1.5 Ø) and 38 mm (2 Ø) for S1 and S2, respectively. A short bond length was placed in the central part of the specimen to focus on the local bond behavior. To avoid cone failure during pull-out loading, unbonded parts were set at the loaded and free ends by inserting PVC tubes. Specimens without and with stirrups over the bonded length were prepared. S2 Series includes specimens with two stirrups (D6) with a 50 mm spacing. Figure 3.7 shows an example of frameworks. All specimens were produced in the same sequence and using the same materials to reduce the discrepancy.

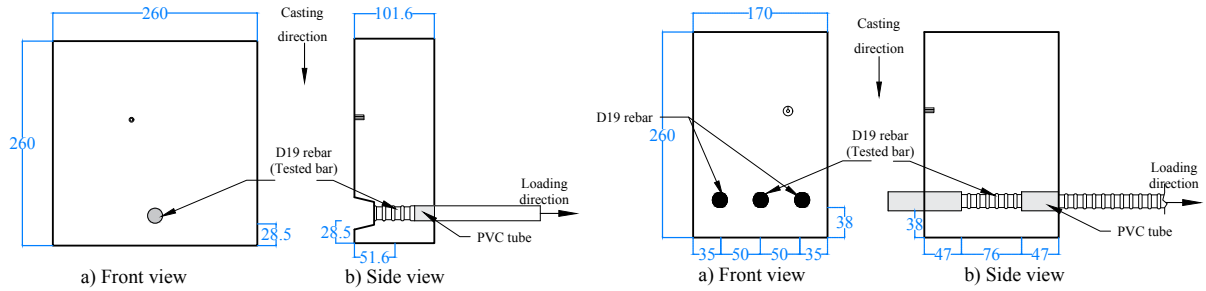

Series S1 Series S2 without stirrup (unit mm)

Figure 3.6 Specimen details

Series S1 Series S2 without stirrup Series S2 with stirrups

Figure 3.7 Framework of specimens

3.3.3 Electrical induced corrosion setup

Figure 3.8 shows the installation for electrical corrosion. The specimen was immersed in a 3% NaCl solution and a direct current was introduced to induce corrosion. One current supply was used for S1 Series. However, the current was separately impressed in the three rebars using three different current supplies in the S2 series. To simulate corrosion reasonably, a constant current intensity of 0.08 A and 0.3 A was applied to S1 Series and S2 Series, respectively. The specimens were divided into three groups according to corrosion time (3, 7, and 14 days for S1 and 4,6 and 14 days for S2). A group includes three corroded specimens and one uncorroded specimen (reference). The current density used in this test was approximately 900μA/cm^2 (a current intensity of 0.08A for D19 rebars), which was greater than the highest corrosion rate obtained in the natural corrosion (100μA/cm^2), as reported by Andrade [103] Although current density has been shown to influence the development of surface crack width [85,104], no definitive findings have been made regarding its influence on crack pattern. As a result, a high current density was used to quickly induce corrosion-related cracks, as reported in earlier studies [105,106].

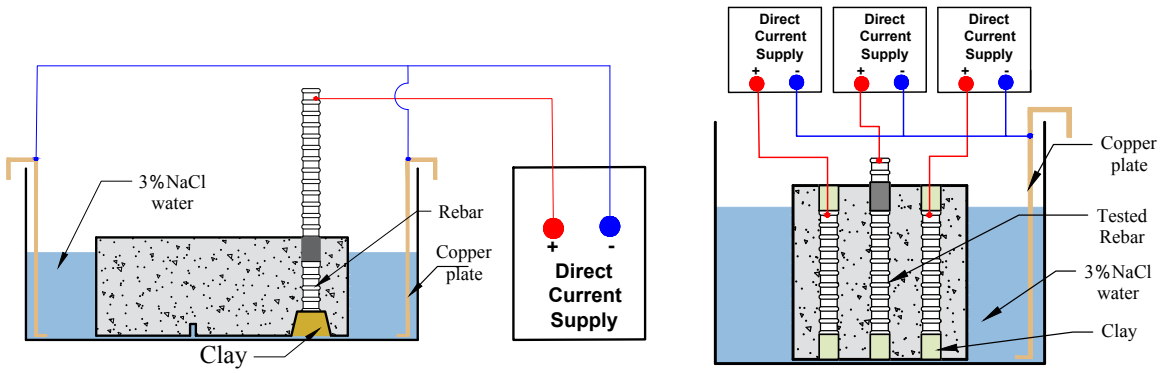

Figure 3.8 Electrical corrosion setup

3.3.4 Loading and measurements

Figure 3.9 shows the test setups for the pull-out test. The specimen was placed on the Teflon sheet to limit friction. Also, not to restrict the lateral deformation of concrete, the loading plate included a hole with a diameter corresponding to the concrete cover. The tested rebar (D19) was subjected to monotonic pull-out loading at a speed of 0.5mm/min, as recommended by ASTM234-91A. Measurement items are pull-out load and slippage at the free end.

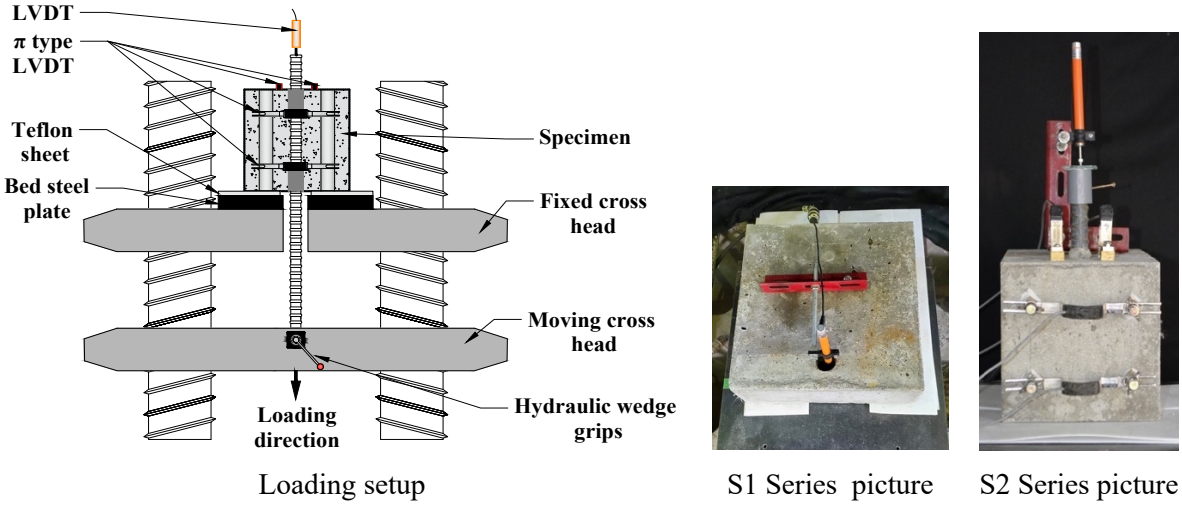

Figure 3.9 Loading and measurement of pull-out test

3.4 Experimental results

Table 3.4 summarizes the experimental results. The specimen ID consists of three sets of characters indicating the Series (S1 or S2), the number of corrosion days (3d, 7d, or 14d), and the specimen number. Moreover, specimen ID in the S2 series includes "NS" and "S" whenever stirrups are provided or not. Specimens ID with "NC" (NC: non-corroded) were immersed in the water without impressing electrical current; therefore, these specimens were not corroded.

Table 3.4 Pull-out results in S1 Series

Specimen ID	Mass loss ratio (%)	At max. load	
		Bond stress (MPa)	Slip (mm)
S1-3d-NC	-	6.14	0.146
S1-7d-NC	-	8.56	0.274
S1-14d-NC	-	6.98	0.128
S1-3d-1	3.85	7.01	0.000
S1-3d-2	4.22	6.11	0.000
S1-3d-3	3.77	6.59	0.106
S1-7d-1	6.54	6.56	0.000
S1-7d-2	6.84	6.88	0.098
S1-7d-3	6.67	8.05	0.012
S1-7d-4	7.19	7.88	0.000
S1-14d-1	11.31	7.24	0.020
S1-14d-2	10.98	6.88	0.006
S1-14d-3	15.27	6.69	0.002
S1-14d-4	13.99	6.33	0.000

Table 3.5 Pull-out results is S2 Series

Specimen ID	Mass loss ratio (%)	Crack width (mm)	At max		Specimen ID	Mass loss ratio. (%)	Crack width (mm)	At max	
			Bond stress (MPa)	Slip (mm)				Bond stress (MPa)	Slip (mm)
S2-NS-NC-1	-	-	11.24	0.346	S2-S-NC-1	-	-	11.87	0.744
S2-NS-NC-2	-	-	11.15	0.564	S2-S-NC-2	-	-	9.83	0.946
S2-NS-NC-3	-	-	9.94	0.674	S2-S-NC-3	-	-	10.72	0.566
S2-NS-2d-1	5.00	0.25	6.86	0.154	S2-S-4d-1	0.68	0.25	10.84	-
S2-NS-2d-2	5.22	0.20	6.47	0.106	S2-S-4d-2	0.56	0.15	13.20	0.700
S2-NS-2d-3	5.83	0.65	6.03	-	S2-S-4d-3	0.72	0.15	10.69	0.704
S2-NS-4d-1	7.17	0.15	6.52	0.304	S2-S-6d-1	0.43	0.2	11.95	0.330
S2-NS-4d-2	9.51	0.20	6.26	0.252	S2-S-6d-2	0.77	0.25	11.06	0.624
S2-NS-4d-3	8.59	0.25	6.28	0.054	S2-S-6d-3	0.77	0.25	9.77	0.316
S2-NS-6d-1	13.18	0.40	5.59	0.468	S2-S-14d-1	9.23	0.35	10.45	0.348
S2-NS-6d-2	9.49	0.20	6.54	0.340	S2-S-14d-2	8.49	0.70	8.62	0.616
S2-NS-6d-3	10.82	0.30	6.84	0.154	S2-S-14d-3	11.08	1.00	7.36	0.596

3.4.1 Corrosion and concrete cracking

After testing, the pulled-out rebar and stirrups were removed. The corroded rebars were cleaned with a hydrochloric acid solution. Then they were cleaned with a wire brush to remove any remaining rust before being weighed to evaluate the mass loss. The mass loss ratio, *c*, was calculated as follows:

$$\boldsymbol{c} = \frac{\boldsymbol{m_0 - m}}{\boldsymbol{m_0}} \times 100 \qquad (3\text{-}1)$$

where c is mass loss ratio, m_0 is the non-corroded rebar weight; m is the weight after rust removal.

3.4.1.1 For S1 series (single rebar)

Figure 3.10 shows an example of the corroded rebar surface and specimen. The mass loss ratio ranged from 3.85% to 15.27 %. Figure 3.10 shows that the rebar corrosion was non-uniform and more severe at the rebar free end. However, the corrosion did not crack the concrete. This is likely because rust did not build up enough hoop pressure to crack the cover when the length of the specimen is small. The rust flowing out at the end of the rebar was observed.

S1-14d-NC S1-14d-3 (15.27) Corroded specimen

Figure 3.10 Example of corroded specimen in S1

3.4.1.2 For S2 series (Three rebars)

Figure 3.11 shows an example of corroded rebars and specimens. The mass loss ratio varied from 5.00 % to 13.18 % in specimens without stirrups and 0.43% to 14.08 % in specimens with stirrups. For the same corrosion time, the specimens without stirrup have higher corrosion levels than specimens with stirrup. The stirrups have a minor concrete cover and are the most vulnerable to corrosion. The corrosion time for S2-S-14d-1, S2-S-14d-2, and S2-S-14d-3 was extended to induce severe corrosion. Side-splitting cracks perpendicular to the rebars was observed in all specimens. Their maximum widths range from 0.15 mm to 0.60 mm and from 0.15 to 1 mm for specimen without stirrup and with stirrup, respectively.

Corroded rebars Corroded specimen Corroded stirrup

Figure 3.11 Example of corroded specimen in S2

3.4.2 Failure mode and bond stress–end slip curves

The specimens have a short bond length, and it is assumed that the bond stress is almost uniform throughout the length. Bond stress is calculated as the pull-out load divided by the surface area

of rebar. Furthermore, the tested bar is assumed to remain in its elastic region due to the small applied pull-out load. Thus, the slip measured at the free end estimated the local slip in the focused bond length. Figure 3.12 and Figure 3.13 shows examples of bond stress–slip relationships for S1 and S2 series, respectively.

For Series S1, the rebar corrosion did not cause cracks that reached the concrete surface. During pull-out testing, all specimens failed due to the splitting of the concrete cover. Corrosion is shown to have caused an increase in initial stiffness and a reduction in slip matching to the peak loads. Generally, the bond strength of the corroded specimen is greater than the reference value. The graphs also show that the concrete failure was very brittle. Once the ultimate strength is reached, stresses decrease significantly, followed by an abrupt increase in slip.

In the S2 series, where corrosion led to concrete cracking-before pull-out loading, specimens failed by concrete splitting due to the widening of existing corrosion-related cracks. Although the bond strengths are lower than those of uncorroded specimens without stirrups, the failure mode by splitting resulted in a similar stress-slip curve.

The influence of stirrup corrosion is clearly shown in Figure 3.13. The bond strengths are mostly not affected by corrosion of around 0.77%, which may be due to the confinement provided by the stirrup. However, when the specimen was severely corroded (S2-S-14d-1, S2-S-14d-2, and S2-S-14d-3), the bond strength was lower than that of the uncorroded specimens.

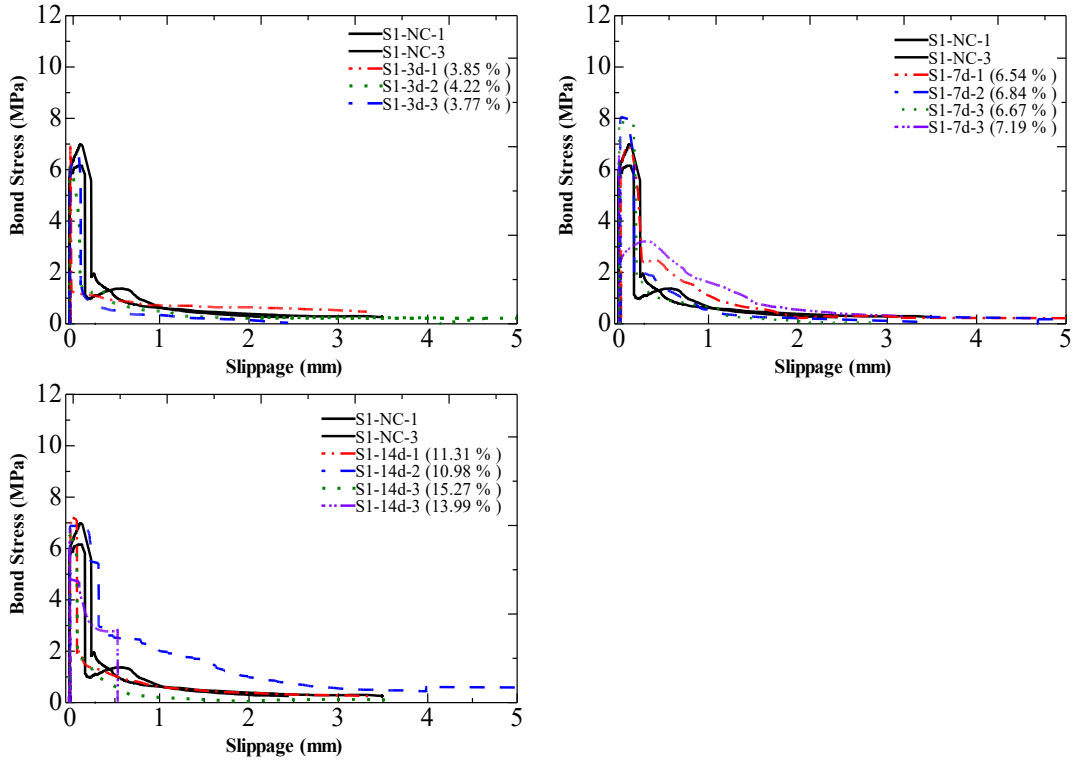

Figure 3.12 Bond stress versus slip curves in S1 Series

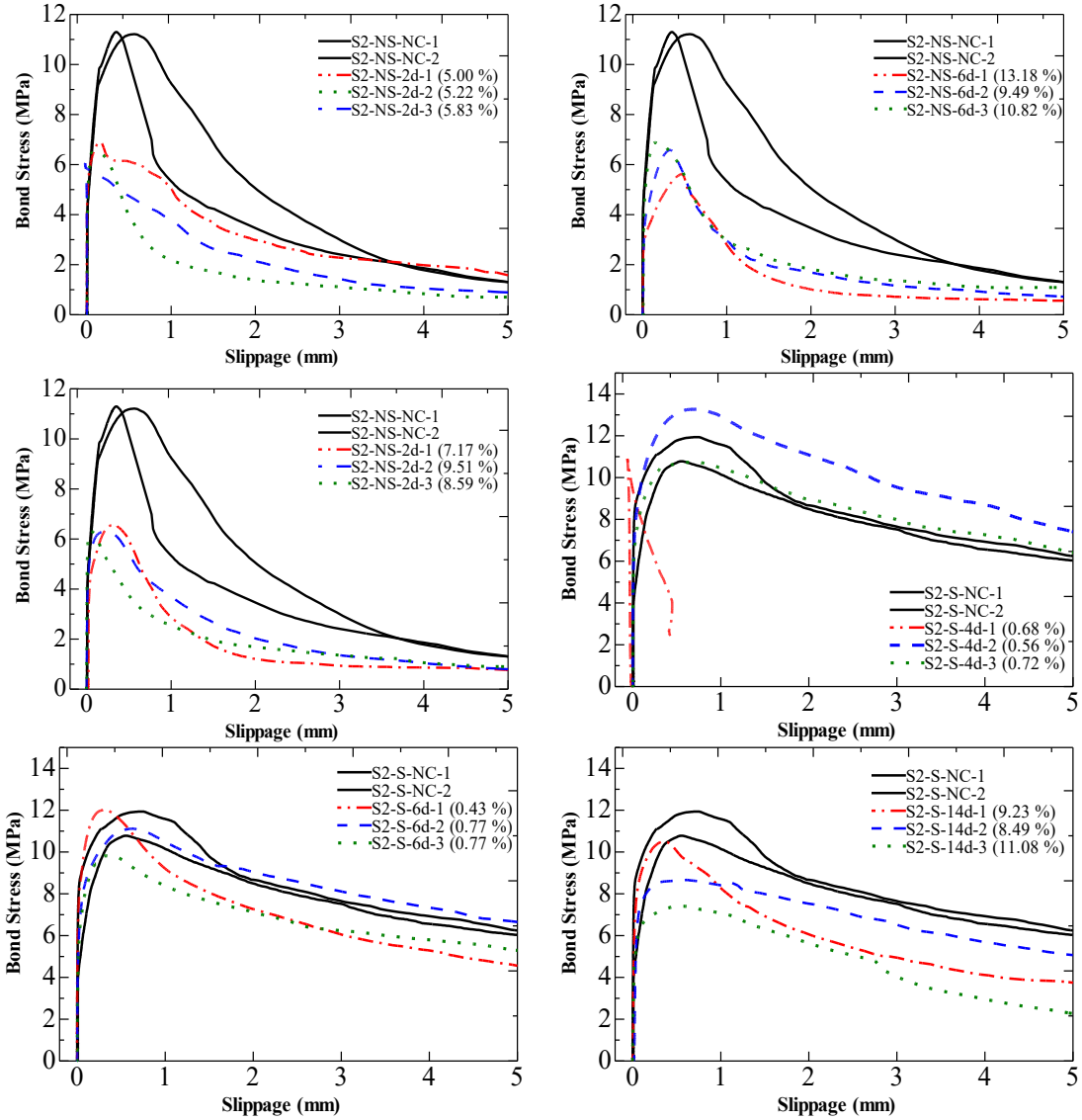

Figure 3.13 Bond stress versus slip curves in S2 Series

3.5 Bond Strength Degradation in Corroded Specimens

The residual bond strength ratio associated with the induced crack width is obtained by normalizing the bond strength of the cracked specimens to that of the uncracked reference specimen. Figure 3.14 and Figure 3.15 shows the relationship between the residual bond strength ratio and the corrosion mass loss or the induced crack width before loading.

3.5.1 Bond strength degradation in S1 series

In the S1 series, the specimens were corroded; however, cracks were not observed prior to loading. Figure 3.14 shows that the residual bond strength ratio is 1.11 to 0.85 for specimens with rebar corrosion mass loss from 3.85% to 15.27 %. The rebar corrosion does not severely affect the residual bond strength when the specimen is not cracked by corrosion. Instead, a

slight increase in bond strength was observed in some corroded specimens. A radial pressure is generated at the rebar-concrete interface by the expansive corrosion product. The corrosion also increases the roughness of the rebar surface. The abovementioned effects increase the friction component, which explains the initial increase in bond strength. Therefore, it can be suggested that corrosion mass loss is not a critical parameter when assessing bond strength degradation in corroded concrete without cracks. We can conclude that corrosion cover cracking did not affect the bond strength.

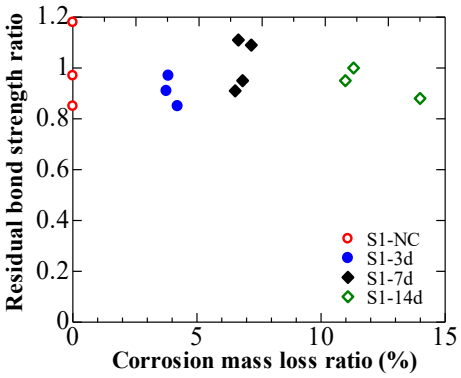

Figure 3.14 Mass loss versus crack width

3.5.2 Bond strength degradation in S2 series

In S2 series, the residual bond strength ratio decreases with the increase in crack width, as shown in Figure 3.15. For specimen without stirrups, the residual bond strength ratios slightly vary from 0.56 to 0.52 for specimens induced cracks widths ranging from 0.15 mm to 0.6 mm. The bond strength was almost constant following the increase of induced cracks width, suggesting that the bond was also strongly affect by the rebar profile change.

For specimens with stirrup, the residual bond strength ratios vary from 1.17 to 0.65 for specimens induced cracks widths ranging from 0.15 mm to 1.00 mm. Furthermore, specimens S2-S-14d-1 (0.35mm), S2-S-14d-2 (0.70 mm), and S2-S-14d-3 (1.00 mm), we voluntarily increased the corrosion time to induce severe damage. We can observe a notable decrease in residual bond strength ratio from 0.92 to 0.65. We conclude that significant bond deterioration begins only when the corrosion of the stirrup is very high. However, some stirrup legs are fractured at the pitting points or almost consumed by uniform corrosion in extreme situations.

A comparison of residual bond strength ratio in specimens without and with a stirrup shows that the bond degradation in specimens without a stirrup is more severe than those with stirrups. (Figure 3.15). Unconfined specimens depend on the surrounding concrete to confine them. Cracked concrete loses its confining stresses, leading to rapid bond strength degradation. In

contrast, stirrups can restrict the widening of the induced crack, increasing the concrete residual confinement and limiting the bond strength deterioration.

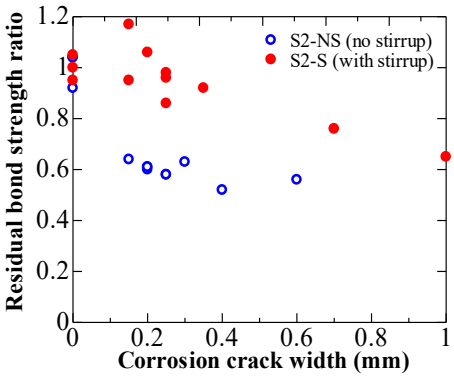

Figure 3.15 Residual bond strength ratio versus crack width

3.6 Summary

Pull-out bond test was conducted on electrically corroded specimens to investigate the bond degradation in corroded concrete. These findings have significant implications for understanding how corrosion affects bond strength. Taken together, these results suggest that:

i. In the S1 series, the specimens were corroded; however, cracks were not observed prior to loading. The residual bond strength ratio is 1.11 to 0.85 for specimens with rebar corrosion mass loss from 3.85% to 15.27 %. The rebar corrosion does not severely affect the residual bond strength when the specimen is not cracked by corrosion.

ii. In S2 series, the residual bond strength ratio decreases with the increase in crack width. The residual bond strength ratios vary from 1.17 to 0.65 for specimens induced cracks widths ranging from 0.15 mm to 1.00 mm in specimen without stirrup. In specimens with stirrup, the residual bond strength ratios vary from 1.17 to 0.65 for specimens induced cracks widths ranging from 0.15 mm to 1.00 mm. This demonstrates that the corrosion-related crack is primarily responsible for bond strength degradation and could be considered the primary variable.

iii. A comparison of residual bond strength ratio in specimens S2 without and with a stirrup shows that the bond degradation in specimens without a stirrup is more severe than those with stirrups. Furthermore, we conclude that significant bond deterioration begins only when the corrosion of the stirrup is very high. However, some stirrup legs are fractured at the pitting points or almost consumed by uniform corrosion in extreme situations.

4 BOND STRENGTH DEGRADATION IN CONCRETE CRACKED BY EXPANSION AGENT FILLED PIPE (EAFP)

4.1 Introduction

In Chapter 3, accelerated corrosion techniques have been adopted to investigate the effect of corrosion on bond strength degradation. Instead of corrosion mass loss, the crack width and pattern induced by corrosion is focused on. However, the results showed that it was challenging to investigate bond loss using electrical corrosion. In electrically corroded specimens corrosion, the corrosion products diffuse randomly in the surrounding concrete around the bar and circulate differently in the internal cracks and the surface crack [107–109]. Therefore, it is difficult to control the crack width and pattern.

Furthermore, corrosion rebar changes the surface properties of the steel, and the rebar shape and cracks the surrounding concrete. This phenomenon altogether affects the bond strength of the corroded specimen. However, the combination of these effects leads to difficulties in analyzing the processes at a fundamental level and negates the overall accuracy of the bond strength degradation prediction. Therefore, a novel method to simulate cracking due to volumetric expansion by expansion agent filled pipe (EAFP) is proposed to overcome the limitation related to electrical corrosion techniques and discretely assess bond deterioration. The alternative approach proposed here focuses on the single effect of crack width on the bond mechanism through interlocking ribs. While ignoring the ambiguity related to corrosion product or rate, the crack width could quantify the exclusive corrosion on bond strength.

The first part of this chapter thoroughly describes the novel method to induce crack and confirms the induced surface and internal crack using various specimens. In the second part, the newly proposed method is used to examine the effect of crack pattern and width on the bond strength degradation. Moreover, the effect of the stirrup on bond loss in the cracked specimen is investigated.

4.2 Cracks Simulated by Expansion Agent Filled Pipe (EAFP)

Most studies on the bond behavior of cracked concrete have used accelerated corrosion techniques. However, these methods often produce inconsistent crack widths and less predictable crack patterns. The bond of rebars in pre-cracked specimens was investigated by Gambarova et al.[110]. The specimens were subjected to transverse tensile stress, cracking the concrete. Thin inserts (e.g., propylene sheet), 3-point bending tests, mechanical expanding cores [105], and controlled splitting experiments [98,111] are all standard methods of introducing cracks in concrete to investigate chloride dispersion. These techniques are not as simple for bond tests and may not accurately reflect cracked concrete.

4.2.1 Principe of crack simulation by EAFP

Expansion agent is also known as a non-explosive demolition agent or soundless cracking demolition agents. It is mainly used to destroy rocks and RC structures. In powder form, it expands when humified. The volumetric expansion is mainly caused by hydration of CaO producing $Ca(OH)_2$ leading to a gradual development of expansive pressures (Figure 4.1) [112].

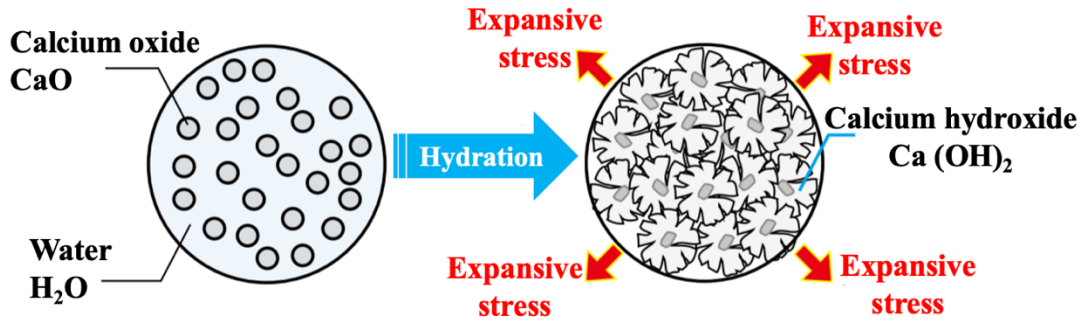

Figure 4.1 Expansion pressure generation [112]

To simulate the expansion of rebars due to corrosion, an aluminum pipe embedded in concrete is filled with an expansion agent. Due to this expansion, cracks are generated in the concrete, as illustrated in Figure 4.2. The mechanism of crack formation is similar to that caused by the rebar's expansion due to corrosion.

EAFP allows one to focus on the effect of the cracking itself while ignoring the other effect of corrosion (section loss or rust around the rebar). It is also beneficial in quickly controlling the cracks (width and position). The following subsections highlight this method.

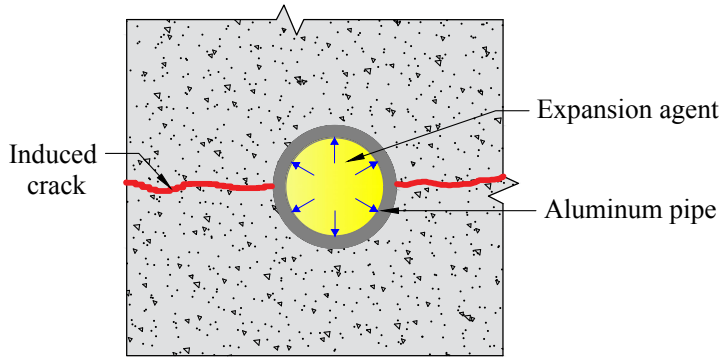

Figure 4.2 Concrete cracking with an EAFP

4.2.2 Specimen for cracking simulation

Figure 4.3 shows the specimens used to test the cracking by EAFP. Its dimensions were 150 mm x 150mm x 400mm. An aluminum pipe with an 18 mm as outer diameter and 1 mm thickness was embedded in the concrete. The crack width was measured with π-type displacement transducers placed in three positions on the specimen. Table 4.1 shows the list of specimens. The concrete cover size was set as the main parameter. The six specimens were divided into two groups with different concrete covers (15 and 20mm).

Table 4.1 List of specimens

No.	Specimen	Common factors	Concrete cover *C* (mm)
1	S-15	Pipe thickness 1mm Pipe diameter 18 mm Water to expansion agent ratio W/B=30% Concrete strength 25.3 MPa	15
2			
3			
4	S-20		20
5			
6			

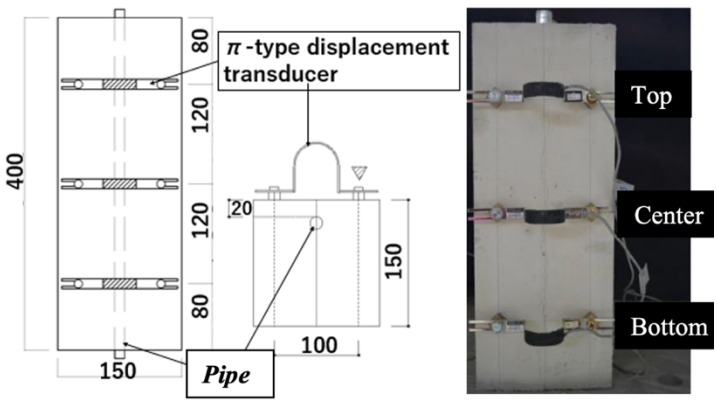

(Unit: mm)

Figure 4.3 Specimen for cracking confirmation (S-20)

4.2.3 Confirmation of cracking simulation

Figure 4.4 exhibits cracks the cover side of the specimen along the EAFP. Table 4.2 shows the average and maximum crack width after 250 hours. Figure 4.5 shows examples of the relationship between the crack width and elapsed time. In all specimens, the crack width increased over time. The induced crack appeared slightly higher in the 20mm concrete cover. Lin et al. [75] observed the same trend using a high current density (600μA/cm^2) to accelerate corrosion. However, given the shallow depths and the slight difference, cover depth might not be the main factor governing the surface crack width.

In this research, the elapsed time and crack width relationship shown in Figure 4.5 is used as a reference to simulate specific crack width.

Table 4.2 Crack width after 250 hours

No	Specimen	Average crack width (mm)	Maximum crack width (mm)
1	S-15-1	0.43	0.50
2	S-15-2	0.43	0.50
3	S-15-3	0.52	0.60
4	S-20-1	0.48	0.55
5	S-20-2	0.52	0.65
6	S-20-3	0.45	0.55

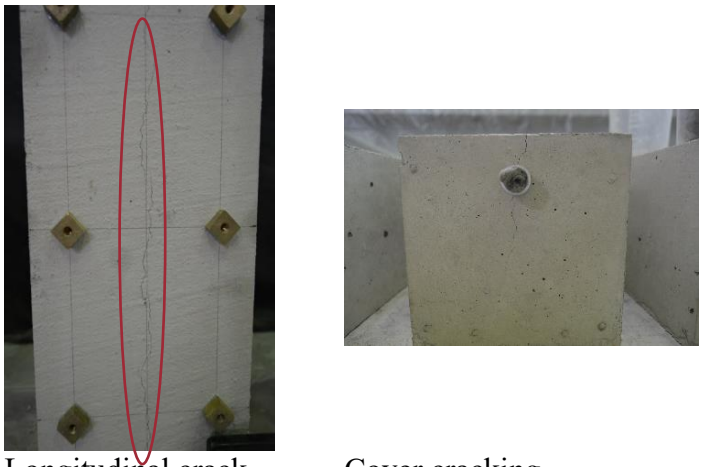

Longitudinal crack Cover cracking

Figure 4.4 Crack after 250 hours (S-20-2)

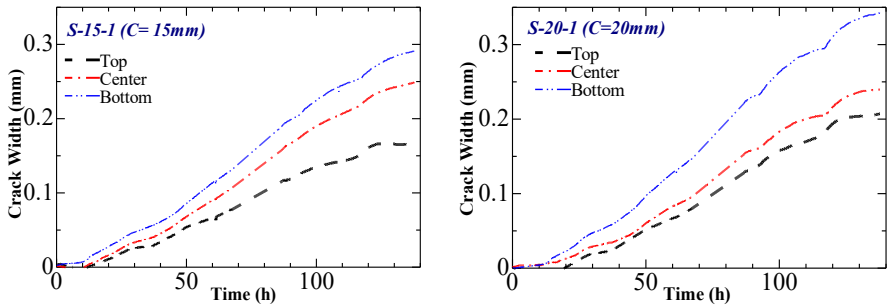

Figure 4.5 Crack width over elapsed time

4.3 Cracking Induced by EAFP in RC Beam

4.3.1 Beam specimen for cracking simulation by EAFP

Researchers commonly conduct structural tests of beams, columns, or slabs to assess the deterioration of RC structures. They designed the size of their tested structural elements according to their objective. Thus, it will be useful to observe the development of cracks induced by EAFP in RC beam. To achieve this, four RC beam specimens with different length are prepared to investigate the surface and internal cracking due to EAFP. EAFPs replaced the main rebars at the corner of the beam. Figure 4.6 shows a specimen with a 220 mm x 420 mm cross-section. The specimen length was 840 mm (short beam) and 1260 mm (long beam). Aluminum pipes with an outer diameter of 22 mm and a thickness of 1 mm were placed at the four corners of the beam. Two deformed reinforcing bars, D19, were placed at the top and bottom of the cross-section. Both specimen (short and long) were reinforced with D10@60 stirrups at their ends. The specimen framework is shown in Figure 4.7.

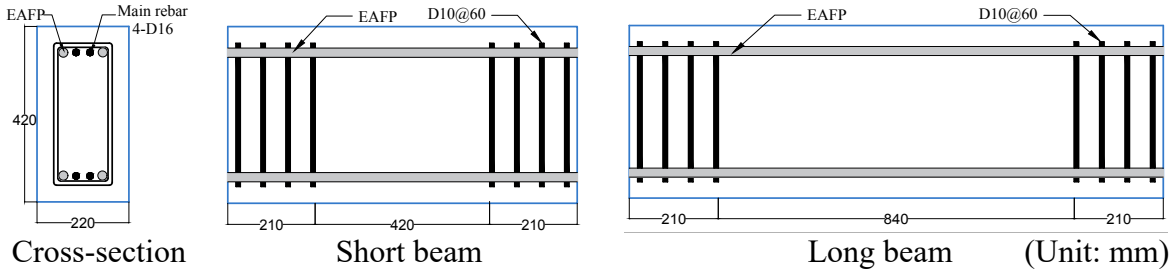

Figure 4.6 Detail of specimen

Figure 4.7 Short beam framework

4.3.2 Expansion agent filling and crack monitoring

The RC beam was vertically raised, and an expansion agent mixed with 30% water was filled into the aluminum pipe. Two beams (one short and one long) were used to observe the evolution of surface crack width. π-type displacement transducers were fixed on the beam to measure the induced cracks' widths accurately. The other two beams were cut transversely to observe the internal crack pattern. Before cutting the beam, the surface cracks were measured using a crack scale.

4.3.3 Result of cracking induced by EAFP

4.3.3.1 surface cracking

Figure 4.8 shows the pattern of surface crack induced by EAFPs. Hours after filling, longitudinal cracks parallel to the reinforcement bars were measured and recorded, as shown in Figure 4.8. The longitudinal cracks are marked in blue, and the maximum crack widths of the picture are measured in each section.

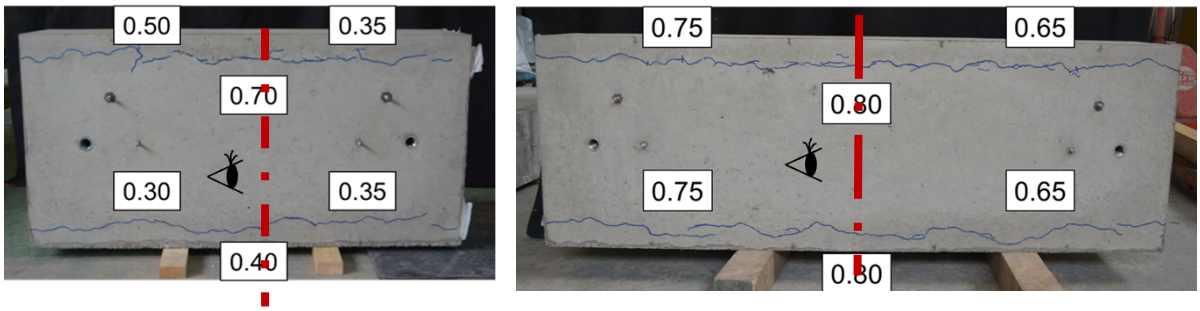

Short beam Long beam (Unit: mm)

Figure 4.8 Surface crack induced by EAFP

Figure 4.9 shows the relationship between the width of the surface crack, the time elapsed after filling the expansion agent (to 300 hours), and the ambient temperature. It plots the average surface crack width measured by two π-type displacement transducers attached along the same rebar. The crack width before filling the agent (sinking cracks) are added to the measured widths. Temperature with a 10-hour interval was acquired from the Automated Meteorological Data Acquisition System (AMeDAS) in Tsukuba.

From Figure 4.9, the crack width tends to increase rapidly from the expansion agent filling to approximately 50 hours. Considering the casting direction, it can be seen that the width of the crack at the top is smaller than that at the bottom of the beam. It seems possible that these results are due to the change in the transmission of EAFP expansion due to the presence of voids during

the cure of the concrete. Additionally, the specimen length and the temperature did not significantly influence the cracking process.

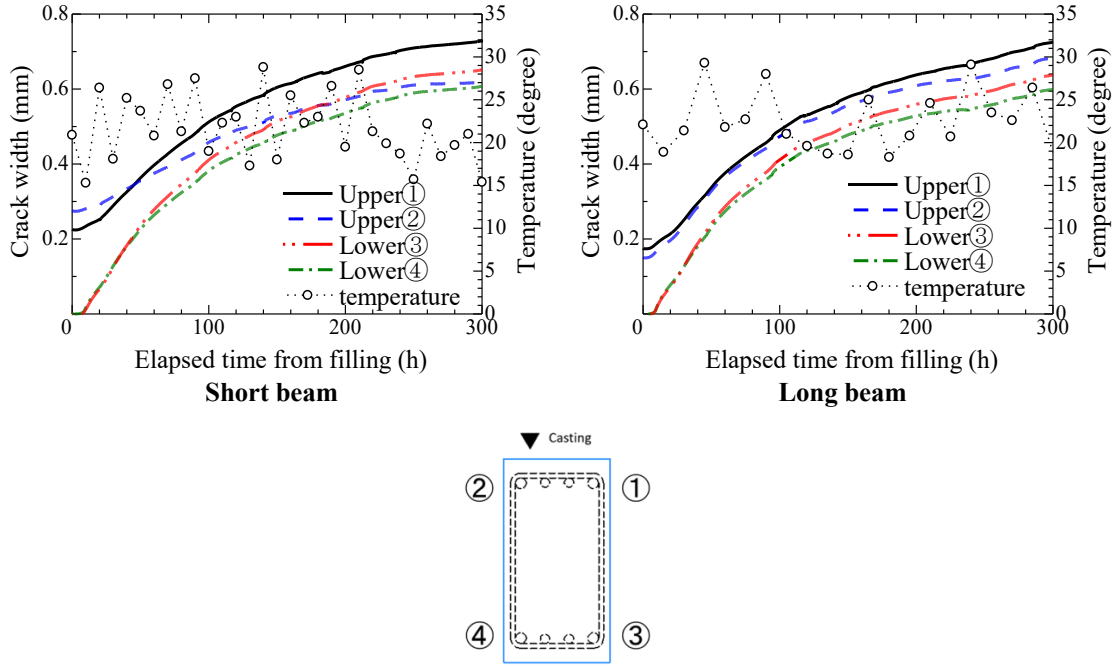

Figure 4.9 Crack width and elapsed time relationship

4.3.3.2 Internal cracking

After measuring the surface crack width (Figure 4.8), the specimens were half-cut to observe internal cracking, as shown in Figure 4.10. EAFP also induces internal cracks in the specimens. In the short beam, side-splitting cracks developed at the top and bottom of the beam ends. In the long beam, side-split-type cracks occurred in the upper part, and corner-splitting cracks occurred in the bottom of the beam. Therefore, we can assume that EAFP mainly induces a side-splitting crack inside the RC beam through this thesis.

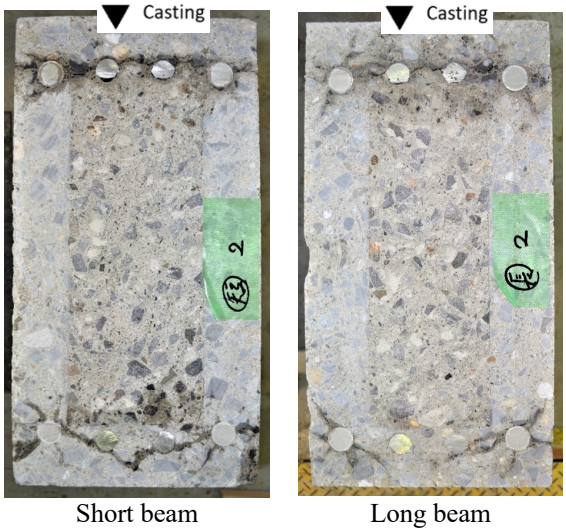

Short beam Long beam

Figure 4.10 EAFP crack pattern observation

4.4 Effect of Cracking Pattern on Bond Strength Degradation

This section investigates the influence of crack patterns on bond degradation due to induced cracks. In Chapter 3, this effect was unclear because the cracking pattern was not easy to control using electrical corrosion. Additionally, the change in corroded rebar and induced cracks affected the bond strength. Therefore, it is challenging to analyze the degradation at a fundamental level. To address these limitations, the crack is induced using the EAFP technique introduced earlier.

4.4.1 Pull-out experimental program

4.4.1.1 Specimen outline

Table 4.3 shows the specimen list. A total of 27 specimens were used in series S1 and S2. The specimens are identical to the ones used to investigate the bond strength degradation in electrically corroded specimens (Chapter 2). The parameters are the induced crack width and crack pattern (single or side-splitting). Moreover, the effect of the stirrup is investigated in Series S2. To better observe the deterioration of the bond, the main parameter is the induced crack width.

Figure 4.11 shows the specimen detail. The specimens in series S1 are designed to incorporate single-splitting cracks due to bar expansion. In those specimens, the crack induced by a ribbed EAFP is located at the cover side along the rebar. The pull-out bar is the ribbed EAFP. On the other hand, S2 specimens include side split cracks on the surrounding concrete toward the side surface. The induced cracks are simulated by two EAFPs located around the D19 rebar. Here, the effect of the stirrup was also investigated. The pull-out bar is the D19 steel rebar. The specimen framework is also shown in Figure 4.12.

The compressive and splitting tensile strengths at the age of the pull-out test were, on average, 24.2 MPa and 2.17 MPa, respectively.

Table 4.3 List of pull-out specimens

Series	S1	S2	
Splitting mode	Single	Side	
Stirrup diameter (mm)	No	No	8
Induced crack range (mm)	No-cracked reference		
	0.08 to 0.85		
Tested rebar	EAFP with ribs	D19 rebar	

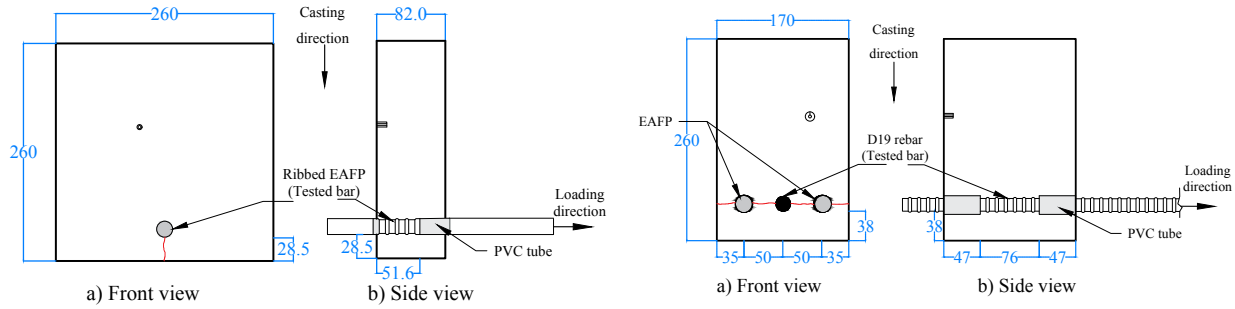

Figure 4.11 Specimen detail

Figure 4.12 Framework of specimens

Figure 4.13 shows an overview of a machined aluminum pipe with ribs geometry set according to JIS G 3112. An aluminum pipe with a 21.7 mm as outer diameter and 2.5 mm thickness was used to mimic the D19 rebar.

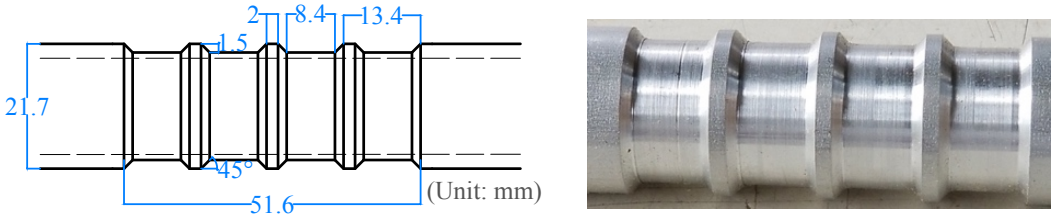

Figure 4.13 Aluminum pipe with ribs

4.4.1.2 Crack simulation by EAFP

The ratio of the water to an expansion agent was set to 30%. The specimen was placed to set the axis of the pipe vertically. In Figure 4.14, the expansion agent was filled from the top of the

pipe. Crack width increases over the time that has elapsed after filling. Thus, this time is controlled to obtain the target crack width.

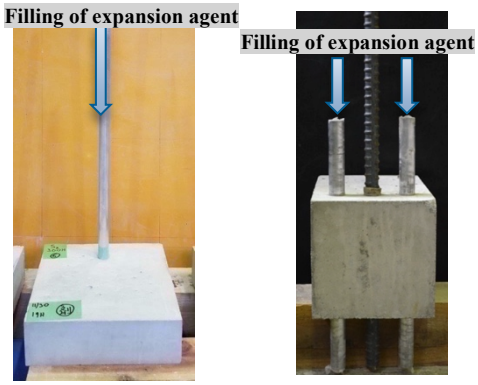

S1 S2

Figure 4.14 Crack simulation with an EAFP

4.4.1.3 Loading and measurement method

The cracks induced by EAFP were sketched, and their widths were measured. The specimens were then subjected to monotonic pull-out loading with a universal testing machine (section 3.3.4).

4.4.2 Results of experiments

All experimental results are summarized in Table 4.4. Specimens S2-NS-NC were subjected to pull-out loading without filling the expansion agent. Thus, there was no induced crack by EAFP in these specimens.

Table 4.4 Result list of S1 specimens

Specimen ID	Induced crack width (mm)	At Maximum	
		Bond stress (MPa)	Slippage (mm)
S1-C-0.10	0.10	2.71	0.146
S1-C-0.15	0.15	2.58	0.088
S1-C-0.20	0.20	2.25	0.218
S1-C-0.35	0.35	1.87	0.144
S1-C-0.50	0.50	1.98	0.198
S1-C-1.5	1.50	1.33	0.262
S1-C-1.80	1.80	1.52	0.658
S1-C-2.00	2.00	1.27	0.768
S1-C-2.00	2.00	1.22	0.572
S1-C-2.60	2.60	0.74	1.380
S1-C-3.00	3.00	0.69	0.804

Table 4.5 Result list of S2 specimens

Specimen ID	Induced crack width (mm)	At Maximum		Specimen ID	Induced crack width (mm)	At Maximum	
		Bond stress (MPa)	Slip (mm)			Bond stress (MPa)	Slip (mm)
S2-NS-NC	-	10.68	0.902	S2-S-NC	0	11.16	0.946
S2-NS-0.15	0.15	8.81	0.586	S2-S-0.15	0.15	9.46	1.090
S2-NS-0.20	0.20	6.27	0.6	S2-S-0.20	0.20	7.93	2.092
S2-NS-0.25	0.25	7.43	0.43	S2-S-0.20	0.20	9.01	1.034
S2-NS-0.30	0.30	6.21	0.464	S2-S-0.25	0.25	7.94	1.562
S2-NS-0.35	0.35	7.29	0.562	S2-S-0.30	0.30	8.82	1.946
S2-NS-0.40	0.40	6.94	0.684	S2-S-0.35	0.35	8.70	1.706
S2-NS-0.50	0.50	4.97	0.656	S2-S-0.35	0.35	7.82	1.340
S2-NS-0.60	0.60	4.43	0.692	S2-S-0.40	0.40	9.41	-
S2-NS-0.85	0.85	2.70	1.118	S2-S-0.40	0.40	9.55	1.886
S2-NS-0.95	0.95	3.69	1.040	S2-S-0.50	0.50	7.84	1.366
				S2-S-0.50[1]	0.50	7.10	1.888
				S2-S-0.50[2]	0.50	8.31	1.690
				S2-S-0.60	0.60	8.16	1.684
				S2-S-0.70	0.70	7.36	1.298

4.4.2.1 Crack simulation by EAFP

Figure 4.15 and 4.16 shows examples of crack patterns after filling the expansion agent. The maximum crack width before pull-out loading in every specimen can be seen in Table 4.4.

Figure 4.15 Crack induced by EAFP in S1 specimens

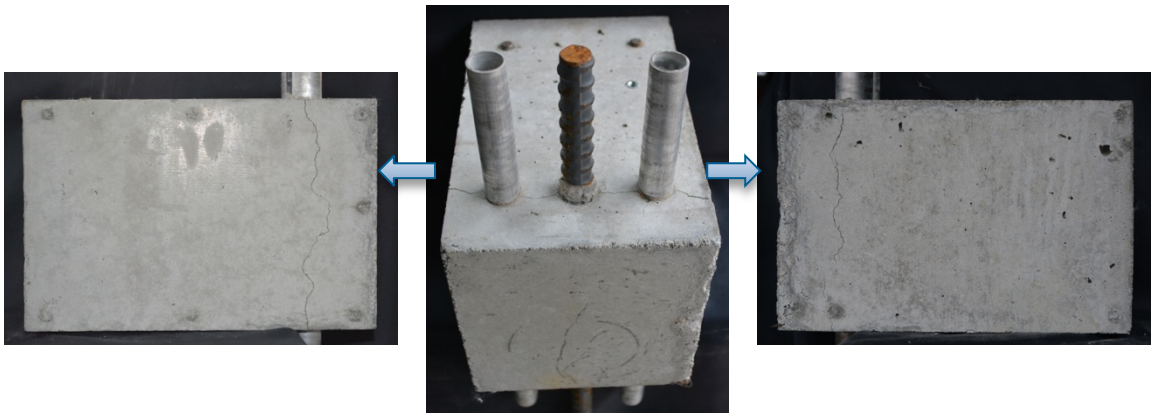

Figure 4.16 Crack induced by EAFP in S2 specimens

4.4.2.2 Failure mode

All specimens experienced failure due to splitting. A group failed due to a newly generated splitting crack, and others due to the widening of the crack induced by EAFP. In the S1 series, some specimens presented new side cracks. On the others hand, S2 specimens without induced cracks failed by single splitting showing cracks toward the cover side, showing that induced crack can switch the failure mode from single to side-splitting. Furthermore, a small crack width (0.15mm, 0.25mm) even leads to a single split in the S2 specimen without stirrup. This may be explained by the fact that concrete does not lose all of its strength at once in cracking, and some ability to transmit stresses across cracks is retained. However, load drop is smoother with the increased slip in specimens with stirrup. This can be simply explained by the fact that the stirrup restrained the development of cracks, leading to a ductile failure.

4.4.2.3 Pull-out load and slippage

Figure 4.17 and 4.18 shows the bond stress and slippage relationship. In S1 series, specimens with crack widths from 0.1 to 1 mm indicated almost linear relationships between load and slip up to the maximum load. After that, the load rapidly drops and continues to show increasing slip at decreasing loads. The sudden drop in the load-slip curve at the maximum load is likely related to the sudden splitting of the concrete cover over the bar. Additionally, no significant correlation was found between slip at maximum load and induced crack width. Further, when the crack width is higher than 2 mm, the stiffness is negatively affected by the induced crack width. Before the observation of failure, significant slip occurred at maximum load. Furthermore, the maximum load slightly varies, ranging from 1.33 MPa to 1.22 MPa for crack width between 1.5 mm and 2 mm, respectively. These observations were also reported by

Cabrera et al. [70]. In a wide induced crack, the bearing action between the rebar rib and concrete is deteriorated by reducing the confinement from surrounding concrete.

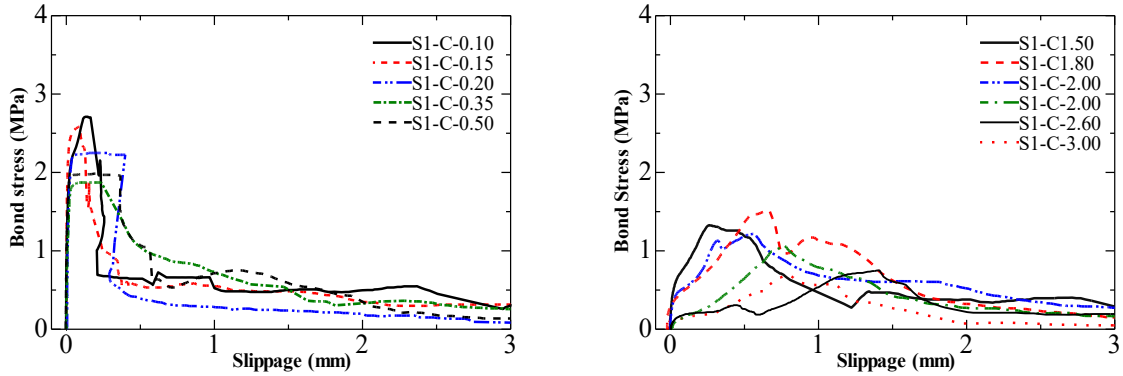

Figure 4.17 Bond stress versus slip curves in S1 Series

The maximum load decreases to 90% following the increase in crack widths in S2. In contrast, the corresponding slip at maximum load shows a similar decreasing tendency. At the same applied load, a higher load and less slip were obtained for specimens with stirrups compared to specimens without stirrups. Moreover, specimen with stirrup has a stiffer response and shows ductile behavior than stirrup without stirrup.

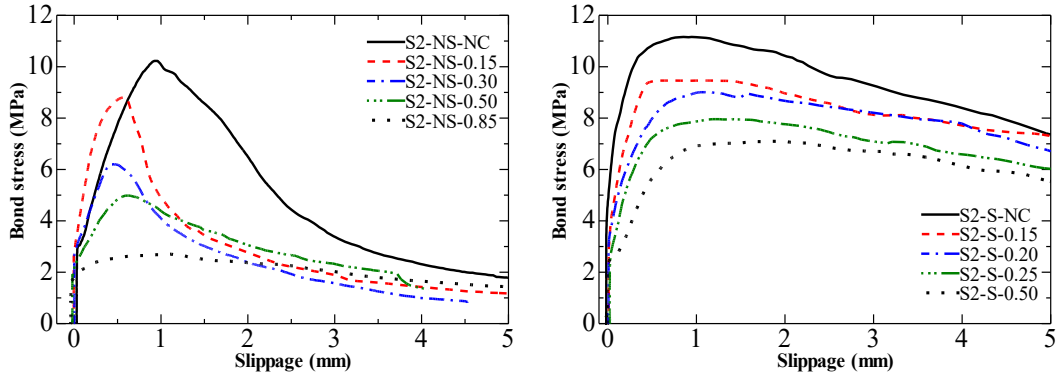

Specimen without stirrup Specimen with stirrups

Figure 4.18 Bond stress versus slip curves in S2 Series

4.4.3 Bond strength degradation and surface crack width relationship

In this section, the residual bond strength ratio, defined as the ratio of the bond strength of a cracked specimen to that of the uncracked specimen, is evaluated to discuss the bond degradation. In S1, for uncracked concrete, the specimen failed by rupturing the aluminum pipe before pulling it out. Consequently, the bond strength of these specimens could not be obtained. Therefore, the following equation, as reported in the previous study [113], is used to calculate the pull-out splitting strength of uncracked specimen:

$$\tau_{b,max} = 0.601 \cdot \sigma_t \cdot \frac{r_u}{d_b} \cdot \cot\alpha \quad (4\text{-}1)$$

Where, $\tau_{b,max}$: bond splitting strength, σ_t: splitting tensile strength of concrete, $\frac{r_u}{d_b} = \frac{C+d_b}{2}$, d_b: diameter of the pipe (19mm), C: the thickness of cover concrete, α: the angle between the longitudinal axis and splitting force (=34 degrees).

Figure 4.19 displays the relationships between residual bond strength ratio and crack width. The data were fitted using an exponential function. The regression curves are also shown in Figure 4.19. As expected, the bond deterioration strongly correlates with the induced crack width before loading. In both series, the bond strength decreases with the increased induced crack by EAFP.

In Series S2, the bond strength degradation of the specimen without a stirrup appears to be more severe than that of specimen with stirrup. This is due to the crucial role of the stirrup in providing additional confinement. First, the stirrups can effectively limit crack propagation due to EAFP. Furthermore, stirrups help to maintain the bearing between the steel bar and the concrete. However, the bond degradation is not significant because of a big diameter of stirrup, leading to a fully confined specimen. There is a possibility that the deterioration of confinement due to corrosion exists between the unconfined and confined specimens. Therefore, a systematic understanding of how the reduction in confinement provided by the stirrup contributes to bond deterioration is needed to build a formula for predicting bond degradation.

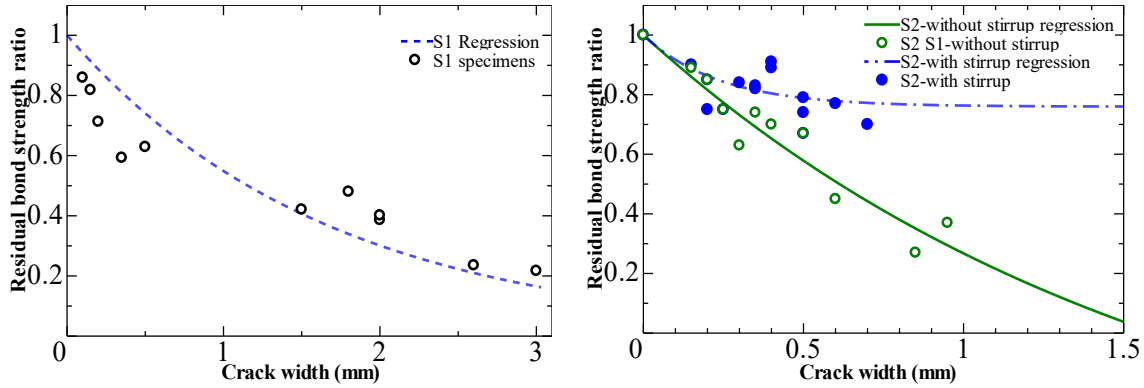

Figure 4.19 Residual bond strength ratio and crack width

4.4.3.1 Effect of crack pattern on bond degradation

Figure 4.20 compares the two prediction formulas. In the range of 0.15 mm to 1 mm crack width, the formula gives a residual bond strength ratio from 0.91 to 0.54 for single-splitting specimens. However, the side-splitting specimens severely deteriorate with a residual bond

strength ratio ranging from 0.73 to 0.12 in the same considered crack width range. Moreover, when the crack width reaches 1.5 mm, the side-splitting specimens (S2) have a residual bond strength ratio close to zero when it remains around 0.30 for single-splitting specimens. The deterioration of the bond strength is more severe in side-splitting specimens (S2) than in single-splitting specimens (S1). This result can confirm the fundamental influence of the type of splitting in reducing the bond strength. This may be explained by the fact that the wedging action of ribs causes circumferential tensile stresses in the concrete surrounding the bar and tends to split the concrete along the weakest plane. The position of cracks in S2 specimens seems to create a weaker side-splitting plane than the single-splitting one.

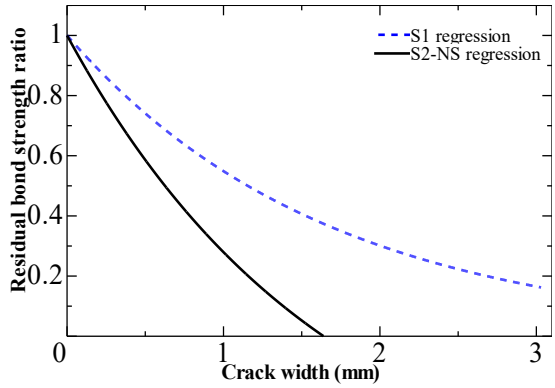

Figure 4.20 Comparison of residual bond strength ratio of S1 and S2

4.5 Summary

This chapter provides insight into the role of crack width on the bond strength between concrete and corroded rebar. A novel method to induce cracking due to the expansion of rebar is proposed. An experimental test program was conducted to investigate the effect of crack pattern and width on bond degradation. Moreover, the importance of stirrup was investigated. The results of the tests indicated that:

i. EAFP was adopted to simulate cracks due to the rebar expansion related to corrosion in RC beams. In this technique is easier to target crack width because the induced crack width increases over elapsed time from filling the aluminum pipe with an expansion agent. Furthermore, the transversal cut of the cracked RC beams shows that internal side-splitting crack pattern mainly occur.

ii. Using EAFP, two series of cracked bond test specimen considering the induced cracks pattern (single or side crack) were tested. It was seen the bond strength exponentially decrease with the increase of induced crack width in both type of specimens. We concluded that cracking without rust fundamentally causes bond strength degradation

in specimen with corrosion related cracks. Additionally, the bond strength degradation is more severe in specimens with a side-splitting crack than with a single-splitting crack.

iii. In Series S2, the bond strength degradation of the specimen without stirrup appears to be more severe than that of specimen with stirrup. This is due to the crucial role of the stirrup in providing additional confinement. First, the stirrups can effectively limit crack propagation due to EAFP. Furthermore, stirrups help to maintain the bearing between the steel bar and the concrete. However, the bond strength degradation is not significant because of a big diameter of stirrup, leading to a fully confined specimen. A systematic understanding of how the reduction in confinement provided by the stirrup contributes to bond deterioration is needed to build a formula for predicting this degradation.

5 BOND STRENGTH PREDICTION IN CONCRETE CRACKED BY EAFP SIMULATING REBAR CORROSION

5.1 Introduction

In Chapter 4, a novel method to simulate cracking due to volumetric expansion using expansion agent filled pipe (EAFP) has been proposed to overcome limitations related to electrical induced corrosion techniques and discretely assess bond strength deterioration. It consists of inserting an aluminum pipe into the concrete and then filling it with an expansion agent to simulate the volumetric expansion of the bar due to corrosion. EAFP is particularly useful for controlling the width and location of the induced crack. In pull-out specimens cracked by EAFP, the single influence of the induced crack width on the bond strength can be observed. This alternative approach is based on the previous findings demonstrating that the bond mechanism through interlocking ribs predominates over friction, even in the case of corroded rebar. In addition, it is assumed that a direct relationship between interlock reduction and crack width excludes the ambiguity related to corrosion product accumulation.

An adequate amount of stirrup can retain the bond action even in cracked concrete [114]. However, stirrups often have a minor concrete cover and are the most vulnerable to corrosion resulting the confinement degradation. Figure 5.1 (data from [115,116]) shows the linear relationship (six times) of the corrosion level between the stirrup and the main rebar. Results in Chapter 3 confirmed that considerable bond strength degradation occurs only when stirrup corrosion is exceptionally high. However, it is challenging to investigate the combined effect of the corroded main bar and stirrup using the electrical corrosion technique.

Furthermore, the pull-out tests on "fully confined" or unconfined concrete cracked by EAFP were conducted to investigate the stirrup effect on cracked concrete in Chapter 4. However, the result shows that the deterioration of the confinement is likely to exist somewhere between. A systematic understanding of how the reduction in confinement provided by the stirrup contributes to bond strength deterioration is still lacking.

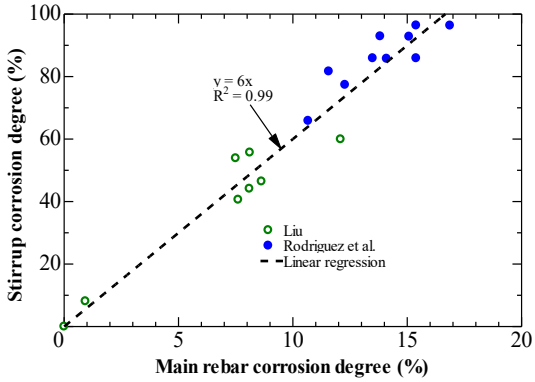

Figure 5.1 Corrosion of main rebar versus stirrup

The discussion above indicated that induced crack width and stirrup diameter reduction due to corrosion are essential parameters for evaluating bond strength deterioration. Therefore, this Chapter aims to propose an empirical prediction for bond strength degradation in cracked concrete. The combined effects of concrete cracking and cross-sectional reduction of stirrups on bond strength are considered. EAFP is adopted to simulate concrete cracking and focus on induced cracks without rust accumulation or change in rebar profile. In addition, rebars with different diameters are used as stirrups to illustrate the reduction in rebar cross-section due to corrosion.

5.2 Experimental Program Outline

5.2.1 Used materials

The compressive and splitting tensile strengths at the age of pull-out test were, on average, 24.2 MPa and 2.17 MPa, respectively.

Figure 5.2 shows the rebar used in this study. The main tested rebar is a deformed bar (D19) with a nominal diameter of 19.1 mm, according to JIS G 3112. The rib height and spacing are 1.2 mm and 13.4 mm, respectively. Stirrups are D3, D4 or D6 rebars with a diameter of 3.13, 4.23 and 6.35 mm, respectively. Tensile tests under JIS Z 2241 were performed on three representative specimens of each type of rebar, and the average results are summarized in Table 5.1. Figure 5.3 shows the stress-strain relationship of the steel rebar.

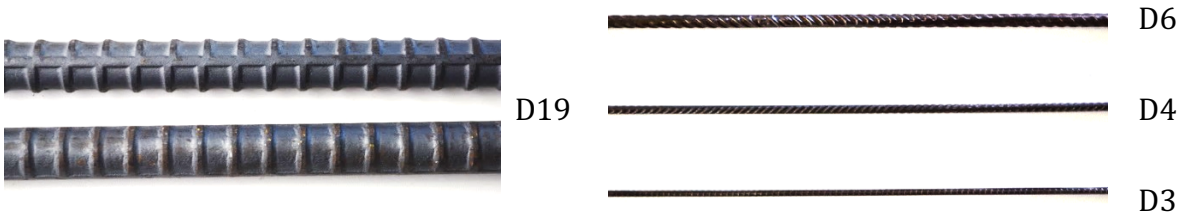

Figure 5.2 Used steel rebar

Table 5.1 Mechanical properties of rebar

Designation by JIS G 3112	Nominal diameter (mm)	Yield strength (MPa)	Tensile strength (MPa)	Elastic modulus (GPa)
D3	3.13	323	458	207
D4	4.23	402*	517	191
D6	6.35	456*	554	201
D19	19.1	366	535	195

*0.2% offset strength

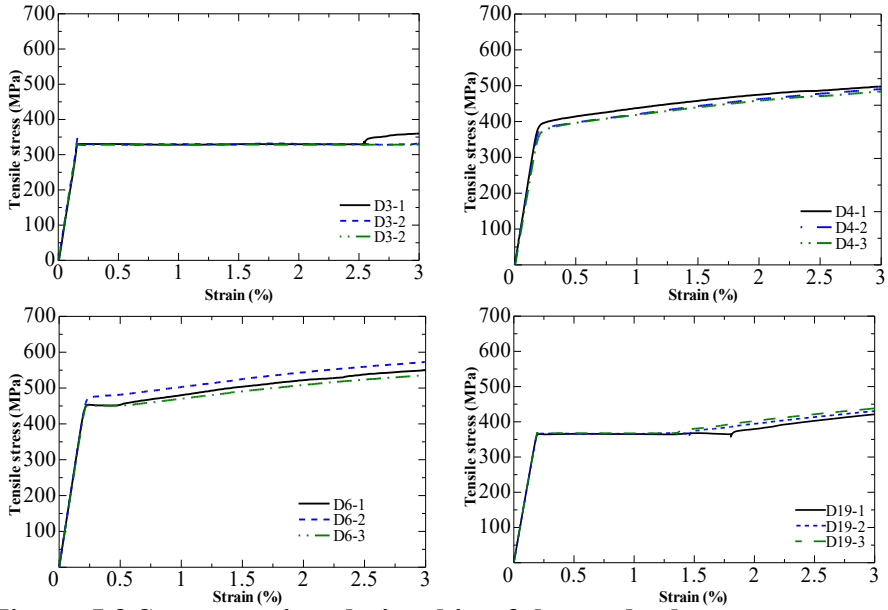

Figure 5.3 Stress-strain relationship of the steel rebar

5.2.2 Test specimens and crack simulation

5.2.2.1 Test specimens

This study performed pull-out tests to investigate the bond strength degradation in concrete specimens with side-splitting cracks. Induced crack width and stirrup ratio were included as main parameters. However, many factors affect bond performance, including bar diameter, cover depth, and concrete strength [117]. These factors were kept constant to focus on induced cracks and stirrups. Table 5.2 summarizes the details of the experimental program. The

specimens were divided into four series with respect to the diameter of the stirrup: no stirrup in Series S0, rebar D3 in Series S1, rebar D4 in Series S2, and rebar D6 in Series S3. In this study, the EAFP method is adopted to simulate concrete cracking. Eq. (5-1). was used to calculate the stirrup ratio.

$$p_w = \frac{a_w}{b \cdot \mathrm{s}} \tag{5-1}$$

Where p_w : stirrup ratio, a_w : stirrup legs cross-sectional area, b: specimen width, and s: stirrup spacing.

Table 5.2 List of pull-out specimens

Series	**S0**	**S1**	**S2**	**S3**
Induced crack width (mm)	No crack			
	0.10 to 1.2			
Confinement level	Unconfined	Poor	Moderate	Good
Stirrup diameter (mm)	No	3.13	4.23	6.35
Stirrup ratio (%)	0	0.18	0.33	0.75

5.2.2.2 Specimens design

Figure 5.4 shows the specimen details. The concrete was cast with the main longitudinal D19 rebar horizontally positioned at the bottom of the framework. A small concrete cover of 38 mm, twice the diameter of the tested rebar, was used. To focus on the local bond behavior, the bonded length was four times the diameter of the tested bar (76 mm). It was placed in the central part of the specimen. To avoid cone failure during pull-out loading, 47 mm unbonded parts were set at the loaded and free ends by inserting PVC tubes. Specimens without and with stirrups over the bonded length were prepared. Different specimens had two stirrups (D3, D4, or D6) with a 50 mm spacing. Two EAFPs parallel to the tested rebar were placed to simulate concrete cracking. Figure 5.5 shows an example of a framework. All specimens were produced in the same sequence and using the same materials to reduce the discrepancy.

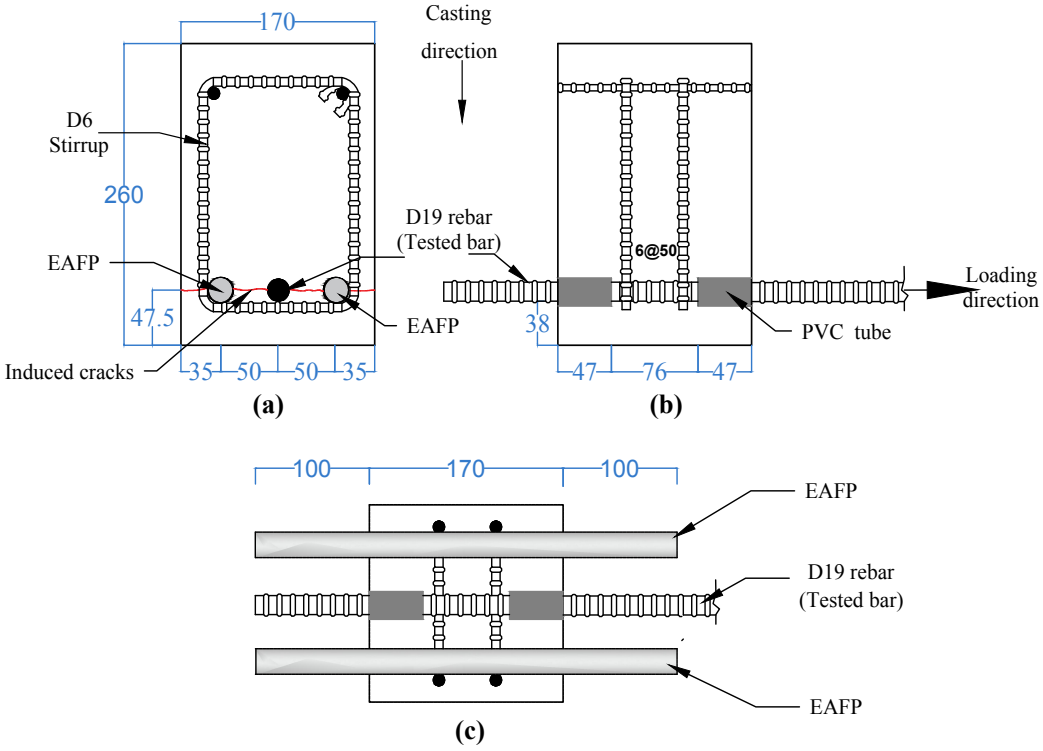

Figure 5.4 Specimen details (Series S3)

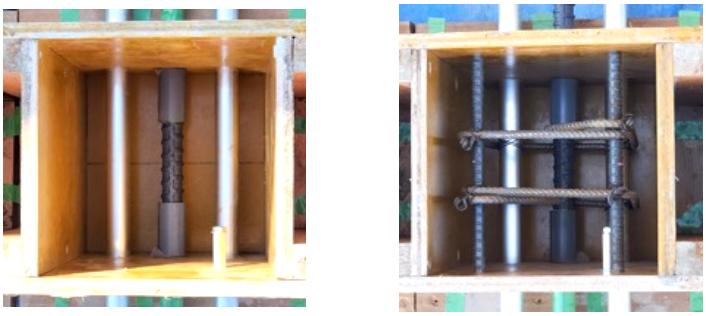

Specimen without stirrup Specimen with stirrup

Figure 5.5 Framework of specimen

5.2.2.2.1 Crack simulation by EAFP

To simulate cracks with EAFP, an expansion agent is poured into aluminum pipes embedded in concrete to simulate the expansion of the rebar volume due to corrosion, as shown in Figure 5.6. The specimens were placed, so the aluminum pipe axis was vertically set to quickly pour the expansion agent, as seen in Figure 5.6. The crack width widens over time that has elapsed after filling.

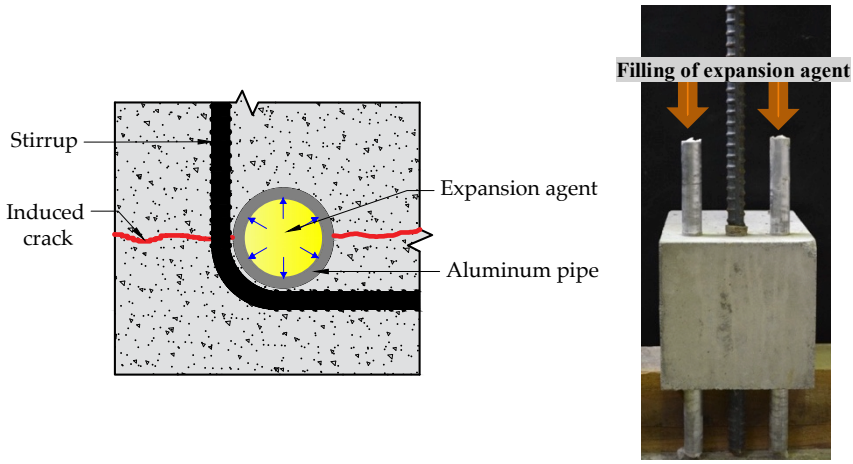

Cracking mechanism Expansion agent filling

Figure 5.6 Crack simulation with an EAFP

5.2.2.3 Loading test and instrumentation

Figure 5.7 shows the general setup for the pull-out test. After each specimen reached the target-induced crack width measured by a crack scale, pull-out tests were conducted using a universal testing machine. The extra section of the aluminum pipe was cut before loading. The specimen was then placed on the fixed head cross of the loading machine, and a monotonic load was applied with a head speed of 0.5 mm/min according to ASTM234-91A. A Teflon sheet was inserted between the bed steel plate and the specimen to reduce the restriction of lateral deformation of the concrete. Measurement items are pull-out load, slippage at free-end, and opening of the induced crack during loading.

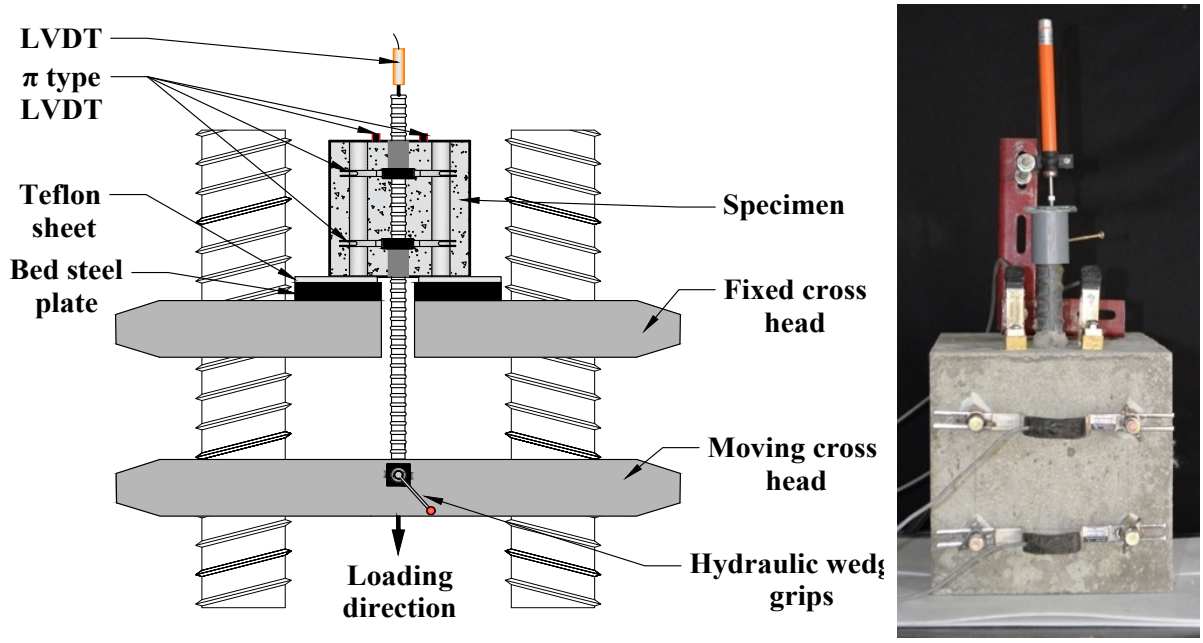

Loading machine Photo of specimen

Figure 5.7 Pull-out test setup

5.3 Experimental Results

Table 5.3 summarizes the experimental results. The specimen ID consists of three sets of characters indicating the Series (S0, S1, S2, or S3), the diameter of the stirrup rebar (D3, D4, or D6), and the induced crack width. Specimens S0-D0-NC, S1-D3-NC, S2-D4-NC, and S3-D6-NC (NC: no crack) were loaded without filling the expansion agent, so these specimens did not have EAFP-induced cracks. The definitions of failure mode (F.M.) will be explained after.

Table 5.3 List of pull-out results

Specimen ID	Induced crack width (mm)	At max. load		F.M.	Specimen ID	Induced crack width (mm)	At max. load		F.M.
		Bond stress (MPa)	Slip (mm)				Bond stress (MPa)	Slip (mm)	
S0-D0-NC 1	-	10.20	0.36	F	S2-D4-NC 1	-	9.58	0.92	F
S0-D0-NC 2	-	9.71	0.15	F	S2-D4-NC 2	-	12.31	0.44	F
S0-D0-NC 3	-	10.98	0.36	F	S2-D4-NC 3	-	11.39	0.31	F
S0-D0-C 0.15	0.15	7.13	0.74	S	S2-D4-C0.10	0.10	9.78	0.96	F
S0-D0-C 0.20	0.20	7.13	0.56	S	S2-D4-C0.15	0.15	9.52	0.23	F
S0-D0-C 0.30	0.30	6.84	0.32	S	S2-D4-C0.30	0.30	9.30	0.13	F
S0-D0-C 0.40	0.40	4.32	0.43	S	S2-D4-C0.40	0.40	7.55	1.36	F
S0-D0-C 0.50	0.50	4.18	0.17	S	S2-D4-C0.50	0.50	7.62	1.10	S
S0-D0-C 0.60	0.60	4.65	0.45	S	S2-D4-C0.80	0.80	6.52	1.06	S
S0-D0-C 0.75	0.75	3.23	1.04	S	S2-D4-C0.90	0.90	6.20	0.92	S
S0-D0-C 1.00	1.00	2.81	1.36	S	S2-D4-C1.00	1.00	6.29	2.30	S
S0-D0-C 1.10	1.10	2.70	1.11	S	S2-D4-C1.10	1.10	5.58	2.07	S
S1-D3-NC 1	-	9.55	0.48	F	S3-D6-NC 1	-	11.42	0.67	F
S1-D3-NC 2	-	11.19	0.41	F	S3-D6-NC 2	-	10.81	0.95	F
S1-D3-NC 3	-	9.35	0.38	F	S3-D6-NC 3	-	10.41	0.77	F
S1-D3-C0.15	0.15	8.83	0.42	F	S3-D6-C0.10	0.10	10.37	0.19	F
S1-D3-C0.25	0.25	7.43	0.72	F	S3-D6-C0.30	0.30	9.80	0.48	F
S1-D3-C0.30	0.30	7.83	0.95	F	S3-D6-C0.40	0.40	9.58	0.92	F
S1-D3-C0.50[1]	0.50	6.41	0.68	F	S3-D6-C0.50	0.50	6.94	0.38	F
S1-D3-C0.50[2]	0.50	6.65	1.18	F	S3-D6-C0.60	0.60	8.03	0.90	F
S1-D3-C0.60	0.60	6.05	0.48	S	S3-D6-C0.70	0.70	7.82	1.71	S
S1-D3-C0.70	0.70	5.49	1.48	S	S3-D6-C0.80	0.80	7.78	0.77	S
S1-D3-C0.80	0.80	5.19	1.71	S	S3-D6-C0.90	0.90	7.35	1.46	S
S1-D3-C1.00	1.00	5.35	2.40	S	S3-D6-C1.20	1.20	5.65	2.39	S

F.M.: failure modes; F: face split; S: side split

5.3.1 Crack simulation by EAFP

An example of crack induced by EAFP is shown in Figure 5.8. The expansion agent was filled simultaneously in the specimens with identical target-induced crack widths. The hoop stress caused by EAFP induces side-splitting cracks. The crack width around the rebar's free end was measured using a crack scale. The considered crack width ranged from 0.15 to 1.10 mm in specimens S0, 0.15 to 1.00 mm in specimen S1, 0.10 to 1.10 mm in specimen S2, and 0.10 to 1.20 mm in specimen S3.

In all specimens, the onset of cracking is observed 15 hours after injecting the expansion agent. Then the crack width increases linearly (0.15 mm after 22 hours). The presence of stirrup does not influence the initiation of crack. However, the crack width tends to increase faster in specimens without stirrup. For example, 300 hours were required to obtain a crack width of 1.10 mm in the specimen without stirrup (S0). Instead, the same crack width is obtained after 320 hours in specimens with stirrup (S2).

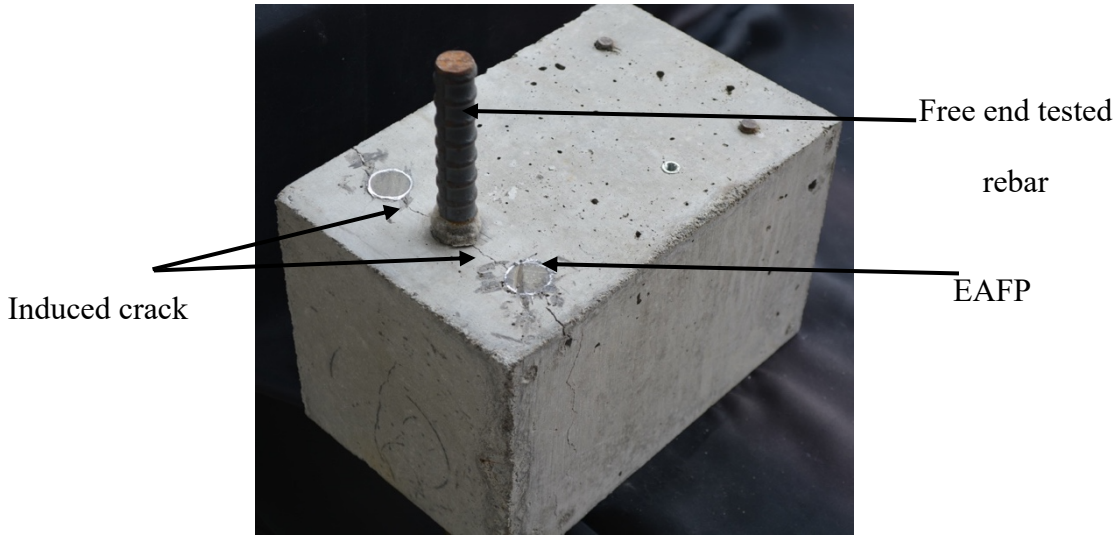

Figure 5.8 Specimen cracked by EAFP

5.3.2 Pull-out failure mode

Figure 5.9 shows typical examples after pull-out loading. All specimens failed due to the splitting of the concrete cover. The most common splitting was characterized by the widening of the induced crack under the pull-out load (namely, "side split"). However, for several specimens with stirrups, a second splitting mode occurs with newly generated longitudinal cracks along the tested rebars toward the cover face (namely, "face split"). After loading, the crack width is smaller in specimens with a higher stirrup ratio. This reflects the capacity of the stirrup to restrict the opening of the initial induced crack. In engineering practice, stirrups are

mainly used to improve shear resistance of RC members. Moreover, the presence of stirrups can increase concrete confinement.

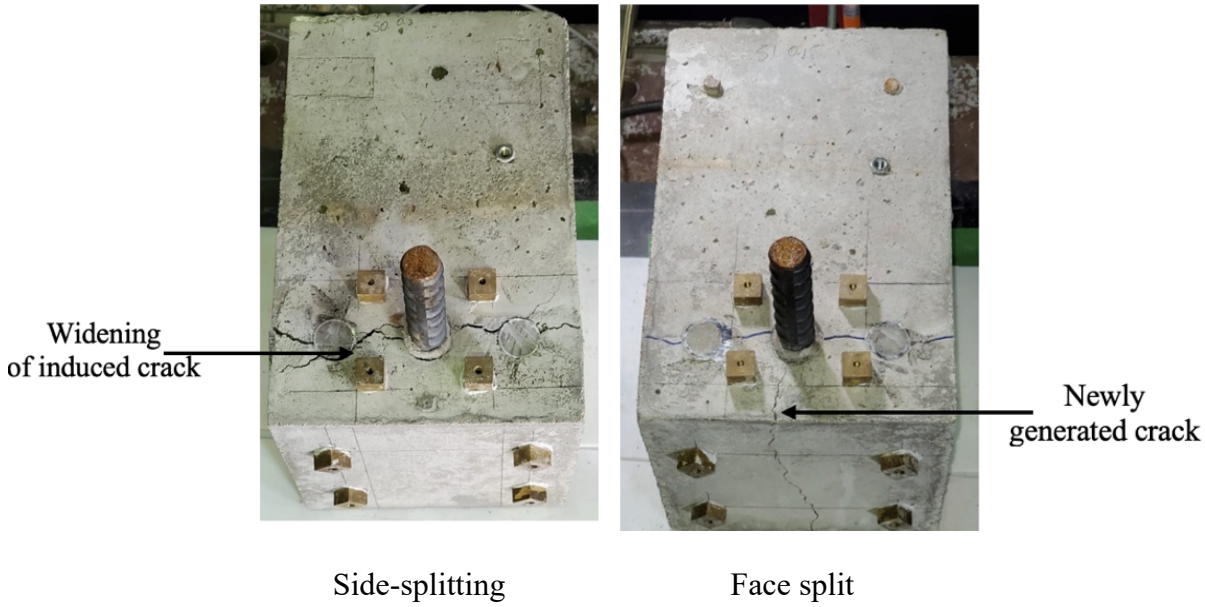

Figure 5.9 Mode of failure

5.3.3 Bond stress–slip relationship

The specimens have a short bond length, and the bond stress is assumed to be almost uniformly distributed throughout the length. Bond stress is calculated as the pull-out load divided by the surface area of rebar. Furthermore, the tested bar is assumed to remain in its elastic region due to the small applied pull-out load. Thus, the slip measured at the free end estimated the local slip in the focused bond length. Figure 5.10 shows examples of bond stress–slip relationships. The pull-out load showed a sudden decrease in specimens without stirrup (S0). However, the bond stress–slip indicated ductile behavior in specimens with stirrups. This also agrees with earlier observations [70], which showed that confinement affects the bond strength and post-peak behavior in cracked concrete.

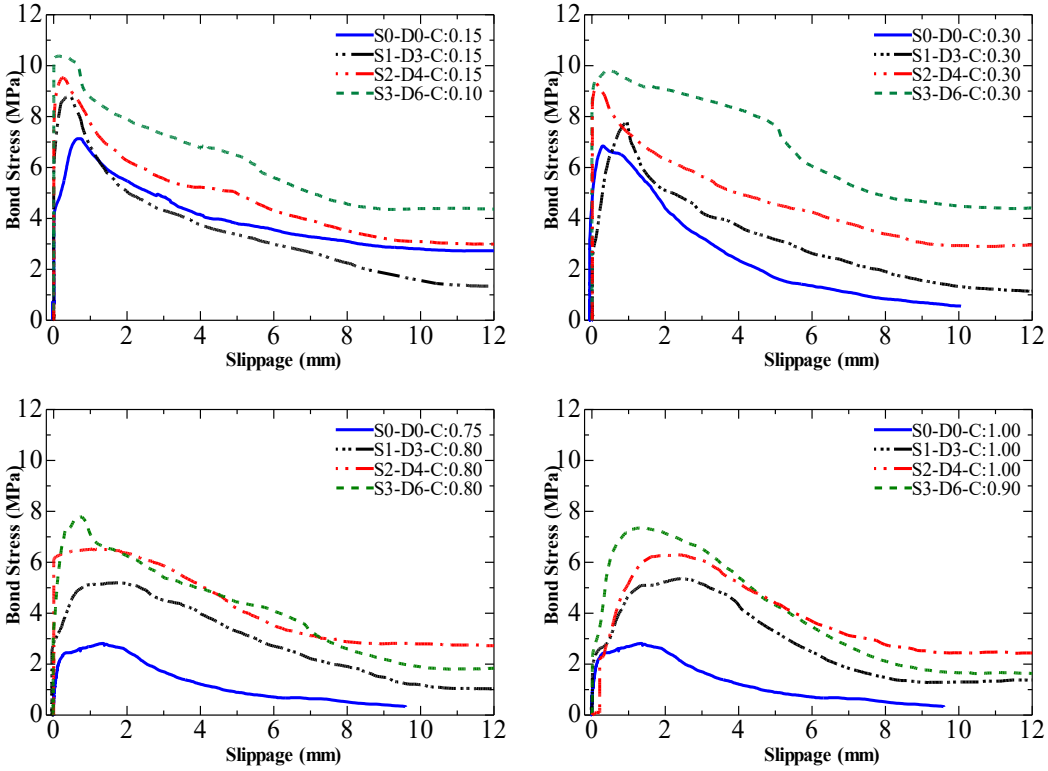

Figure 5.10 Examples of bond stress versus slip curves

5.3.4 Bond strength

The test results in terms of bond strength are shown in Figure 5.11. The bond strengths of the uncracked specimens are the average of three specimens. Their values are 10.29 MPa, 10.03 MPa, 11.09 MPa, and 10.87 MPa for S0, S1, S2, and S3 specimens, respectively. As expected, bond strength decreases when the induced crack width increases. Furthermore, the bond strength of the specimens with stirrups is less affected by induced cracks than those without stirrups. This highlights the importance of stirrup confinement for retaining the bond after concrete cover cracking.

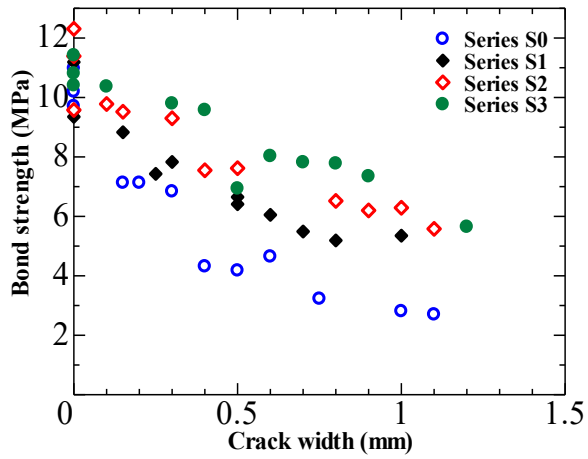

Figure 5.11 Bond strength vs. induced crack width relationship

5.4 Evaluation of bond strength degradation due to induced crack

5.4.1 Residual bond strength and induced crack width relationship

In this study, the residual bond strength ratio (R_B) associated with the induced crack width is obtained by normalizing the bond strength of the cracked specimens with respect to that of the uncracked reference specimen.

Figure 5.12 shows the residual bond strength ratio and the crack width relationships. The residual bond strength decreases in most specimens with increasing induced crack width.

The residual bond strength ratio was fitted using the exponential function introduced in Eq. 5-2.

$$\boldsymbol{R_B = 1 - a\left(1 - \left(e^{b \cdot w_{c_R}}\right)\right)} \qquad (5\text{-}2)$$

Where a and b: are empirical coefficients and w_{CR}: induced crack width in mm.

The results of the regression analysis are shown in Table 5.4. Figure 5.13 compares the fitting results obtained for S0, S1, S2, and S3 specimens. This revealed that confinement by stirrups contributes to the rate of bond strength degradation in cracked concrete. In specimens without stirrups, the residual bond strength severely decreases at a ratio of 0.28 caused by an induced crack width of 1 mm. In contrast, specimens S1, S2, and S3 show slightly higher residual bond strengths of 0.46, 0.54, and 0.66, respectively. The unconfined specimens depend on the surrounding concrete to confine them. Cracked concrete loses its confining stresses, leading to rapid bond strength degradation. In contrast, stirrups can restrict the widening of the induced crack, increasing concrete's residual confinement and limiting the bond strength's deterioration.

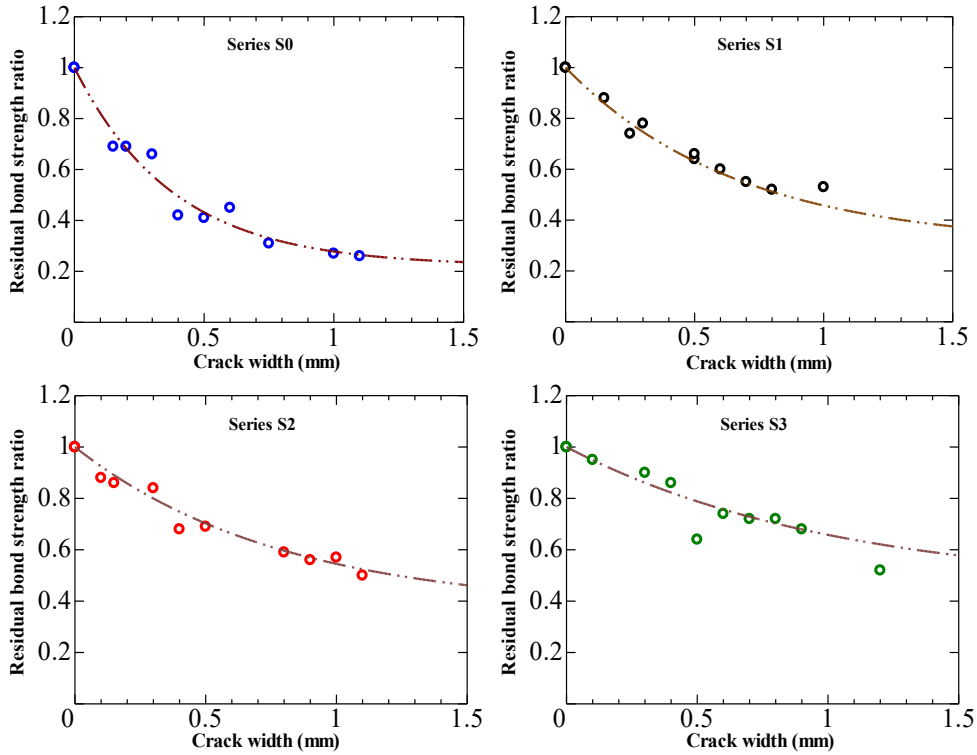

Figure 5.12 Residual bond strength ratio versus crack width

Table 5.4 Results of the regression analysis

Series	p_w (%)	a	b	R^2
S0	0	0.77	-2.62	0.97
S1	0.18	0.70	-1.50	0.98
S2	0.33	0.63	-1.27	0.98
S3	0.75	0.55	-0.97	0.94

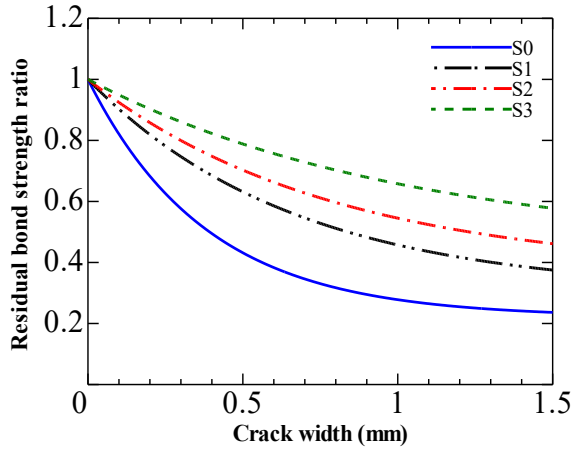

Figure 5.13 Proposed formulas comparison

5.4.2 Effect of stirrup on the empirical coefficient

The results show that bond strength degradation resulting from induced cracks is strongly associated with the passive confinements provided by stirrups. Figure 5.14 shows the relationship between the empirical coefficients a and b and stirrup ratio p_w. Coefficient a decreases and b increase when the stirrup ratio increases. To evaluate the coefficients a and b as functions of p_w, the exponential function gives a better fit than the linear one. Furthermore, for the coefficient b, using $\sqrt{p_w}$ instead of p_w increase the value of R^2 from 0.78 to 0.99. Therefore, Eq. (5-3) and Eq. (5-4) evaluate the coefficients a and b:

$$a = 0.8\mathbf{e}^{-0.5p_w} \quad (5\text{-}3)$$

$$b = -2.6\mathrm{e}^{-1.3\sqrt{p_w}} \quad (5\text{-}4)$$

Here the stirrup ratio p_w is expressed in %.

Substituting Eq. (5-3) and Eq. (5-4) in Eq. (5-2), the model of bond degradation due to induced cracks can be expressed as follows:

$$R_B = 1 - 0.8\mathbf{e}^{-0.5p_w}\left(1 - \left(\mathbf{e}^{-2.6\mathbf{e}^{-1.3\sqrt{p_w}}.w_{cR}}\right)\right) \quad (5\text{-}5)$$

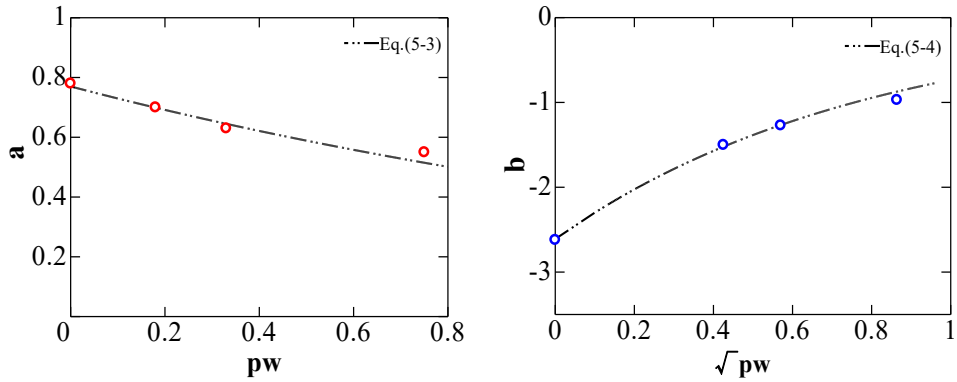

Figure 5.14 Influence of p_w on empirical coefficients a and b

5.4.3 Influence of corrosion product and rebar change on bond strength

Figure 5.15 shows the relationship between the residual bond strength ratio and the induced crack width in specimens cracked by electrical induced corrosion (S2 series specimens without stirrup in Chapter 3) or by EAFP (S0 series specimens in Chapter 5). Both methods can lead to identical crack patterns (side-splitting). Thus, the main difference between these two specimens is the rust presence and rebar profile change due to corrosion. It is confirmed that residual bond decreases in most specimens with increasing induced crack width. Interestingly, we can see that the residual bond strength ratio can be estimated by considering the single effect of cracking,

ignoring the rust presence or rebar profile change. It is also confirmed that a direct relationship between bearing and crack width can ignore ambiguity related to the accumulation of corrosion products. Furthermore, the result suggests that a crack-based approach can lead to more accurate results because corrosion-induced surface cracks represent the net amount of corrosion. Conclusively, it is practical to have a direct and visible damage indicator that can be measured on the outer concrete surface.

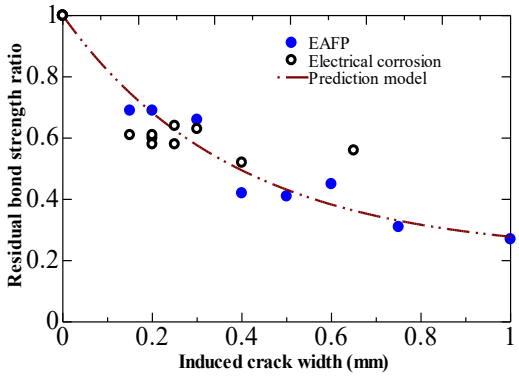

Figure 5.15 Bond strength degradation in electrical corrosion and EAFP specimen

5.4.4 Influence of corrosion product and rebar change on bond-slip curve

Figure 5.16 compares bond-slip relationship in specimens cracked by electrical corrosion (S2 series specimens without stirrup in Chapter 3) or by EAFP (S0 series specimens in Chapter 5). For instance, specimens with the same induced crack width are compared to depict better the influence of rust presence or rebar profile change. It is confirmed that corrosion products do not influence bond strength. However, the post-peak curves decrease rapidly in specimens cracked by electrical corrosion compared to ones cracked by EAFP. It is confirmed that the corrosion products can lead to more brittle failure. After the maximum load, the bond behavior is mainly governed by the friction between the rebar and surrounding concrete. Thus, the corroded rebars greatly influence the bond behavior in this section. Furthermore, this demonstrates that the bond strength through the bearing is predominant with respect to frictional influence after cracking. Jiradilok et al. [118] confirm that corrosion cracks have a dominant effect on bond behavior. Furthermore, they stated that the commonly used experimental method could not capture the real bond-slip relationship in corroded specimens. However, only the effect of surface cracking could be observed in the final result.

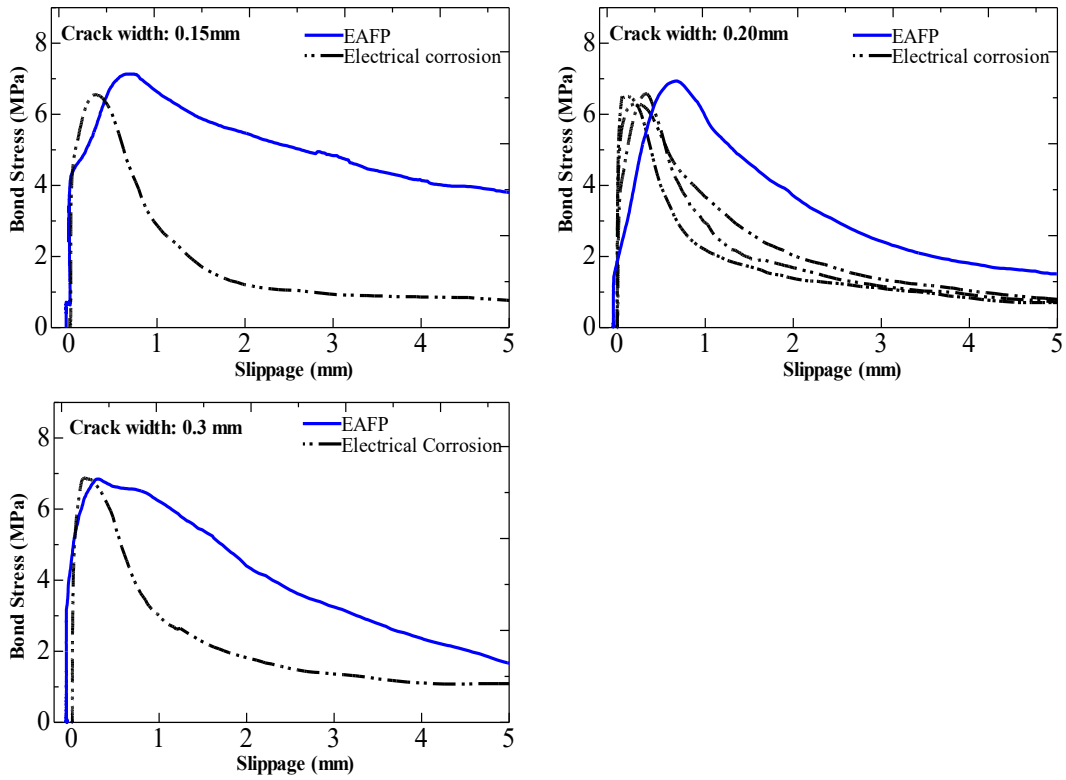

Figure 5.16 Bond-slip relationship in specimen crack by electrical corrosion and EAFP

5.4.5 Comparison of predictions and experimental results from the literature

5.4.5.1 Comparison of test results with fib model

The fib model code (2010) [119] proposed a bond strength degradation estimated based on the induced crack width (hereafter, fib model). Mainly based on various experimental results, fib model suggested a residual bond strength are for a specific range of surface crack widths. Theses crack widths were calculated using the linear relationship between corrosion penetration and induced corrosion cracks. Comparisons of the evaluations in this study and the fib model are shown in Figure 5.17. In specimens without stirrups (S0), Figure 5.17 shows that the prediction, suggesting an abrupt deterioration of the bond strength, is in excellent safety agreement with the fib model. On the other hand, the limits proposed by the fib model for specimens with stirrups predict the bond strength deterioration of specimen S3 (good confinement). However, predictions for series S1 and S2 show a more severe bond strength degradation, overestimating the residual bond strength when compared to the fib model.

The fib model considers only the existence of stirrups without including the effect of their quantity on bond strength degradation due to cracks. A prediction formula, including the effect of stirrup ratio variation, is needed to estimate bond strength degradation accurately.

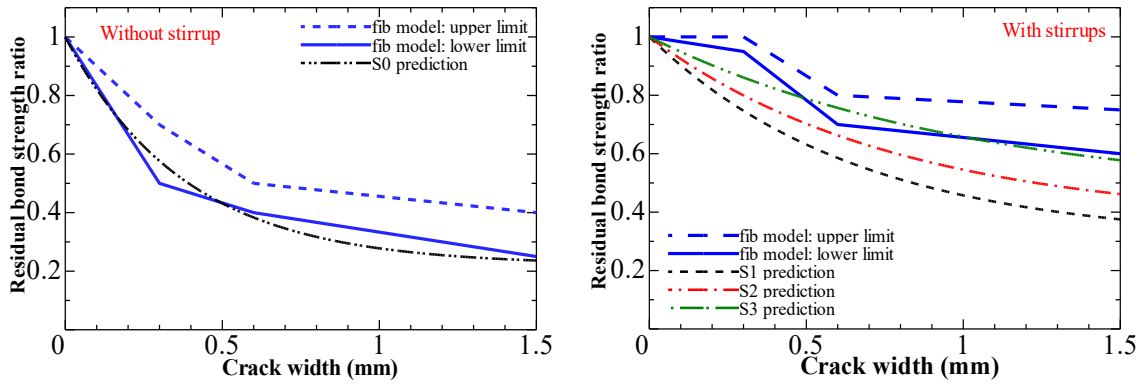

Without stirrup With stirrup

Figure 5.17 Results compared with the fib model

5.4.5.2 Comparison of predictions with previous experimental data

The empirical predictions developed in this study are further compared with the experimental results in the literature [74,75,77]. The details of the corroded specimens for comparison purposes are summarized in Table 5.5. Figures 5.18, 5.19, and 5.20 compare the residual bond strength ratio between the predictions and the experimental results. The average and the coefficient of variation (CV) of the ratio of the predicted bond strength to the experimental one are also shown in Figures 5.18, 5.19, and 5.20. The predictions closely match the experimental results in most situations. Despite the scattering of data from the literature, the predictions are conservative and safe. In general, the beneficial influence of stirrups on bond strength degradation is clearly illustrated. Furthermore, it is confirmed that the direct relationship between interlock reduction and crack width can exclude the ambiguity related to corrosion product accumulation.

In conclusion, EAFP-induced cracks can effectively quantify the net amount of corrosion-induced damage. Because the induced crack width is the most apparent indication of corrosion, it is appropriate to connect the degradation of the bond directly with an easy-to-measure damage indicator. Today, the acquisition of excellent visual records of structures (e.g., cracks) is possible thanks to the remarkable progress of automated monitoring surveys (inspection drones). Models that use visible damage indicators could be beneficial for making faster and more accurate degradation predictions.

Table 5.5 Previous experimental investigations

References	Specimen type	Tested rebar diameter (mm)	C/D*	Concrete compressive strength (MPa)	Stirrup ratio (%)
Lin et al. [75]	Pull-out	20	1.5 2 3	33	No 0.33 0.67 1.34
Apostolopoulos al. [77]	Pull-out	16	1.5 2.5	30	No 0.21 0.42 0.84
Law et al.[74]	Beam end	12 16	3	40	No 0.38

**C*: cover thickness, *D*: rebar diameter

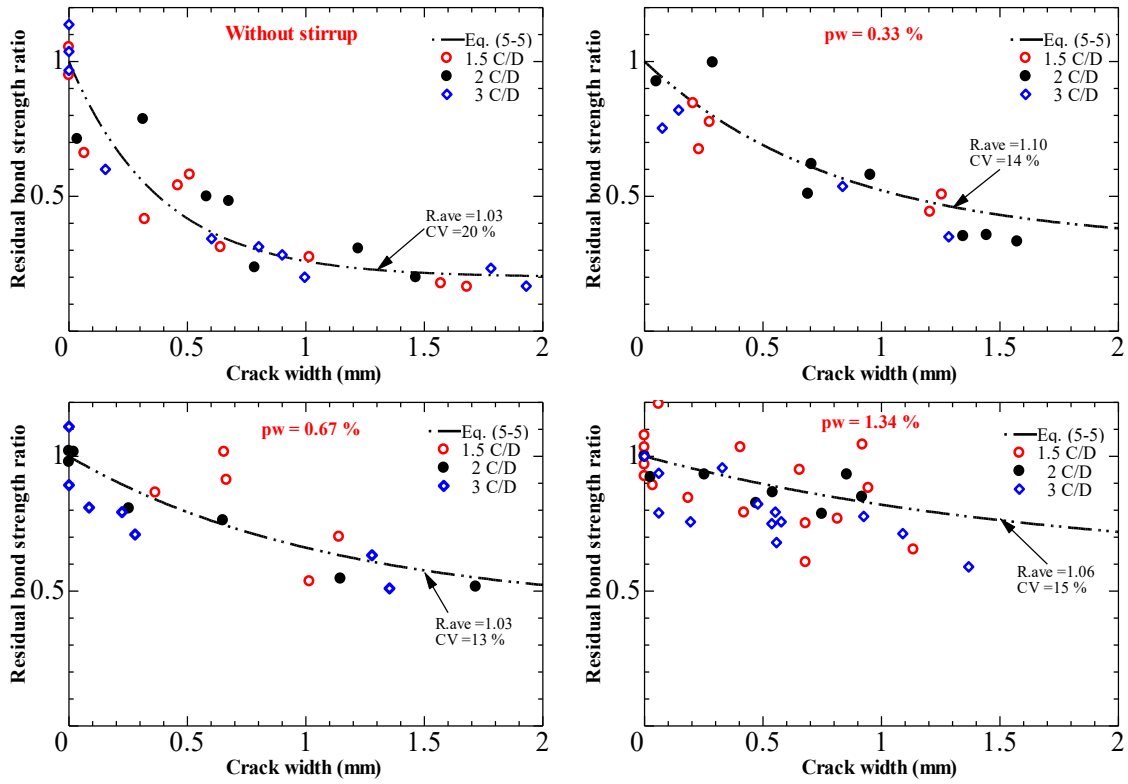

Figure 5.18 Comparison of the proposed formulas with experimental test results of Lin et al. [75]

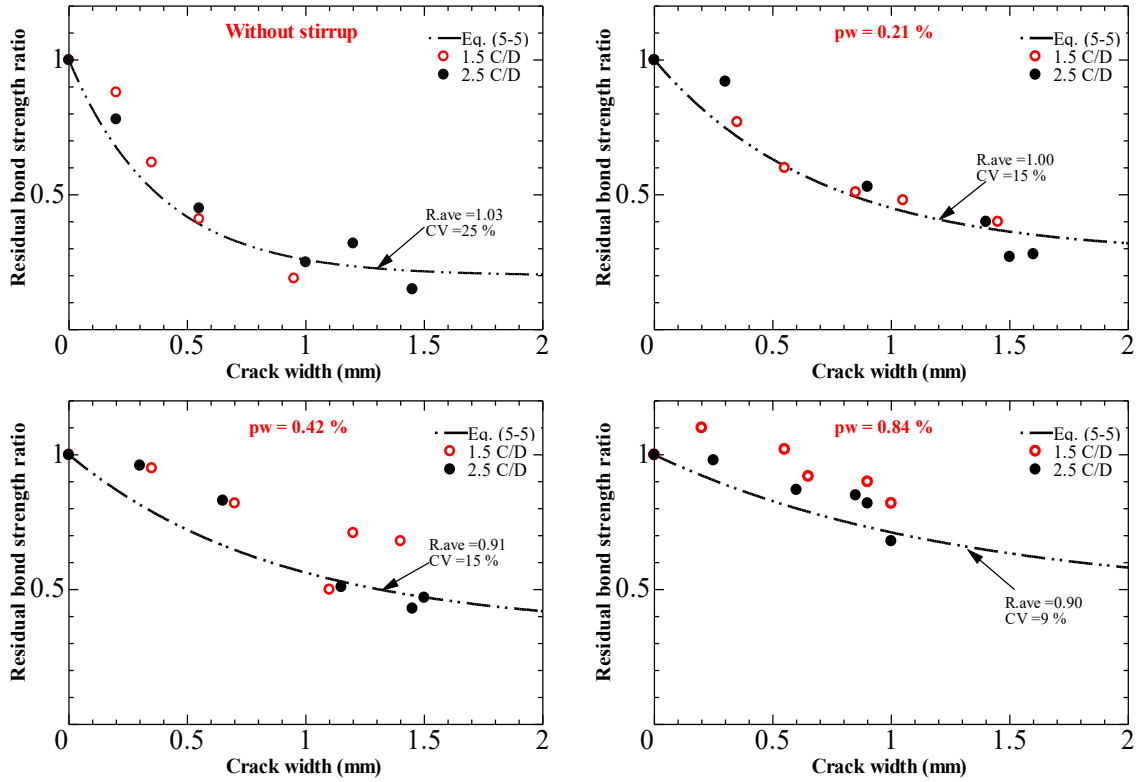

Figure 5.19 Comparison of the proposed formulas with experimental test results of Apostolopoulos al. [77]

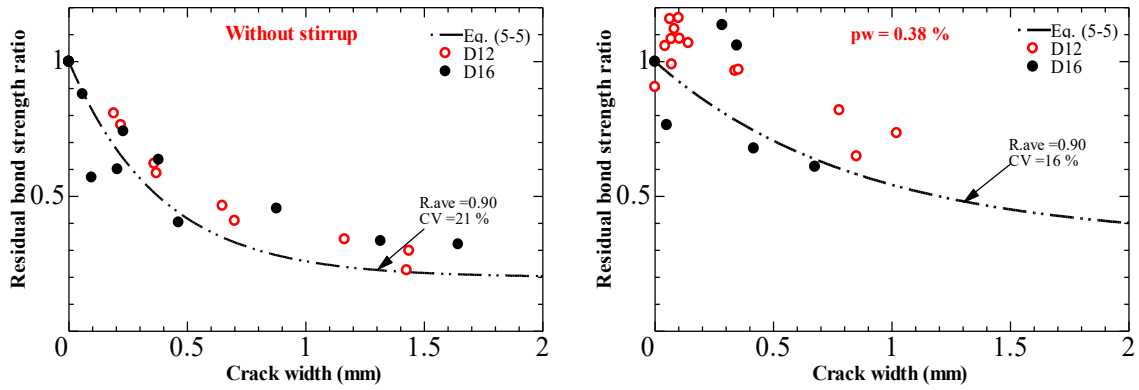

Figure 5.20 Comparison of the proposed formulas with experimental test results of Law et al. [74]

5.5 Summary

The pull-out bond test was conducted on specimens with different induced crack widths and stirrup ratios to propose formula predicting the bond strength degradation due to corrosion. The following conclusions are drawn based on the results of this experimental investigation.

i. To focus on the combined effect of cracking and stirrup diameter reduction on bond strength degradation, side-splitting cracks with different widths are simulated in pull-out bond specimens using EAFP.

ii. The test result reflects the crucial role of the stirrup on the bond degradation mechanism due to induced cracks. The bond strength degradation rate is considerably fast in specimens without stirrups. However, bond degradation is limited in specimens with stirrup, respectively, to the stirrup ratio increase. Moreover, the stirrup can also restrict the opening of cracks induced by EAFP, leading to a more ductile failure mode.

iii. To investigate the effect of corroded rebar shape on bond degradation, the bond degradation in specimens cracked by electrical-induced corrosion or EAFP was compared. The main difference between these two specimens is the rust presence and rebar profile change due to corrosion. The result shows no significant difference in bond degradation. Thus, we conclude that the residual bond strength ratio can be estimated by considering the single effect of cracking, ignoring the rust presence or rebar profile change. It is also confirmed that a direct relationship between bearing and crack width can ignore ambiguity related to the accumulation of corrosion products

iv. An empirical model has been proposed to assess the bond strength degradation considering the induced crack width and the stirrup ratio. Comparisons with previous data of corroded specimens show that the proposed model can give reasonable estimations.

6 STRUCTURAL PERFORMANCE OF RC BEAMS CRACKED BY EXPANSION AGENT FILLED PIPE (EAFP)

6.1 Introduction

Numerous countries with a high risk of earthquakes, including Japan, Italy, California, and New Zealand, have major populated cities along coastal areas. Therefore, RC structures are vulnerable to corrosion and seismic effects in these regions. In recent years, structural behavior under the combined impacts of reinforcement corrosion and seismic damage [39–41] has received increasing attention. However, the observed seismic behavior of corroded RC beams has not been given enough consideration. Under seismic reversed loading circumstances, flexural and shear strengths of RC beams degrade more severely than under monotonic loading. Ou et al.[120–122], Kato et al. [121], and Kobayashi [124] examined the seismic behavior of corroded RC beams subjected to cyclic loads. Kato et al. and Kobayashi [123,124] examined RC beams subjected to cyclic four-point bending; hence, shear did not affect the critical center zone. However, Ou et al. [120–122] tested an RC cantilever beam manner with cyclic loading applied to the free end. As a result, the critical region around the fixed end was subjected to flexure and shear, which is more representative of the loading due to the earthquake. The ultimate drift, ductility, and beams energy dissipation increased initially and decreased following the corrosion degree in the beam with corroded longitudinal rebar and stirrup. Furthermore, the beams flexural strength was not significantly impacted in specimens with severely corroded stirrups. However, the deformation capacity was drastically reduced.

The accelerated corrosion techniques have been adopted in several studies on the performance degradation of cracked concrete RC structures. In these techniques, it can be challenging to control the widths or patterns of the cracks. Also, the combination of concrete cracking and sectional defect of the rebar leads to difficulties in analyzing the degradation process at a fundamental level. In the previous chapter, it is confirmed that the bond strength is affected by corrosion-induced cracking. This bond degradation is more critical than the sectional loss of corroded rebar. During loading, cracks on RC members highly depend on the bond capacity between concrete and rebar. Although bond degradation due to corrosion has been intensively

studied, there are few references investigating their effect on RC structural performance. Therefore, there is necessary to cover such a topic because understanding the effect of bond strength degradation is necessary to evaluate the residual performance of corroded RC members.

This chapter aims to contribute to this growing area of research by exploring the effect of bond deterioration on the structural capacity (shear and flexural) of deteriorated RC beams. To achieve this goal, different damage levels (crack width) are simulated in the specimens by inducing cracks using an EAFP. Then, anti-symmetrical loading tests of the damaged beam are carried out to grasp the mechanical performance of the damaged beam.

6.2 Experimental program

6.2.1 Test specimens

The specimen consisted of a beam that was designed according to the guideline by the Architectural Institute of Japan [125,126]. Two types of beam specimens were designed to fail in shear or flexure. One type of specimen has lower shear capacity than flexural and bond ones, leading to a shear failure (namely "S_{hear} specimen"). The second type of specimen has lower flexural capacity than shear and bond ones ("F_{lex} specimen"). Moreover, F_{lex} specimens are divided into two categories according to their shear span ratio (1.5 and 2.0). The structural capacities of the specimen are listed in Table 6.1.

Table 6.1 Calculation of capacities

Specimen	Shear span ratio	Flexural strength Q_{Mu} (kN)	Shear strength V_u (kN)	Bond strength V_{bu} (kN)	Shear margin index V_u / Q_{Mu}	Bond margin index V_{bu} / Q_{Mu}
S_{hear}	1.5	204	180	251	0.88	1.23
F_{lex}-1.5	1.5	111	220	179	1.99	1.62
F_{lex}-2.0	2	78	144	109	1.85	1.40

6.2.1.1 S_{hear} specimens

The specimen’s rebar details are shown in Figure 6.1. The specimen's cross-section is 220 mm x 420 mm with a central target region of 1260mm and a shear span ratio of 1.5. Four D16 deformed rebars in two layers and D10@200 deformed rebars were used as main rebars and a stirrup, respectively. To simulate the cracking damage, four aluminum pipes with an outer diameter of 22mm and thickness of 1mm were used as EAFP. Series S_{hear} includes four

specimens; one is transversally cut (Monitor specimen) to observe the condition of internal induced cracking. Then, the three others were subjected to an anti-symmetrical loading.

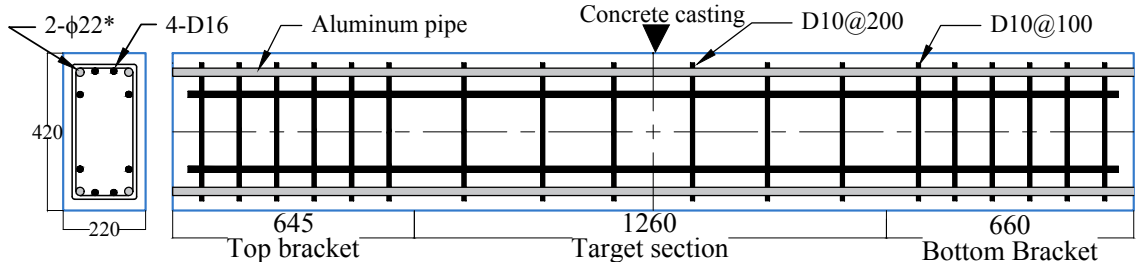

Figure 6.1 S_{hear} specimen detail

6.2.1.2 F_{lex} specimens

The specimen's rebar details are shown in Figure 6.2. F_{lex} specimens were divided into two categories. Although the beams have the same amount of rebar, their cross sections are different to vary the shear span ratio (from 1.5 to 2.0). Specimens F_{lex}-1.5, with a shear span of 1.5, have a cross-section of 220 mm x 420 mm. However, specimens F_{lex}-2.0, with a shear span of 2.0, have a smaller cross-section of 235 mm x 315 mm. A central target region of 1260 mm is similar for all specimens. Two D19 deformed rebars and D10@200 deformed rebars were used as main rebars and stirrups, respectively. To simulate the cracking damage, four aluminum pipes with an outer diameter of 22 mm and thickness of 1mm were used as EAFP.

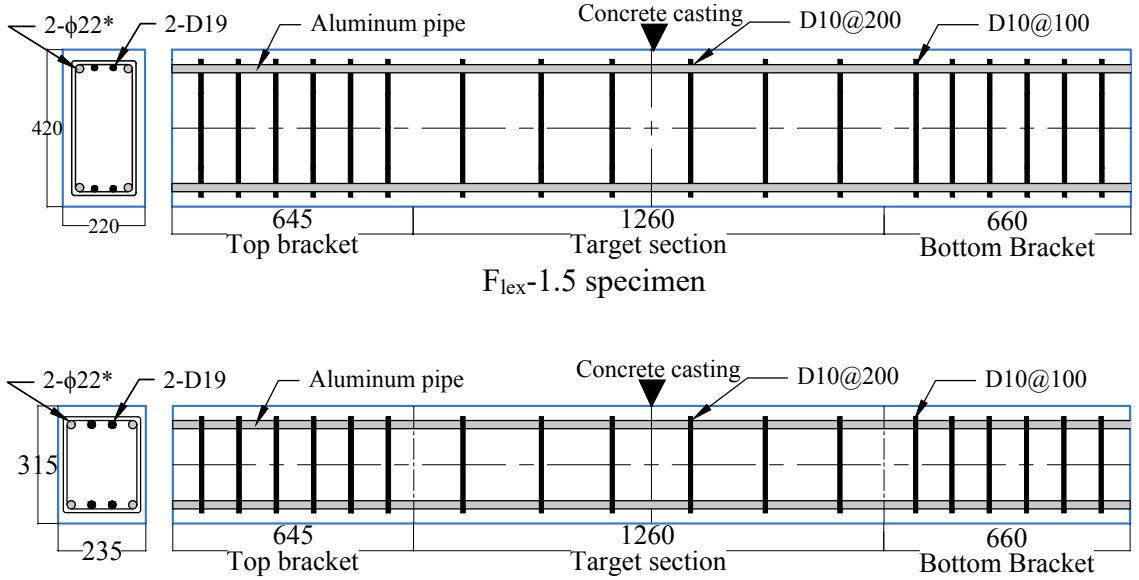

Figure 6.2 F_{lex} specimen detail

6.2.2 Used materials

The concrete, provided by a local ready-mixed concrete factory, was made with ordinary Portland cement with a content of 248 kg/m^3, a water-cement ratio of 78.5%, and a maximum aggregate grain size of 20 mm. The mechanical characteristics of the concrete measured at loading day on ϕ100 mm×200 mm cylinder is summarized in Table 6.2. The tensile test results of rebars are listed in Table 6.3. An aluminum pipe with an outer diameter of 22mm and thickness of 1mm was used as EAFP. The tensile test results of the aluminum pipe are listed in Table 6.4.

Table 6.2 Mechanical characteristics of concrete

Specimen series	Compressive strength (MPa)	Elastic modulus (GPa)	Splitting tensile strength (MPa)
S_{hear}	20.5	18.2	2.07
Flex-1.5	23.8	19.4	2.27
Flex-2.0	22.2	19.9	2.07

Table 6.3 Mechanical characteristics of reinforcing bar

Type	Yield strength (MPa)	Tensile strength (MPa)	Elastic modulus (GPa)	Elongation at rupture (%)
D10	352	481	190	30.4
D16	526	703	192	14.8
D19	355	532	187	24.0

Table 6.4 Mechanical characteristics of aluminum pipe

Offset strength (MPa)	Tensile strength (MPa)	Elastic modulus (GPa)	Poisson's ratio
207	235	60	0.338

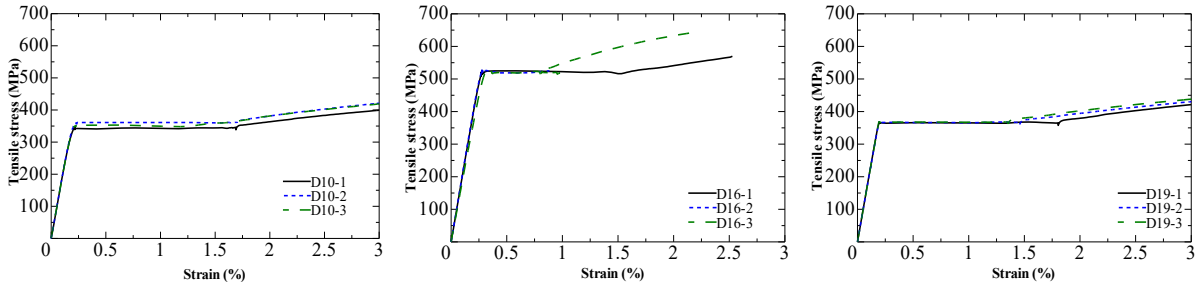

Figure 6.3 Stress-strain relationship of the steel rebar

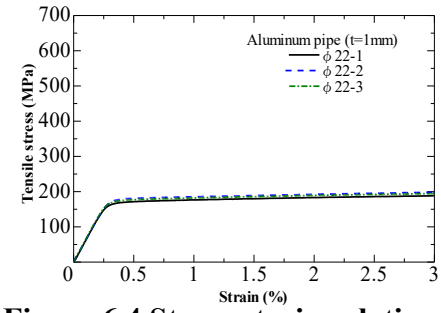

Figure 6.4 Stress-strain relationship of the aluminum pipe

6.2.3 Crack simulation with EAFP

EAFP is an aluminum pipe embedded in concrete and filled with an expansion agent to simulate the expansion of the rebar volume due to corrosion, as shown in Figure 6.5. The specimens were placed to vertically set the pipe axis to fill the aluminum pipe with an expansion agent. The crack width increases over time that has elapsed after filling. Thus, one can quickly obtain a target crack width by monitoring the time.

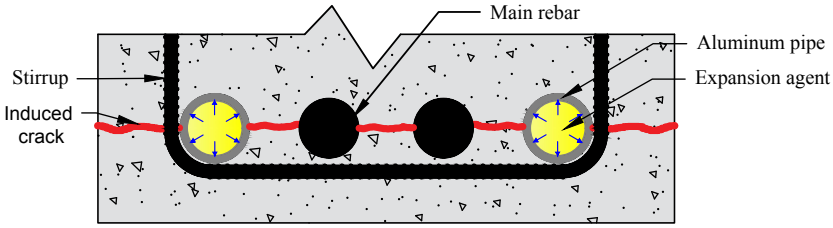

Figure 6.5 Crack induced by EAFP

6.2.4 Cyclic antisymmetrical static loading and measurement method

Figure 6.6 illustrates the loading test setup. The specimens were vertically raised. Two vertical jacks restricted the rotation of the top bracket attached on a specimen. It resulted in the anti-symmetric moment distribution of the central beam test region. In this system, vertical deformation of the specimen was free; that is, no additional axial load was applied to the specimen. A horizontal 100 tons actuator applied lateral shear force. During the test, the drift angle of the specimen was controlled. Shear force, the relative displacement between the end of the specimen, the axial displacement between stubs, and the strain of main bars, stirrups, and aluminum pipes were measured. The drift angle is obtained from relative displacement between the end of the specimen divided by clear span length. The static loading history is shown in Figure 6.7. The loading cycle is twice of ±1/400, ±1/200, ±1/100, ±1/50, ±1/33, and once of ±1/20 and ±1/15.

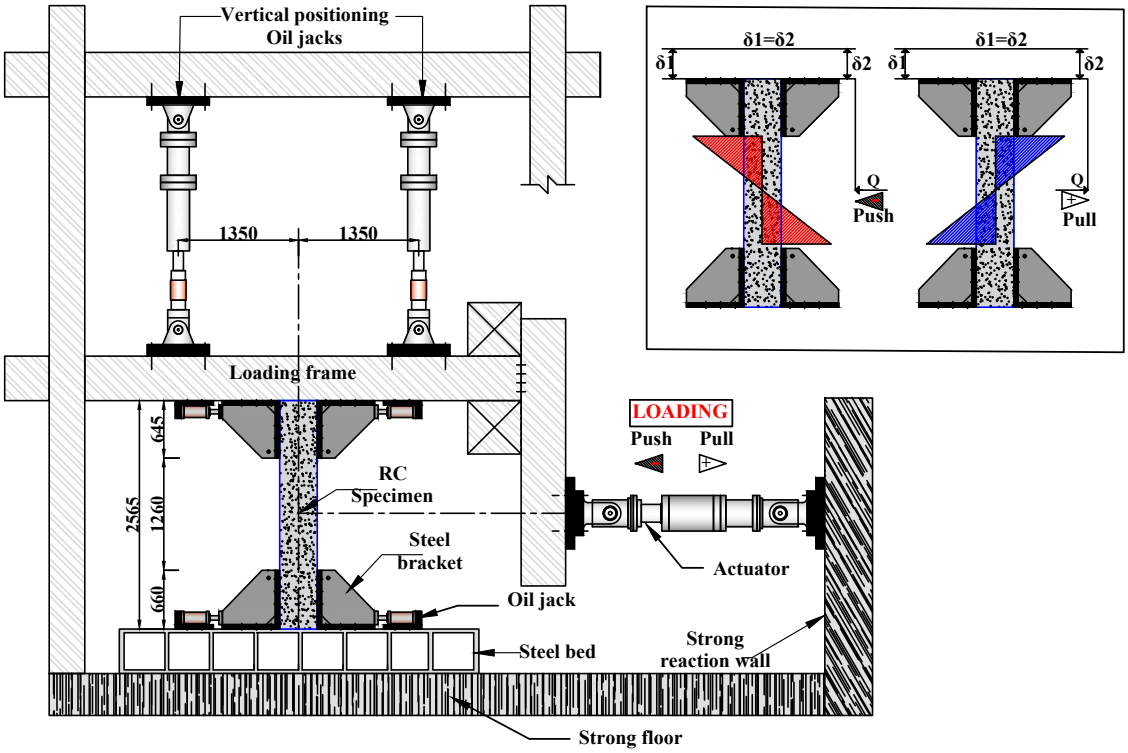

Figure 6.6 Loading system

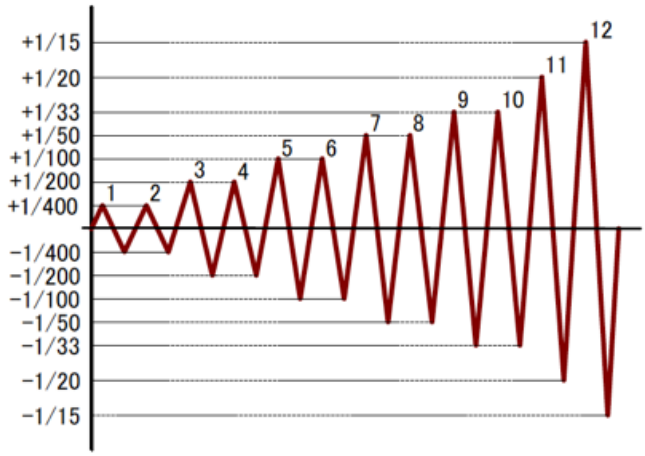

Figure 6.7 Loading history

6.3 Experimental results

6.3.1 Visual assessment of induced crack by EAFP

The main goal of this study is to evaluate the structural degradation of damaged beams using a visual damage indicator (crack width). The crack was induced with an EAFPs technique described previously. In Figure 6.8, longitudinal cracks run parallel to main rebar in S_{hear} specimens. These cracks were measured in many sections of the beams using a crack scale. The value in the figure indicates the maximum crack. Considering casting direction, it can be

observed that the crack width at the top is smaller than those at the bottom of the beam. It is likely possible that the presence of voids under the top rebar can alter EAFP expansion transmission, leading to smaller crack width on the beam top. This study considers the maximum surface crack width to assess the structural degradation due to induced crack.

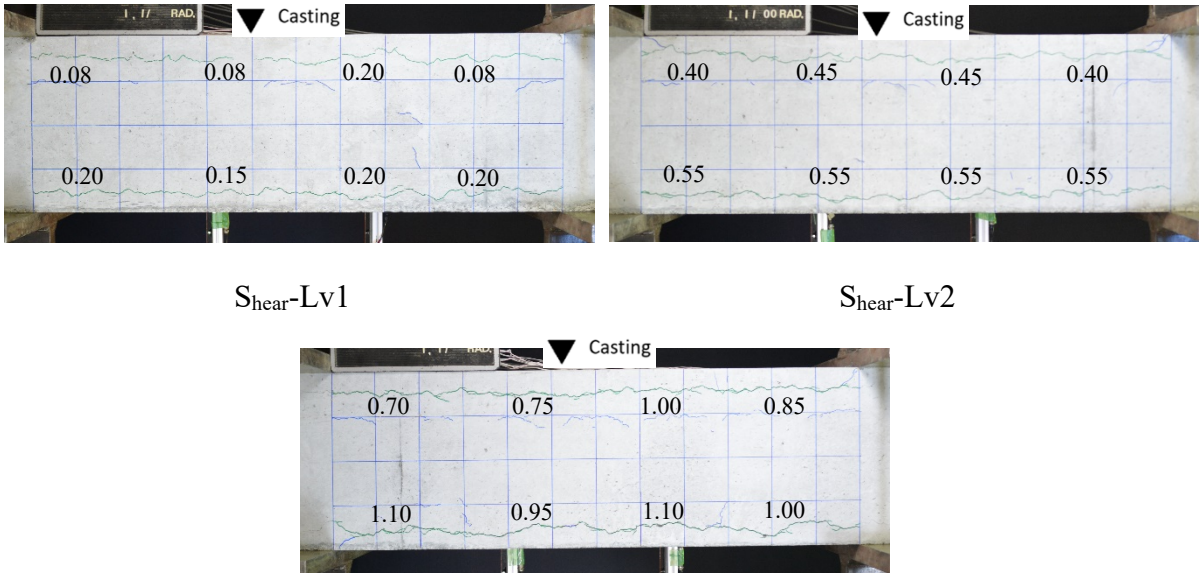

S_{hear}-Lv1 S_{hear}-Lv2

S_{hear}-Lv3 (unit: mm)

Figure 6.8 Example of crack simulated by EAFP

Although the surface crack is the most apparent visual damage in actual concrete structures, it is well-known that the internal crack can influence the structural behavior of damaged beams. Thus, three transversal cuts were performed on a S_{hear}-Lv3 monitor specimen to observe the internal cracking condition. The detail of internal cracking can be seen in Figure 6.9. The value in the figure expresses the surface crack width. It can be seen that the crack width distribution was non-uniform along the axis of the beam. Moreover, side split cracks mainly occurred around the first layer due to the expansion of EAFP. In some cases, cracks progressed till the main bar of the second layer.

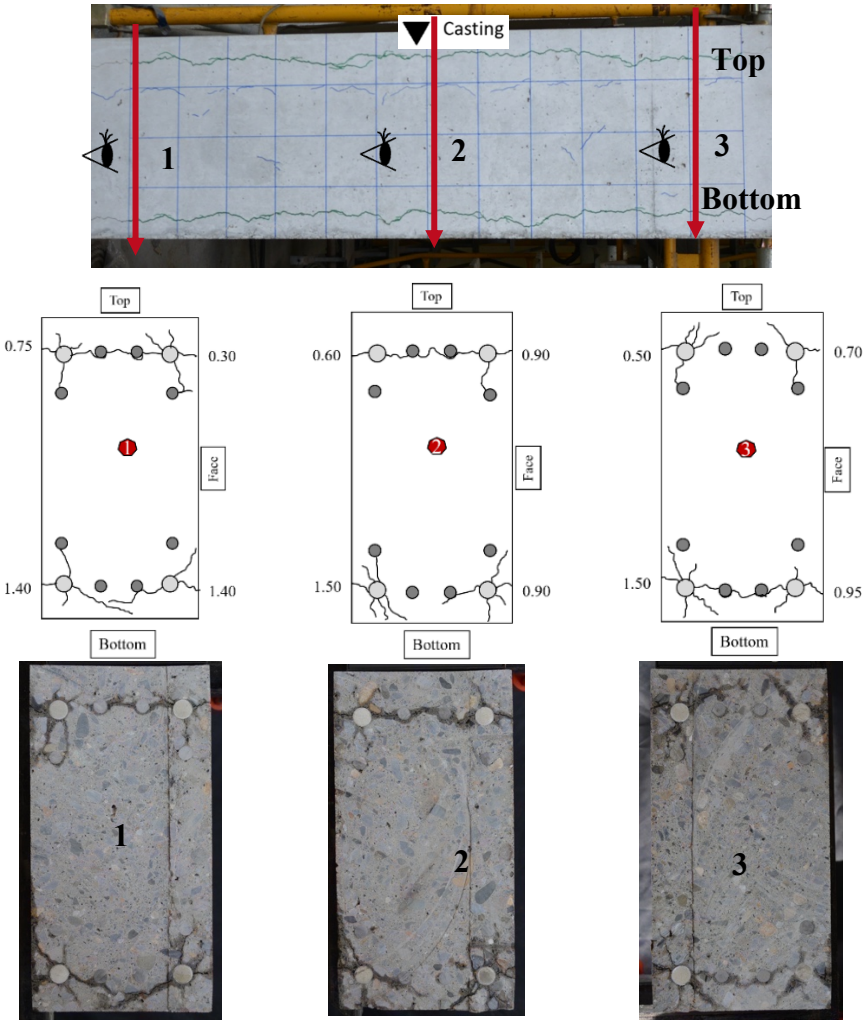

Figure 6.9 Detail of internal cracking

6.3.2 Damage mechanism during loading

Figure 6.10-6.12 shows the crack patterns of the damaged specimen before loading and 1/50 rad as the drift angle. The cracks induced by EAFP before the anti-symmetrical loading are marked in green color. During the loading, the cracks that occurred at positive loading are in black and red when the loading is negative. All sets of pictures in every cycle can be seen in appendix 1.

6.3.2.1 S_{hear} specimens

For S_{hear}-Lv1 with 0.20mm as induced crack width, flexural and flexural-shear cracks occurred when the drift angle reached 1/400 rad. At 1/200 rad, bond-splitting and shear cracks occurred near the main bar of the first layer. Finally, cracks expanded and led to shear failure.

For the S_{hear}-Lv2 with 0.55mm as induced crack width, similarly to S_{hear}-Lv1, flexural and flexural-shear cracks occurred when the drift angle reached 1/400 rad. At 1/200 rad, shear

cracks took place and drastically widened just before 1/100 rad. At 1/50 rad, bond-splitting cracks also developed around the rebar of the second layer. Finally, the spread of these cracks led to a complex failure mode dominated by shear.

For S_{hear}-Lv3 with 1.10mm as induced crack width, flexural and flexural-shear cracks occurred when the drift angle reached 1/400 rad. At 1/100 rad, bond-splitting cracks occurred near the main bar of the first layer. This was followed by bond-splitting cracks around the rebar of the second layer at 1/50 rad. Finally, the specimen failed by bond splitting.

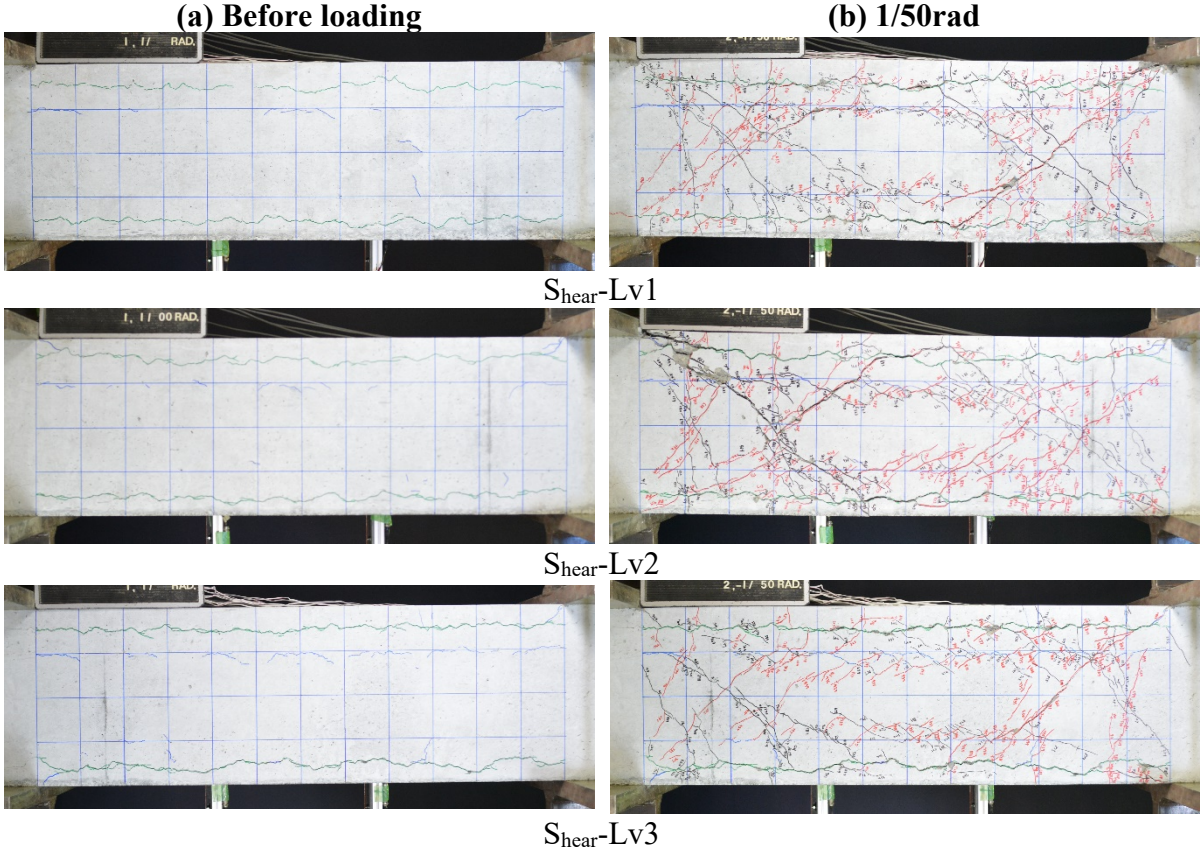

Figure 6.10 S_{hear} specimens

6.3.2.2 F_{lex}-1.5 specimens

The specimen F_{lex}-1.5-Lv1 have a maximum crack width of 0.05mm induced by EAFP. During the loading cycle of 1/400 rad, flexural cracks and flexural shear cracks took place. During the loading cycle of 1/100 rad, bond-splitting cracks occurred at the upper bar position. The flexural shear and bond splitting cracks spread and finally failed by bond splitting.

The specimen F_{lex}-1.5-Lv2 have a maximum crack width of 0.4mm induced by EAFP. During the loading cycle of 1/400 rad, flexural cracks and flexural shear cracks occurred. During the loading cycle of 1/200 rad, bond-splitting cracks occurred at the upper bar position. During the loading cycle of 1/100 rad, flexural shear and bond-splitting cracks occurred at lower bar

positions. The flexural shear cracks and bond splitting cracks spread and failed by bond splitting similarly as specimen F_{lex}-1.5-Lv1.

The specimen F_{lex}-1.5-Lv2 have a maximum crack width of 1.6mm induced by EAFP. During the loading cycle of 1/400 rad, flexural cracks occurred. During the loading cycle of 1/200 rad, bond-splitting cracks occurred at the upper bar position. No new bond-splitting crack was observed around the induced cracks of 0.8mm width or more; only the induced cracks widened

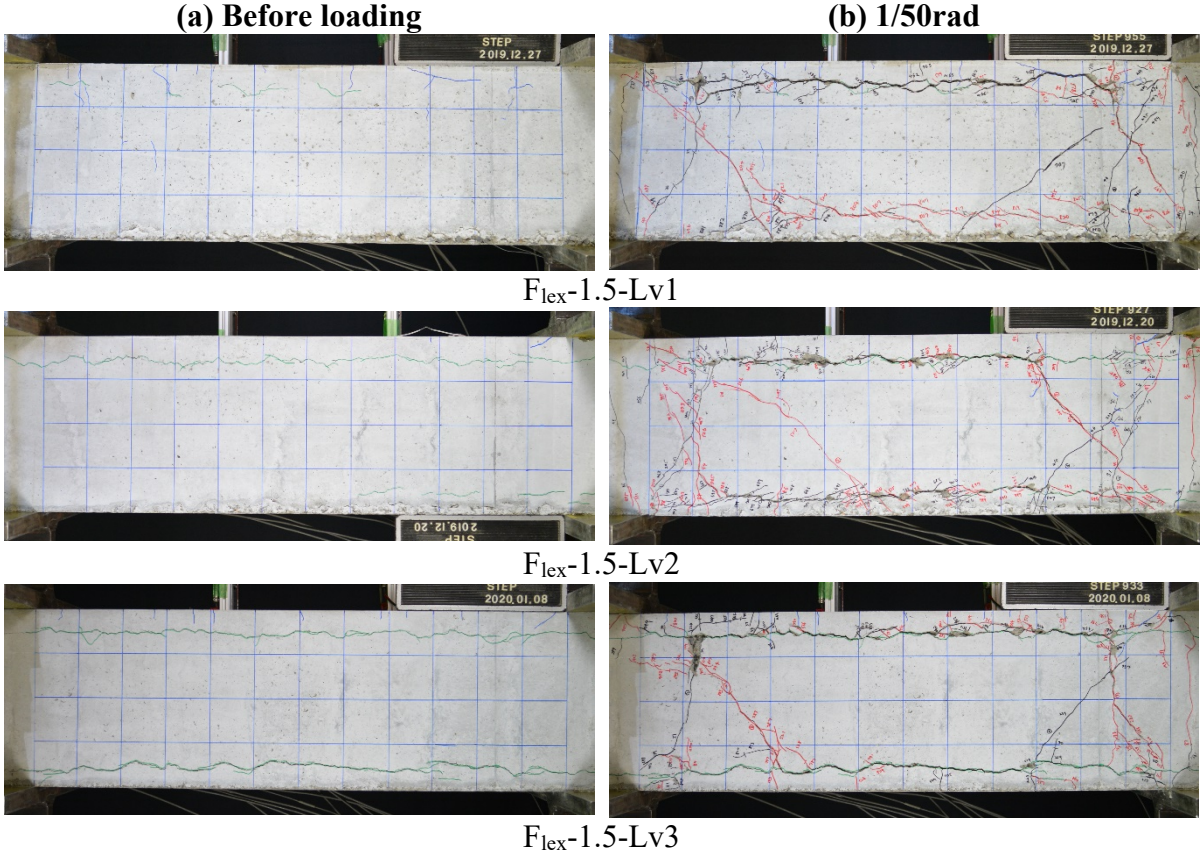

Figure 6.11 F_{lex}-1.5

6.3.2.3 F_{lex}-2.0 specimens

The specimen F_{lex}-2.0-NC is a sound reference beam without induced crack. During the loading cycle of 1/400 rad, flexural cracks and flexural shear cracks occurred. Then, bond-splitting cracks were observed along the top rebar of the beam at 1/100 rad. Further, flexural shear and bond-splitting cracks expanded, leading to bond-splitting failure of the beam.

The specimen F_{lex}-2.0-Lv1 have a maximum crack width of 0.20 mm induced by EAFP. Flexural cracks and flexural shear cracks occurred 1/400 rad as drift angle. Bond splitting cracks occurred along the top rebar of the beam at 1/100 rad. Further, flexural shear cracks and bond-splitting cracks along the top rebar lead to shear-bond failure.

The specimen F_{lex}-2.0-Lv2 have a maximum crack width of 0.60 mm induced by EAFP. Flexural cracks occurred at +1/400 rad, followed by flexural shear cracking. Flexural shear -1/400 rad. Bond splitting cracks developed top rebar at 1/100 rad. Further, the bond-splitting cracks expanded along both the top and bottom rebar. Finally, the beam failed due to extensive bond-splitting cracks.

The specimen F_{lex}-2.0-Lv3 have a maximum crack width of 1.30 mm induced by EAFP. Flexural cracks occurred after +1/400 rad. Flexural shear cracking developed at -1/400 rad. Bond splitting cracks developed along the top and bottom rebar at 1/100 rad. Further, the crack induced by EAFP widened, leading to the bam failure.

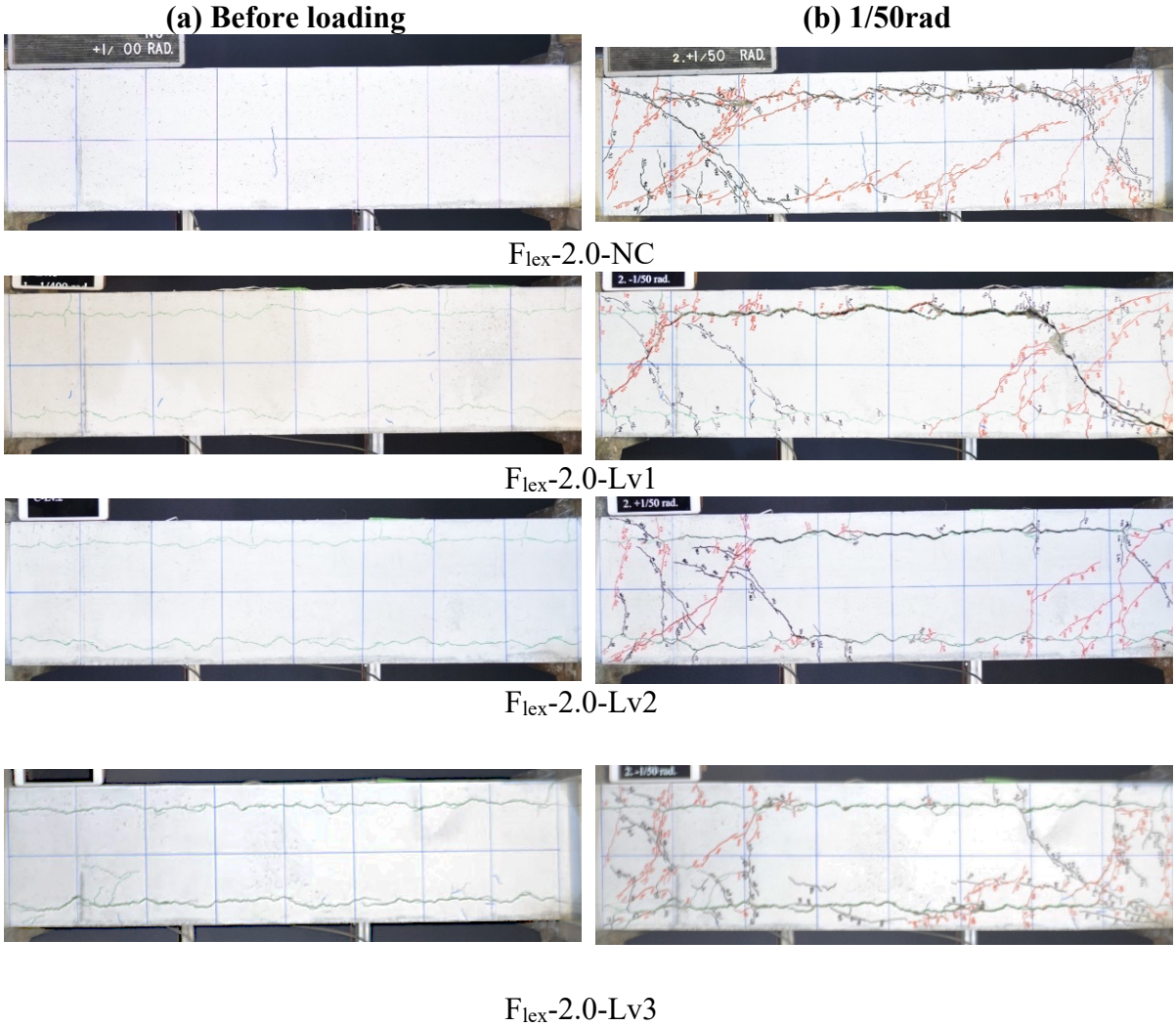

Figure 6.12 F_{lex}-2.0

6.3.3 Responses of the test specimens

6.3.3.1 Lateral force-drift angle relationships

Lateral force-drift angle responses are presented in Figure 6.13. The lateral force is the load applied by the actuator while the drift angle is calculated as the ratio of the relative displacement between the end of the specimen divided by clear span length. In general, the shear response showed a cyclic degradation defined by loss of strength and stiffness in successive cycles. Moreover, severe pinching was observed in every specimen due to the shear and slipping of main rebars opening and closing of cracks.

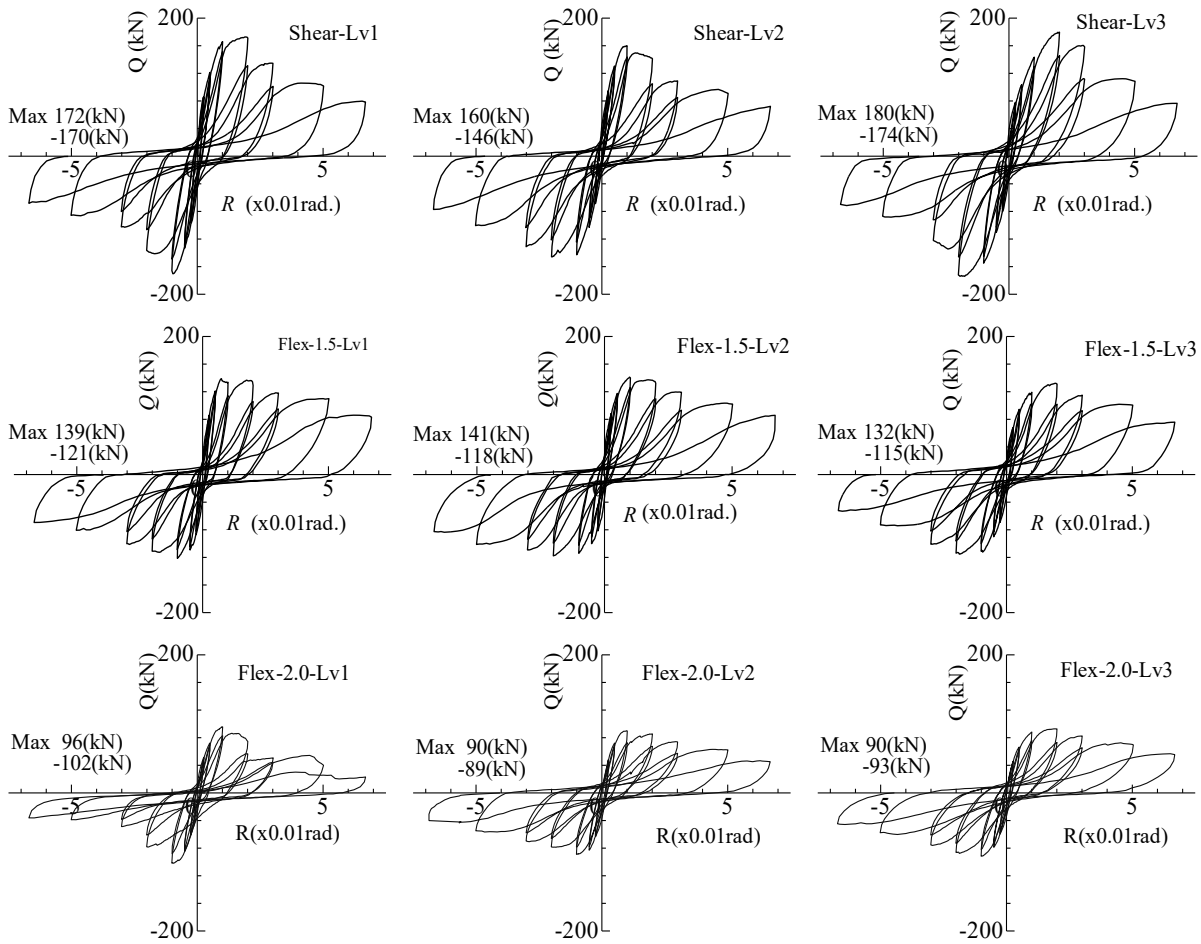

Figure 6.13 Hysteresis curve

Table 6.5 compares the maximum capacity and drift angle of tested beams. Also, the average of their positive and negative values is expressed. The width of the induced cracks before loading can switch the failure mode during antisymmetrical bending. However, no clear evidence of the reduction of maximum lateral force due to induced crack was found. The slightly seen maximum lateral force variation could be attributed to the different degradation levels of the bond, which is essential to the truss mechanism in RC beams. Although the effect

of induced crack on the maximum lateral force is complicated, the drift angle at maximum lateral force tends to increase with the increase of induced crack.

Table 6.5 Test results

Specimen ID	Induced crack width (mm)	Max. lateral force (kN)		Drift angle (x0.01rad)		Ave. Max. lateral force (kN)	Ave. drift angle (x0.01rad)	Failure mode
S_{hear}-Lv1	0.20	-170	172	-0.91	1.94	171	1.43	Shear
S_{hear}-Lv2	0.55	-146	160	-1.94	1.01	153	1.48	Shear
S_{hear}-Lv3	1.10	-174	180	-1.92	2.01	177	1.97	Bond
F_{lex}-1.5-Lv1	0.05	-121	139	-0.98	0.75	130	0.87	Bond
F_{lex}-1.5-Lv2	0.40	-118	141	-2.01	0.98	130	1.5	Bond
F_{lex}-1.5-Lv3	1.60	-115	132	-1.91	1.95	124	1.93	Induced crack widening
F_{lex}-2.0-NC	-	-91	99	-1.91	1.01	95	1.46	Bond
F_{lex}-2.0-Lv1	0.20	-102	96	-0.95	1.01	99	0.98	Shear-bond
F_{lex}-2.0-Lv2	0.60	-89	90	-0.98	0.98	90	0.98	Bond
F_{lex}-2.0-Lv3	1.30	-91	93	-1.01	1.9	92	1.46	Induced crack widening

6.3.3.2 Influence of induced cracks on maximum lateral force

The specimen "S_{hear}" is designed with lower shear resistance. Thus, a failure due to shear is expected during loading-EAFP induced a crack width of 0.20, 0.55, and 1.10 mm in specimens S_{hear}-Lv1, S_{hear}-Lv2, and S_{hear}-Lv3, respectively. Figure 6.14 shows that the shear capacity slightly decreased in S_{hear}-Lv1 and S_{hear}-Lv2 when the specimen failed by shear. However, Shear-Lv3, which is supposed to have the worst bond damage shows a higher shear capacity. This finding is consistent with Ikeda and Uji [125], who experimentally demonstrated that the shear capacity of RC beams is improved when the bond between tension rebars and concrete is destroyed. The observed increase in shear could be attributed to the arch mechanism, which is forced to form, or diagonal shear crack formation is considerably delayed.

The specimens "F_{lex}-1.5 and F_{lex}-2.0" are designed with lower flexural resistance. Thus, a failure due to higher flexure demand is expected during loading. EAFP induced a crack width of 0.05, 0.4, and 1.60 mm in specimens F_{lex}-1.5-Lv1, F_{lex}-1.5-Lv2, and F_{lex}-1.5-Lv3, respectively. F_{lex}-1.5-Lv1 and F_{lex}-1.5-Lv2 specimens failed due to bond-splitting cracks after flexural yielding. However, F_{lex}-1.5-Lv3 was affected by the widening of cracks induced by EAFP. In addition, the maximum shear forces are not influenced by the mentioned bond degradation since every beam reached maximum capacity by flexural yielding.

A crack width of 0.2, 0.6, and 1.30 mm were induced by EAFP in specimens F_{lex}-2.0-Lv1, F_{lex}-2.0-Lv2, and F_{lex}-2.0-Lv3, respectively. Specimens failed due to bond splitting cracks after flexural yielding, except F_{lex}-2.0-Lv1, which failed in shear bond. Here again, the bond deterioration due to induced cracks does not influence the maximum capacity.

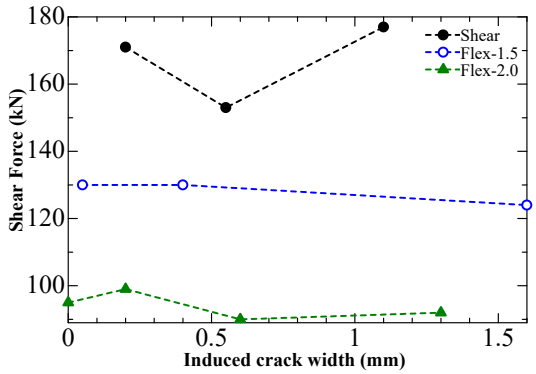

Figure 6.14 Maximum shear - induced cracks width relationships

6.3.4 Comparison of skeleton curve

A skeleton curve is the envelope of all cycle loading during antisymmetrical loading, which can reflect the seismic performance indicators of the specimen, such as shear capacity, stiffness, and ductility. The comparison of skeleton curves of tested beams is shown in Figure 6.15. The skeleton curves generally show a reduction of initial stiffness as increasing the induced crack width when the drift angle between 1/400 to 1/100rad in almost every specimen. This is likely related to the bond deterioration mainly due to cracks induced by EAFP. Further, it can be seen that the shear response slightly varies on positive and negative sides. It seems possible that the difference in the width of the induced cracks following the casting direction (as described in section 6.3.1) is also reflected in the cyclic behavior of the beams.

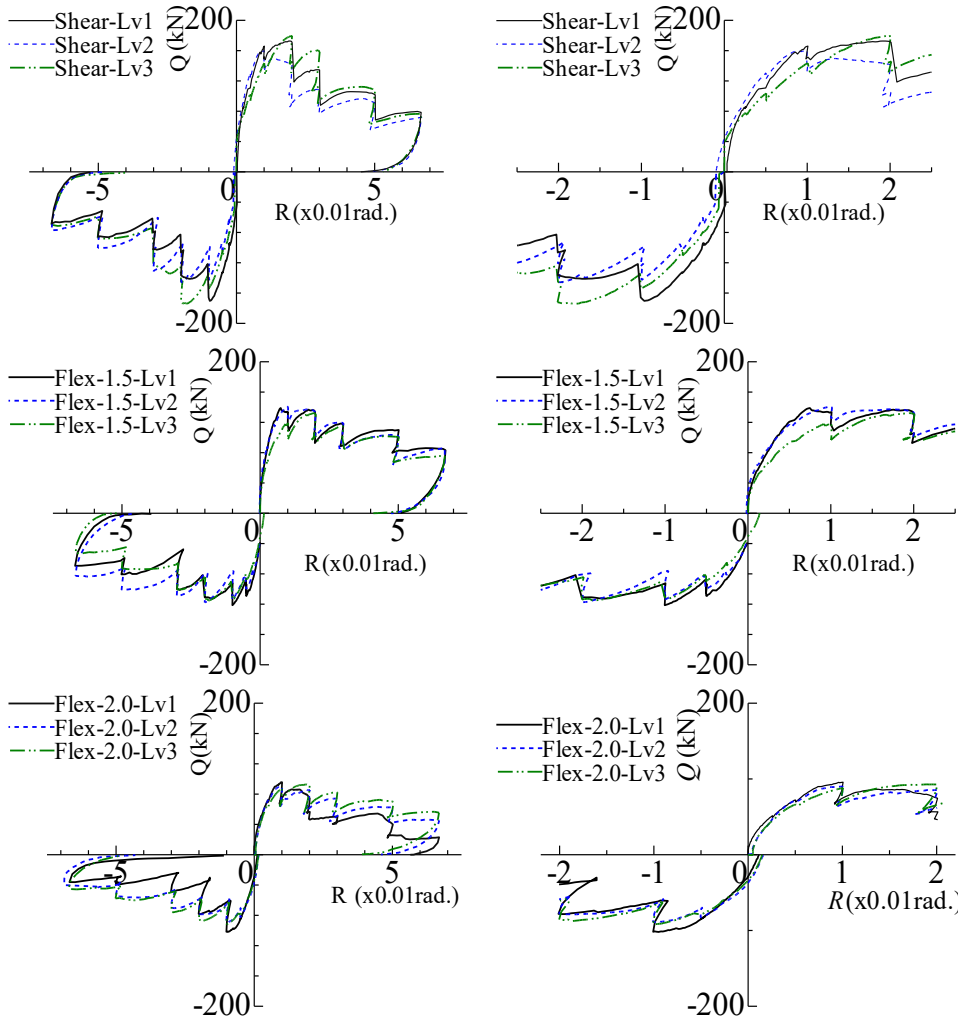

Figure 6.15 Skeleton curve

6.3.5 Peak stiffness in cracked beams

Figure 6.16 shows the stiffness at peaks in each cycle. The stiffness was calculated as the average peak in positive and negative loadings divided by the corresponding deflections at each cycle. Until 1/200 rad, the stiffness reduces with increased induced crack width before loading. This is likely related to the deterioration of tension stiffening due to local bond degradation caused by induced cracks. From 1/100 rad, the stiffness is not correlated to the induced crack width. Until this stage, the peak load almost reached a maximum capacity. Experiments carried out in this study are not enough to quantitatively evaluate the stiffness degradation due to induced crack.

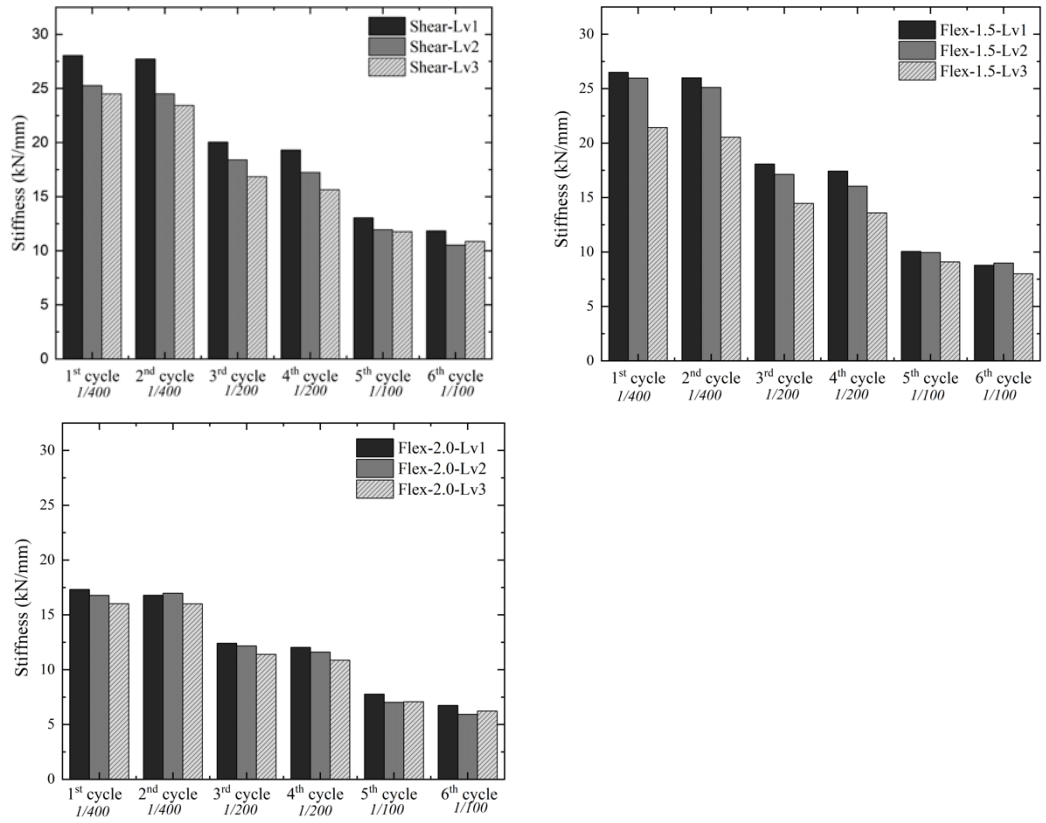

Figure 6.16 Stiffness of cracked beams

6.3.6 Energy dissipation

The energy dissipation capacity is an important indicator to evaluate the seismic behavior of specimens, which can be determined by the enclosed area of the hysteresis curve. It is noteworthy that the structure can consume or absorb most seismic energy if it has better energy dissipation capacity under earthquake loading. Here the absorbed energy quantity for every specimen is normalized by the one obtained from Level 1 or NC specimens. The comparison of this ratio is shown in Figure 6.17. As observed, the energy dissipation capacities tend to decrease with the increase of induced crack width until around 1/50 rad. This difference is partly caused by stiffness degradation due to induced crack. Furthermore, specimens with higher induced crack width show higher energy dissipation capacities after 1/50 rad. In these specimens, the bond was severely deteriorated by induced cracks. As a result, main rebars lose their ability to transmit stress to the concrete. Therefore, the concrete is not much damaged, leading to better energy dissipation.

Moreover, the energy dissipation capacity of specimens with a slight decrease in shear force was the lowest among the beams due to the combined effects of force reduction, drift capacity, and pinching seen in the hysteresis curve.

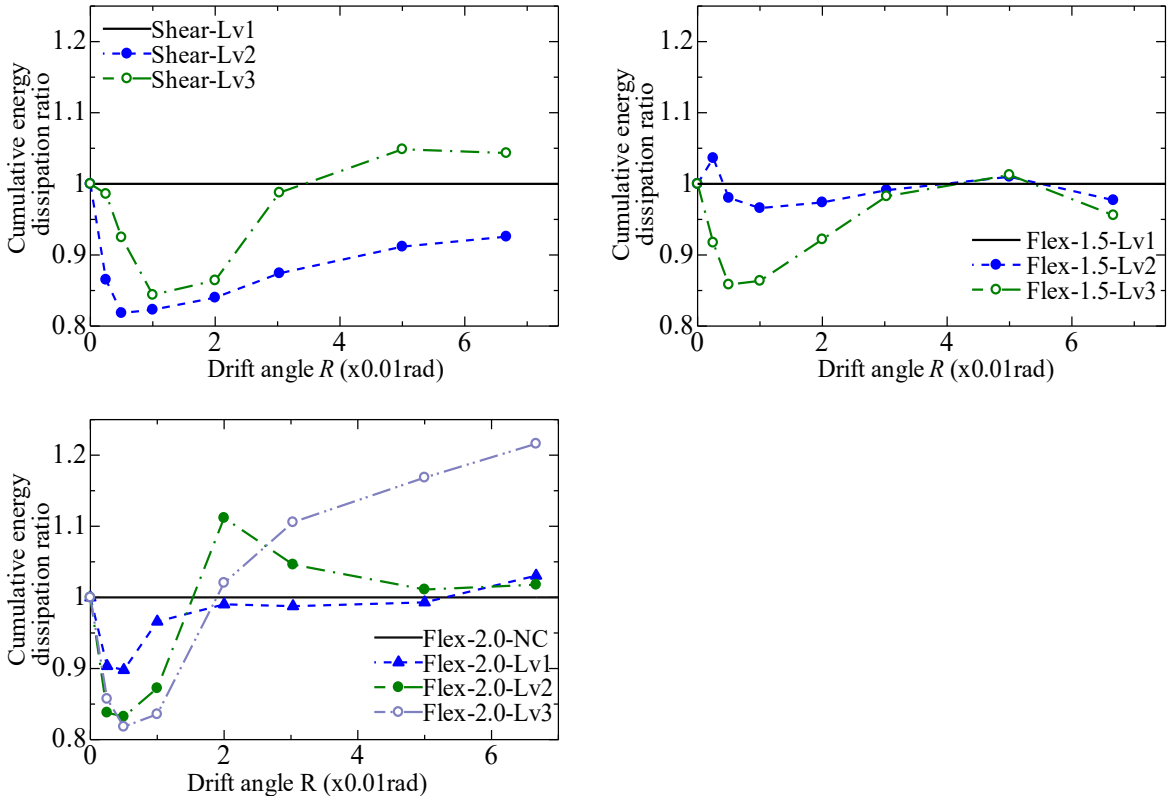

Figure 6.17 Energy dissipation

6.4 Summary

Ten RC beam specimens with different damage levels (induced crack width) were tested under antisymmetrical loading. Moreover, the effects of induced crack on the seismic behavior, such as shear capacity, stiffness and energy dissipation, are described. The following conclusions can be drawn from this study.

i. The bond degradation due to induced cracks changes the failure mode of the specimen under antisymmetric loading.

ii. The test results showed that the correlation between the maximum lateral force of specimens and induced crack width was not clear enough. Results suggest that the beam capacity degradation due to induced crack cannot be merely evaluated with the crack width as a main parameter.

iii. Significant modifications of service behavior were observed due to the bond degradations: loss of initial stiffness and reduction of energy dissipation until 1/50 rad loading.

7 CONCLUSIONS AND FUTURE RESEARCH

7.1 Conclusions

This study aims to better understand the structural behavior of deteriorated RC structures, focusing on the bond strength between deformed bars and concrete. The research program investigates degradation in concrete structures due to corrosion, considered the most common threat. At the material level, the research approach evaluates bond strength deterioration due to induced cracks caused by corrosion. Moreover, the effect of bond deterioration on the structural perforce of an RC beam is investigated at a structural level. This chapter summarizes the most relevant findings from this work.

Chapter 2: Researchers have extensively examined the impact of corrosion on the bond strength between concrete and rebar to propose empirical, theoretical, or numerical predictive models. Therefore, research programs on this topic have increased rapidly in recent years. To begin with, the literature was systematically reviewed to explore experimental methods, outcomes, and trends on this topic. Key factors that affect bond strength degradation, including concrete cover, concrete strength, and stirrups, have been documented. However, a general model is still unavailable due to discrepancies caused by differences in testing methods to evaluate the effect of corrosion on bond strength. Furthermore, researchers attempted to clarify the degradation mechanism of bond strength affected by corrosion. As a result, new alternatives have been proposed to build a practical model to assess the bond strength deterioration of corroded structures.

Chapter 3: Pull-out bond test was conducted on electrically corroded specimens to investigate the bond strength degradation in corroded concrete. These findings have significant implications for understanding how corrosion affects bond strength. Taken together, these results suggest that:

In the S1 series, the specimens were corroded; however, cracks were not observed prior to loading. The residual bond strength ratio is 1.11 to 0.85 for specimens with rebar corrosion mass loss from 3.85% to 15.27 %. The rebar corrosion does not severely affect the residual bond strength when the specimen is not cracked by corrosion.

In S2 series, the residual bond strength ratio decreases with the increase in crack width. The residual bond strength ratios vary from 1.17 to 0.65 for specimens induced cracks widths ranging from 0.15 mm to 1.00 mm in specimen without stirrup. In specimens with stirrup, the residual bond strength ratios vary from 1.17 to 0.65 for specimens induced cracks widths ranging from 0.15 mm to 1.00 mm. This demonstrates that the corrosion-related crack is primarily responsible for bond strength degradation and could be considered the primary variable.

A comparison of residual bond strength ratio in specimens S2 without and with a stirrup shows that the bond degradation in specimens without a stirrup is more severe than those with stirrups. Furthermore, we conclude that significant bond deterioration begins only when the corrosion of the stirrup is very high. However, some stirrup legs are fractured at the pitting points or almost consumed by uniform corrosion in extreme situations.

Chapter 4: EAFP was adopted to simulate cracks due to the rebar expansion related to corrosion in RC beams. In this technique is easier to target crack width because the induced crack width increases over elapsed time from filling the aluminum pipe with an expansion agent. Furthermore, the transversal cut of the cracked RC beams shows that internal side-splitting crack pattern mainly occur.

Using EAFP, two series of cracked bond test specimens considering the induced cracks pattern (single or side crack) were tested. It was seen the bond strength exponentially decrease with the increase of induced crack width in both type of specimens. We concluded that cracking without rust fundamentally causes bond strength degradation in specimen with corrosion related cracks. Additionally, the bond strength degradation is more severe in specimens with a side-splitting crack than with a single-splitting crack.

In Series S2, the bond strength degradation of the specimen without stirrup appears to be more severe than that of specimen with stirrup. This is due to the crucial role of the stirrup in providing additional confinement. First, the stirrups can effectively limit crack propagation due to EAFP. Furthermore, stirrups help to maintain the bearing between the steel bar and the concrete. However, the bond strength degradation is not significant because of a big diameter of stirrup, leading to a fully confined specimen. A systematic understanding of how the reduction in confinement provided by the stirrup contributes to bond deterioration is needed to build a formula for predicting bond degradation.

Chapter 5: To focus on the combined effect of cracking and stirrup diameter reduction on bond strength degradation, side-splitting cracks with different widths are simulated in pull-out bond specimens using EAFP.

The test result reflects the crucial role of the stirrup on the bond degradation mechanism due to induced cracks. The bond strength degradation rate is considerably fast in specimens without stirrups. However, bond strength degradation is limited in specimens with stirrup, respectively, to the stirrup ratio increase. Moreover, the stirrup can also restrict the opening of cracks induced by EAFP, leading to a more ductile failure mode.

To investigate the effect of corroded rebar shape on bond degradation, the bond degradation in specimens cracked by electrical-induced corrosion or EAFP was compared. The main difference between these two specimens is the rust presence and rebar profile change due to corrosion. The result shows no significant difference in bond degradation. Thus, we conclude that the residual bond strength ratio can be estimated by considering the single effect of cracking, ignoring the rust presence or rebar profile change. It is also confirmed that a direct relationship between bearing and crack width can ignore ambiguity related to the accumulation of corrosion products

An empirical model has been proposed to assess the bond strength degradation considering the induced crack width and the stirrup ratio. Comparisons with previous data of corroded specimens show that the proposed model can give reasonable estimations.An empirical model has been proposed to assess the bond strength degradation in specimens cracked by EAFP. The proposed degradation prediction is mainly based on induced crack width. The formula also reflects the critical role of the stirrup in limiting bond degradation. Comparisons with previous data of corroded specimens show that the proposed model can give reasonable estimations.

Chapter 6: Finally, RC beam specimens cracked by EAFP were tested under antisymmetrical loading. Moreover, the effects of induced crack on the seismic behavior, such as shear capacity, stiffness and energy dissipation, are described. It is found that bond degradation due to induced cracks change the failure mode of the specimen under antisymmetrical loading. The results showed that the correlation between the maximum capacity of specimens and induced crack width was not clear enough. As a result, it is considered that the beam capacity degradation due to induced crack cannot be merely evaluated with the crack width as the main parameter. Furthermore, it is shown that significant modifications of service behavior were observed due

to the bond degradations, namely: loss of initial stiffness and reduction of energy dissipation until 1/50 rad loading.

7.2 Suggestions for future research

This study was limited to the effect of a stirrup cross section reduction on bond strength degradation due to induced crack width. However, it is also necessary to carry out more investigation to evaluate the stirrup diameter reduction owing to corrosion.

This study showed that the induced crack width affects the initial stiffness of damaged beams. A model that describes the tension stiffening effect in cracked RC specimens is needed to evaluate the residual stiffness quantitively.

Bond strength input can be enough in hand calculations of RC beam capacity. However, a model describing the bond-slip relationship in cracked concrete is needed to conduct a numerical model that can provide a more accurate description of structural behavior.

8 REFERENCES

1. Cairns, J.; Du, Y.; Law, D. Residual Bond Strength of Corroded Plain Round Bars. *Magazine of Concrete Research* **2006**, *58*, 221–231, doi:10.1680/macr.2006.58.4.221.
2. Calvi, G.M.; Moratti, M.; O'Reilly, G.J.; Scattarreggia, N.; Monteiro, R.; Malomo, D.; Calvi, P.M.; Pinho, R. Once upon a Time in Italy: The Tale of the Morandi Bridge. *Structural Engineering International* **2019**, *29*, 198–217, doi:10.1080/10168664.2018.1558033.
3. Lu, X.; Guan, H.; Sun, H.; Li, Y.; Zheng, Z.; Fei, Y.; Yang, Z.; Zuo, L. A Preliminary Analysis and Discussion of the Condominium Building Collapse in Surfside, Florida, US, June 24, 2021. *Frontiers of Structural and Civil Engineering* **2021**, *15*, 1097–1110, doi:10.1007/s11709-021-0766-0.
4. Tepfers, R. Cracking of Concrete Cover along Anchored Deformed Reinforcing Bars. *Magazine of Concrete Research* **1979**, *31*, 3–12, doi:10.1680/macr.1979.31.106.3.
5. Auyeung, Y.; Balaguru, P.; Lan, C. Bond Behavior of Corroded Reinforcement Bars. *ACI Materials Journal* **2000**, *97*, doi:10.14359/826.
6. Li, C.Q.; Zheng, J.J. Propagation of Reinforcement Corrosion in Concrete and Its Effects on Structural Deterioration. *Magazine of Concrete Research* **2005**, *57*, 261–271, doi:10.1680/macr.2005.57.5.261.
7. Lundgren, K. Effect of Corrosion on the Bond between Steel and Concrete: An Overview. *Magazine of Concrete Research* **2007**, *59*, 447–461, doi:10.1680/macr.2007.59.6.447.
8. Mancini, G.; Tondolo, F. Effect of Bond Degradation Due to Corrosion – a Literature Survey. *Structural Concrete* **2014**, *15*, 408–418, doi:10.1002/suco.201300009.
9. Lin, H.; Zhao, Y.; Feng, P.; Ye, H.; Ozbolt, J.; Jiang, C.; Yang, J.-Q. State-of-the-Art Review on the Bond Properties of Corroded Reinforcing Steel Bar. *Construction and Building Materials* **2019**, *213*, 216–233, doi:10.1016/j.conbuildmat.2019.04.077.
10. Palmatier, R.W.; Houston, M.B.; Hulland, J. Review Articles: Purpose, Process, and Structure. *Journal of the Academy of Marketing Science* **2018**, *46*, 1–5, doi:10.1007/s11747-017-0563-4.
11. Denyer, D.; Tranfield, D. Producing a Systematic Review. In *The Sage handbook of organizational research methods.*; Sage Publications Ltd: Thousand Oaks, CA, 2009; pp. 671–689 ISBN 978-1-4129-3118-2.
12. Vieira, E.L.; Costa, S.E.G. da; Lima, E.P. de; Ferreira, C.C. Application of the Proknow-C Methodology in the Search of Literature on Performance Indicators for Energy Management in Manufacturing and Industry 4.0. *Procedia Manufacturing* **2019**, *39*, 1259–1269, doi:https://doi.org/10.1016/j.promfg.2020.01.343.
13. Page, M.J.; McKenzie, J.E.; Bossuyt, P.M.; Boutron, I.; Hoffmann, T.C.; Mulrow, C.D.; Shamseer, L.; Tetzlaff, J.M.; Akl, E.A.; Brennan, S.E.; et al. The PRISMA 2020 Statement: An Updated Guideline for Reporting Systematic Reviews. *BMJ* **2021**, *372*, doi:10.1136/bmj.n71.

14. Haddaway, N.R.; Macura, B.; Whaley, P.; Pullin, A.S. ROSES Reporting Standards for Systematic Evidence Syntheses: Pro Forma, Flow-Diagram and Descriptive Summary of the Plan and Conduct of Environmental Systematic Reviews and Systematic Maps. *Environmental Evidence* **2018**, *7*, 7, doi:10.1186/s13750-018-0121-7.
15. Zavadskas, E.K.; Skibniewski, M.J.; Antucheviciene, J. Performance Analysis of Civil Engineering Journals Based on the Web of Science® Database. *Archives of Civil and Mechanical Engineering* **2014**, *14*, 519–527, doi:10.1016/j.acme.2014.05.008.
16. Https://Www.Webofscience.Com/Wos/Woscc/Summary/Fec308eb-7829-4714-Ba99-38eee89b981e-3df70ef2/Relevance/1e 2022.
17. Lundgren, K.; Tahershamsi, M.; Zandi, K.; Plos, M. Tests on Anchorage of Naturally Corroded Reinforcement in Concrete. *Materials and Structures* **2015**, *48*, 2009–2022, doi:10.1617/s11527-014-0290-y.
18. Tahershamsi, M.; Fernandez, I.; Lundgren, K.; Zandi, K. Investigating Correlations between Crack Width, Corrosion Level and Anchorage Capacity. *Structure and Infrastructure Engineering* **2017**, *13*, 1294–1307, doi:10.1080/15732479.2016.1263673.
19. Tahershamsi, M.; Zandi, K.; Lundgren, K.; Plos, M. Anchorage of Naturally Corroded Bars in Reinforced Concrete Structures. *Magazine of Concrete Research* **2014**, *66*, 729–744, doi:10.1680/macr.13.00276.
20. Robuschi, S.; Sumearll, J.; Fernandez, I.; Lundgren, K. Bond of Naturally Corroded, Plain Reinforcing Bars in Concrete. *Structure and Infrastructure Engineering* **2021**, *17*, 792–808, doi:10.1080/15732479.2020.1768273.
21. Lundgren, K.; Robuschi, S.; Zandi, K. Methodology for Testing Rebar-Concrete Bond in Specimens from Decommissioned Structures. *International Journal of Concrete Structures and Materials* **2019**, *13*, 38, doi:10.1186/s40069-019-0350-3.
22. Feng, W.; Tarakbay, A.; Ali Memon, S.; Tang, W.; Cui, H. Methods of Accelerating Chloride-Induced Corrosion in Steel-Reinforced Concrete: A Comparative Review. *Construction and Building Materials* **2021**, *289*, 123165, doi:10.1016/j.conbuildmat.2021.123165.
23. Shang, H.; Chai, X. Bond Behavior between Corroded Steel Bar and Concrete under Reciprocating Loading History of Beam Type Specimens. *Engineering Structures* **2021**, *247*, 113112, doi:10.1016/j.engstruct.2021.113112.
24. Chai, X.; Shang, H.; Zhang, C. Bond Behavior between Corroded Steel Bar and Concrete under Sustained Load. *Construction and Building Materials* **2021**, *310*, 125122, doi:10.1016/j.conbuildmat.2021.125122.
25. Zhang Xuhui; Wang Lei; Zhang Jianren; Liu Yongming Bond Degradation–Induced Incompatible Strain between Steel Bars and Concrete in Corroded RC Beams. *Journal of Performance of Constructed Facilities* **2016**, *30*, 04016058, doi:10.1061/(ASCE)CF.1943-5509.0000921.
26. Zhao, Y.; Lin, H.; Wu, K.; Jin, W. Bond Behaviour of Normal/Recycled Concrete and Corroded Steel Bars. *Construction and Building Materials* **2013**, *48*, 348–359, doi:10.1016/j.conbuildmat.2013.06.091.
27. Mangat, P.S.; Elgarf, M.S. Bond Characteristics of Corroding Reinforcement in Concrete Beams. *Materials and Structures* **1999**, *32*, 89–97, doi:10.1007/BF02479434.

28. ACI Committee 408 408R-03: Bond and Development of Straight Reinforcing Bars in Tension. *Technical Documents* **2003**.

29. Chana, P.S. A Test Method to Establish Realistic Bond Stresses. *Magazine of Concrete Research* **1990**, *42*, 83–90, doi:10.1680/macr.1990.42.151.83.

30. Hanjari, K.Z.; Coronelli, D.; Lundgren, K. Bond Capacity of Severely Corroded Bars with Corroded Stirrups. *Magazine of Concrete Research* **2011**, *63*, 953–968, doi:10.1680/macr.10.00200.

31. Almusallam, A.A.; Al-Gahtani, A.S.; Aziz, A.R.; Rasheeduzzafar Effect of Reinforcement Corrosion on Bond Strength. *Construction and Building Materials* **1996**, *10*, 123–129, doi:10.1016/0950-0618(95)00077-1.

32. G. J. Al-Sulaimani, M.K., I.A. Basunbul, and Rasheeduzzafar Influence of Corrosion and Cracking on Bond Behavior and Strength of Reinforced Concrete Members. *ACI Structural Journal* **1990**, *87*, doi:10.14359/2732.

33. Lamya Amleh and Saeed Mirza Corrosion Influence on Bond between Steel and Concrete. *ACI Structural Journal* **1999**, *96*, doi:10.14359/676.

34. Banba, S.; Abe, T.; Nagaoka, K.; Murakami, Y. Evaluation Method for Bond-Splitting Behavior of Reinforced Concrete with Corrosion Based on Confinement Stress of Concrete against Corrosion Expansion. *Journal of Advanced Concrete Technology* **2014**, *12*, 7–23, doi:10.3151/jact.12.7.

35. Ma, Y.; Guo, Z.; Wang, L.; Zhang, J. Experimental Investigation of Corrosion Effect on Bond Behavior between Reinforcing Bar and Concrete. *Construction and Building Materials* **2017**, *152*, 240–249, doi:10.1016/j.conbuildmat.2017.06.169.

36. Jiang, C.; Wu, Y.-F.; Dai, M.-J. Degradation of Steel-to-Concrete Bond Due to Corrosion. *Construction and Building Materials* **2018**, *158*, 1073–1080, doi:10.1016/j.conbuildmat.2017.09.142.

37. Choi, Y.S.; Yi, S.-T.; Kim, M.Y.; Jung, W.Y.; Yang, E.I. Effect of Corrosion Method of the Reinforcing Bar on Bond Characteristics in Reinforced Concrete Specimens. *Construction and Building Materials* **2014**, *54*, 180–189, doi:10.1016/j.conbuildmat.2013.12.065.

38. Coccia, S.; Imperatore, S.; Rinaldi, Z. Influence of Corrosion on the Bond Strength of Steel Rebars in Concrete. *Materials and Structures* **2016**, *49*, 537–551, doi:10.1617/s11527-014-0518-x.

39. Fang, C.; Lundgren, K.; Chen, L.; Zhu, C. Corrosion Influence on Bond in Reinforced Concrete. *Cement and Concrete Research* **2004**, *34*, 2159–2167, doi:10.1016/j.cemconres.2004.04.006.

40. Fang, C.; Lundgren, K.; Plos, M.; Gylltoft, K. Bond Behaviour of Corroded Reinforcing Steel Bars in Concrete. *Cement and Concrete Research* **2006**, *36*, 1931–1938, doi:10.1016/j.cemconres.2006.05.008.

41. Yalciner, H.; Eren, O.; Sensoy, S. An Experimental Study on the Bond Strength between Reinforcement Bars and Concrete as a Function of Concrete Cover, Strength and Corrosion Level. *Cement and Concrete Research* **2012**, *42*, 643–655, doi:10.1016/j.cemconres.2012.01.003.

42. Yalciner Hakan; Marar Khaled Experimental Study on the Bond Strength of Different Geometries of Corroded and Uncorroded Reinforcement Bars. *Journal of Materials in Civil Engineering* **2017**, *29*, 05017002, doi:10.1061/(ASCE)MT.1943-5533.0001914.

43. Chung, L.; Jay Kim, J.-H.; Yi, S.-T. Bond Strength Prediction for Reinforced Concrete Members with Highly Corroded Reinforcing Bars. *Cement and Concrete Composites* **2008**, *30*, 603–611, doi:10.1016/j.cemconcomp.2008.03.006.

44. Zhou, H.; Qiao, M.; Du, Y.; Liu, J.; Zhou, Y.; Mo, Y.; Xing, F.; Zhao, Y. Bond Degradation of Rebar and Concrete Confined with Corroded Stirrups: Effects of Concrete Grade and Casting Position. *Magazine of Concrete Research* **2022**, *0*, 1–17, doi:10.1680/jmacr.21.00122.

45. Zhou, H.; Liang, X.; Wang, Z.; Zhang, X.; Xing, F. Bond Deterioration of Corroded Steel in Two Different Concrete Mixes. *Structural Engineering and Mechanics* **2017**, *63*, 725–734, doi:10.12989/sem.2017.63.6.725.

46. Zhou, H.J.; Liang, X.B.; Zhang, X.L.; Lu, J.L.; Xing, F.; Mei, L. Variation and Degradation of Steel and Concrete Bond Performance with Corroded Stirrups. *Construction and Building Materials* **2017**, *138*, 56–68, doi:10.1016/j.conbuildmat.2017.02.007.

47. Wu, Y.F.; Zhao, X.M. Unified Bond Stress Slip Model for Reinforced Concrete. *Journal of Structural Engineering* **2013**, *139*, 1951–1962, doi:10.1061/(ASCE)ST.1943-541X.0000747.

48. Lin, H.; Zhao, Y.; Yang, J.-Q.; Feng, P.; Ozbolt, J.; Ye, H. Effects of the Corrosion of Main Bar and Stirrups on the Bond Behavior of Reinforcing Steel Bar. *Construction and Building Materials* **2019**, *225*, 13–28, doi:10.1016/j.conbuildmat.2019.07.156.

49. Lin, H.; Zhao, Y. Effects of Confinements on the Bond Strength between Concrete and Corroded Steel Bars. *Construction and Building Materials* **2016**, *118*, 127–138, doi:10.1016/j.conbuildmat.2016.05.040.

50. Moodi, Y.; Sohrabi, M.R.; Mousavi, S.R. Corrosion Effect of the Main Rebar and Stirrups on the Bond Strength of RC Beams. *Structures* **2021**, *32*, 1444–1454, doi:10.1016/j.istruc.2021.03.096.

51. Tondolo, F. Bond Behaviour with Reinforcement Corrosion. *Construction and Building Materials* **2015**, *93*, 926–932, doi:10.1016/j.conbuildmat.2015.05.067.

52. Zheng, Y.; Zheng, S.-S.; Yang, L.; Dong, L.-G.; Zhang, Y.-B. Experimental Study and Analytical Model of the Bond Behavior of Corroded Reinforcing Steel Bars in Concrete. *Construction and Building Materials* **2022**, *327*, 126991, doi:https://doi.org/10.1016/j.conbuildmat.2022.126991.

53. Zhou, H.; Lu, J.; Xv, X.; Dong, B.; Xing, F. Effects of Stirrup Corrosion on Bond–Slip Performance of Reinforcing Steel in Concrete: An Experimental Study. *Construction and Building Materials* **2015**, *93*, 257–266, doi:10.1016/j.conbuildmat.2015.05.122.

54. Feng, Q.; Zhang, Y.; Visintin, P.; Xu, R. Stirrup Effects on the Bond Properties of Corroded Reinforced Concrete. *Magazine of Concrete Research* **2021**, *73*, 1151–1166, doi:10.1680/jmacr.19.00531.

55. Moodi, Y.; Sohrabi, M.R.; Mousavi, S.R. Effects of Stirrups in Spliced Region on the Bond Strength of Corroded Splices in Reinforced Concrete (RC) Beams. *Construction and Building Materials* **2020**, *230*, doi:10.1016/j.conbuildmat.2019.116873.

56. Arnaud Castel, I.K., Raoul François, and Raymond Ian Gilbert Modeling Steel Concrete Bond Strength Reduction Due to Corrosion. *ACI Structural Journal* **2016**, *113*, doi:10.14359/51688925.
57. Wang, X.; Liu, X. Bond Strength Modeling for Corroded Reinforcement in Reinforced Concrete. *Structural Engineering and Mechanics* **2004**, *17*, 863–878, doi:10.12989/sem.2004.17.6.863.
58. Wang, X.; Liu, X. Bond Strength Modeling for Corroded Reinforcements. *Construction and Building Materials* **2006**, *20*, 177–186, doi:10.1016/j.conbuildmat.2005.01.015.
59. Bhargava, K.; Ghosh, A.K.; Mori, Y.; Ramanujam, S. Models for Corrosion-Induced Bond Strength Degradation in Reinforced Concrete. *ACI Materials Journal* **2007**, *104*, 594–603.
60. Bhargava, K.; Ghosh, A.K.; Mori, Y.; Ramanujam, S. Corrosion-Induced Bond Strength Degradation in Reinforced Concrete—Analytical and Empirical Models. *Nuclear Engineering and Design* **2007**, *237*, 1140–1157, doi:10.1016/j.nucengdes.2007.01.010.
61. Prieto, M.; Tanner, P.; Andrade, C. Multiple Linear Regression Model for the Assessment of Bond Strength in Corroded and Non-Corroded Steel Bars in Structural Concrete. *Materials and Structures* **2016**, *49*, 4749–4763, doi:10.1617/s11527-016-0822-8.
62. Güneyisi, E.M.; Mermerdaş, K.; Gültekin, A. Evaluation and Modeling of Ultimate Bond Strength of Corroded Reinforcement in Reinforced Concrete Elements. *Materials and Structures* **2016**, *49*, 3195–3215, doi:10.1617/s11527-015-0713-4.
63. Concha, N.C.; Oreta, A.W.C. Investigation of the Effects of Corrosion on Bond Strength of Steel in Concrete Using Neural Network. *Computers and Concrete* **2021**, *28*, 77–91, doi:10.12989/cac.2021.28.1.077.
64. Tanyildizi Harun Predicting Bond Strength of Corroded Reinforcement by Deep Learning. *Computers and Concrete* **2022**, *29*, 145–159, doi:10.12989/CAC.2022.29.3.145.
65. Wang, Y.; Geem, Z.W.; Nagai, K. Bond Strength Assessment of Concrete-Corroded Rebar Interface Using Artificial Neutral Network. *Applied Sciences* **2020**, *10*, doi:10.3390/app10144724.
66. Dauji, S. Bond Strength of Corroded Reinforcement in Concrete: Neural and Tree Based Approaches. *Structural Monitoring and Maintenance* **2021**, *8*, 235–255, doi:10.12989/smm.2021.8.3.235.
67. Blomfors, M. Data for: Engineering Bond Model for Corroded Reinforcement 2017.
68. Bhargava, K.; Ghosh, A.K.; Mori, Y.; Ramanujam, S. Suggested Empirical Models for Corrosion-Induced Bond Degradation in Reinforced Concrete. *Journal of Structural Engineering* **2008**, *134*, 221–230, doi:10.1061/(ASCE)0733-9445(2008)134:2(221).
69. Lee, H.; Noguchi, T.; Tomosawa, F. Evaluation of the Bond Properties between Concrete and Reinforcement as a Function of the Degree of Reinforcement Corrosion. *Cement and Concrete Research* **2002**, *32*, 1313–1318, doi:10.1016/S0008-8846(02)00783-4.
70. Cabrera, J.G. Deterioration of Concrete Due to Reinforcement Steel Corrosion. *Cement and Concrete Composites* **1996**, *18*, 47–59, doi:10.1016/0958-9465(95)00043-7.
71. Stanish, K.; Hooton, R.; Pantazopoulou, S. Corrosion Effects on Bond Strength in Reinforced Concrete. *ACI Structural Journal* **1999**, *96*, 915–921.

72. Denglei Tang, D.W.L., and Rebecca Gravina, Thomas K.C. Molyneaux Influence of Surface Crack Width on Bond Strength of Reinforced Concrete. *ACI Materials Journal* **2011**, *108*, doi:10.14359/51664213.

73. Law, D.W.; Molyneaux, T.C.K. Impact of Corrosion on Bond in Uncracked Concrete with Confined and Unconfined Rebar. *Construction and Building Materials* **2017**, *155*, 550–559, doi:10.1016/j.conbuildmat.2017.08.112.

74. Law, D.W.; Tang, D.; Molyneaux, T.K.C.; Gravina, R. Impact of Crack Width on Bond: Confined and Unconfined Rebar. *Materials and Structures* **2011**, *44*, 1287–1296, doi:10.1617/s11527-010-9700-y.

75. Lin, H.; Zhao, Y.; Ožbolt, J.; Reinhardt, H.-W. Bond Strength Evaluation of Corroded Steel Bars via the Surface Crack Width Induced by Reinforcement Corrosion. *Engineering Structures* **2017**, *152*, 506–522, doi:10.1016/j.engstruct.2017.08.051.

76. Walraven, J. *Model Code 2010 - First Complete Draft, Volume 2*; 2010; ISBN 978-2-88394-095-6.

77. Apostolopoulos, C.Alk.; Koulouris, K.F.; Apostolopoulos, A.Ch. Correlation of Surface Cracks of Concrete Due to Corrosion and Bond Strength (between Steel Bar and Concrete). *Advances in Civil Engineering* **2019**, *2019*, doi:10.1155/2019/3438743.

78. Koulouris, K.; Apostolopoulos, C. An Experimental Study on Effects of Corrosion and Stirrups Spacing on Bond Behavior of Reinforced Concrete. *Metals* **2020**, *10*, doi:10.3390/met10101327.

79. Koulouris, K.; Apostolopoulos, C. Study of the Residual Bond Strength between Corroded Steel Bars and Concrete—A Comparison with the Recommendations of Fib Model Code 2010. *Metals* **2021**, *11*, doi:10.3390/met11050757.

80. Fu, X.; Chung, D. Effect of Corrosion on the Bond between Concrete and Steel Rebar. *Cement and Concrete Research* **1997**, *27*, 1811–1815, doi:10.1016/S0008-8846(97)00172-5.

81. Saether, I. Bond Deterioration of Corroded Steel Bars in Concrete. *Structure and Infrastructure Engineering* **2011**, *7*, 415–429, doi:10.1080/15732470802674836.

82. Kurklu, G.; Baspinar, M.S.; Ergun, A. A Comparative Study on Bond of Different Grade Reinforcing Steels in Concrete under Accelerated Corrosion. *Steel and Composite Structures* **2013**, *14*, 229–242.

83. Alonso, C.; Andrade, C.; Rodriguez, J.; Diez, J.M. Factors Controlling Cracking of Concrete Affected by Reinforcement Corrosion. *Materials and Structures* **1998**, *31*, 435–441, doi:10.1007/BF02480466.

84. Coronelli, D. Corrosion Cracking and Bond Strength Modeling for Corroded Bars in Reinforced Concrete. *ACI Structural Journal* **2002**, *99*, 267–276.

85. El Maaddawy Tamer A.; Soudki Khaled A. Effectiveness of Impressed Current Technique to Simulate Corrosion of Steel Reinforcement in Concrete. *Journal of Materials in Civil Engineering* **2003**, *15*, 41–47, doi:10.1061/(ASCE)0899-1561(2003)15:1(41).

86. Zhu, W.; Dai, J.-G.; Poon, C.-S. Prediction of the Bond Strength between Non-Uniformly Corroded Steel Reinforcement and Deteriorated Concrete. *Construction and Building Materials* **2018**, *187*, 1267–1276, doi:10.1016/j.conbuildmat.2018.07.139.

87. Fu, C.; Fang, D.; Ye, H.; Huang, L.; Wang, J. Bond Degradation of Non-Uniformly Corroded Steel Rebars in Concrete. *Engineering Structures* **2021**, *226*, doi:10.1016/j.engstruct.2020.111392.

88. Li, C.; Song, L.; Qu, F.; Li, X.; Zhao, S. Study on Sectional Nonuniform Corrosion and Bond Strength of Plain Rebar Embedded in Concrete. *KSCE Journal of Civil Engineering* **2021**, *25*, 3031–3040, doi:10.1007/s12205-021-1729-7.

89. Abouhussien, A.A.; Hassan, A.A.A. Acoustic Emission-Based Analysis of Bond Behavior of Corroded Reinforcement in Existing Concrete Structures. *Structural Control and health Monitoring* **2017**, *24*, doi:10.1002/stc.1893.

90. Tian, Y.; Liu, J.; Xiao, H.; Zhang, Y.; Mo, Q.; Shen, J.; Shi, J. Experimental Study on Bond Performance and Damage Detection of Corroded Reinforced Concrete Specimens. *Advances in Civil Engineering* **2020**, *2020*, doi:10.1155/2020/7658623.

91. Avadh, K.; Jiradilok, P.; Bolander, J.E.; Nagai, K. Direct Observation of the Local Bond Behavior between Corroded Reinforcing Bars and Concrete Using Digital Image Correlation. *Cement and Concrete Composites* **2021**, *123*, doi:10.1016/j.cemconcomp.2021.104180.

92. Ouglova, A.; Berthaud, Y.; Fcot, F.; Francois, M.; Ragueneau, F.; Petre-Lazar, I. The Influence of Corrosion on Bond Properties between Concrete and Reinforcement in Concrete Structures. *Materials and Structures* **2008**, *41*, 969–980, doi:10.1617/s11527-007-9298-x.

93. Yang, Y.; Nakamura, H.; Miura, T.; Yamamoto, Y. Effect of Corrosion-Induced Crack and Corroded Rebar Shape on Bond Behavior. *Structural Concrete* **2019**, *20*, 2171–2182, doi:10.1002/suco.201800313.

94. Mak, M.W.T.; Desnerck, P.; Lees, J.M. Corrosion-Induced Cracking and Bond Strength in Reinforced Concrete. *Construction and Building Materials* **2019**, *208*, 228–241, doi:10.1016/j.conbuildmat.2019.02.151.

95. Kearsley, E.P.; Joyce, A. Effect of Corrosion Products on Bond Strength and Flexural Behaviour of Reinforced Concrete Slabs. *Journal of the South Africa Institution of Civil Engineering* **2014**, *56*, 21–29.

96. Jiradilok, P.; Wang, Y.; Nagai, K.; Matsumoto, K. Development of Discrete Meso-Scale Bond Model for Corrosion Damage at Steel-Concrete Interface Based on Tests with/without Concrete Damage. *Construction and Building Materials* **2020**, *236*, 117615, doi:10.1016/j.conbuildmat.2019.117615.

97. Jiradilok, P.; Nagai, K.; Matsumoto, K. Meso-Scale Modeling of Non-Uniformly Corroded Reinforced Concrete Using 3D Discrete Analysis. *Engineering Structures* **2019**, *197*, 109378, doi:10.1016/j.engstruct.2019.109378.

98. Desnerck, P.; Lees, J.M.; Morley, C.T. Bond Behaviour of Reinforcing Bars in Cracked Concrete. *Construction and Building Materials* **2015**, *94*, 126–136, doi:10.1016/j.conbuildmat.2015.06.043.

99. Mousavi, S.S.; Guizani, L.; Ouellet-Plamondon, C.M. On Bond-Slip Response and Development Length of Steel Bars in Pre-Cracked Concrete. *Construction and Building Materials* **2019**, *199*, 560–573, doi:10.1016/j.conbuildmat.2018.12.039.

100. Callahan, J.P.; Lott, J.L.; Kesler, C.E. Bridge Deck Deterioration and Crack Control. *Journal of the Structural Division* **1970**, *96*, 2021–2036, doi:10.1061/JSDEAG.0002714.

101. Bažant, Z.P. Physical Model for Steel Corrosion in Concrete Sea Structures-Application. *Journal of the Structural Division* **1979**, *105*, 1155–1166, doi:10.1061/JSDEAG.0005169.

102. Tsusumi, T.; Matsushima, M.; Murakami, Y.; Seki, H. Study on crack models caused by pressure due to corrosion products. *Japan Society Civil Engineer (JSCE) ronbbun shu* **1996**, *30 (2)*, 159–166, doi:10.2208/jscej.1996.532_159.

103. Andrade, C.; Alonso, C. Corrosion Rate Monitoring in the Laboratory and On-Site. *Construction and Building Materials* **1996**, *10*, 315–328, doi:10.1016/0950-0618(95)00044-5.

104. Alonso, C.; Andrade, C.; Rodriguez, J.; Diez, J.M. Factors Controlling Cracking of Concrete Affected by Reinforcement Corrosion. *Materials and Structures* **1998**, *31*, 435–441, doi:10.1007/BF02480466.

105. Mangat, P.S.; Elgarf, M.S. Bond Characteristics of Corrding Reinforcement in Concrete Beams. *Materials and Structures* **1999**, *32*, 89, doi:10.1007/BF02479434.

106. Yuan, Y.; Ji, Y.; Shah, S.P. Comparison of Two Accelerated Corrosion Techniques for Concrete Structures. *ACI Structural Journal* **2007**, *104*, 344–347.

107. Jamali, A.; Angst, U.; Adey, B.; Elsener, B. Modeling of Corrosion-Induced Concrete Cover Cracking: A Critical Analysis. *Construction and Building Materials* **2013**, *42*, 225–237, doi:10.1016/j.conbuildmat.2013.01.019.

108. Mak, M.W.T.; Desnerck, P.; Lees, J.M. Corrosion-Induced Cracking and Bond Strength in Reinforced Concrete. *Construction and Building Materials* **2019**, *208*, 228–241, doi:https://doi.org/10.1016/j.conbuildmat.2019.02.151.

109. Zhao, Y.; Yu, J.; Hu, B.; Jin, W. Crack Shape and Rust Distribution in Corrosion-Induced Cracking Concrete. *Corrosion Science* **2012**, *55*, 385–393, doi:10.1016/j.corsci.2011.11.002.

110. Gambarova, P.G.; Rosati, G.P.; Zasso, B. Steel-to-Concrete Bond after Concrete Splitting: Test Results. *Materials and Structures* **1989**, *22*, 35–47, doi:10.1007/BF02472693.

111. Djerbi, A.; Bonnet, S.; Khelidj, A.; Baroghel-bouny, V. Influence of Traversing Crack on Chloride Diffusion into Concrete. *Cement and Concrete Research* **2008**, *38*, 877–883, doi:10.1016/j.cemconres.2007.10.007.

112. De Silva, R.V.; Pathegama Gamage, R.; Anne Perera, M.S. An Alternative to Conventional Rock Fragmentation Methods Using SCDA: A Review. *Energies* **2016**, *9*, doi:10.3390/en9110958.

113. Yasojima, A.; Kanakubo, T. Bond Splitting Strength of RC Members Based on Local Bond Stress and Slip Behaviour.; 2005.

114. Giuriani, E.; Plizzari, G.; Schumm, C. Role of Stirrups and Residual Tensile Strength of Cracked Concrete on Bond. *Journal of Structural Engineering* **1991**, *117*, 1–18, doi:10.1061/(ASCE)0733-9445(1991)117:1(1).

115. Liu, S. The Research on Shear Capacity of Corroded Rc Beams. PhD Thesis, PhD Thesis, Master's thesis, Central South University, China, 2013.

116. Rodriguez, J.; Ortega, L.; Casal, J. Load Carrying Capacity of Concrete Structures with Corroded Reinforcement. *Construction and Building Materials* **1997**, *11*, 239–248, doi:10.1016/S0950-0618(97)00043-3.

117. Wu, Y.F.; Zhao, X.M. Unified Bond Stress Slip Model for Reinforced Concrete. *Journal of Structural Engineering* **2013**, *139*, 1951–1962, doi:10.1061/(ASCE)ST.1943-541X.0000747.

118. Jiradilok, P.; Wang, Y.; Nagai, K.; Matsumoto, K. Development of Discrete Meso-Scale Bond Model for Corrosion Damage at Steel-Concrete Interface Based on Tests with/without Concrete Damage. *Construction and Building Materials* 2020, *236*.

119. Interface Characteristics. In *fib Model Code for Concrete Structures 2010*; International Federation for Structural Concrete (fib): Lausanne, Switzerland, 2013; pp. 152–189 ISBN 978-3-433-60409-0.

120. Ou, Y.-C.; Tsai, L.-L.; Chen, H.-H. Cyclic Performance of Large-Scale Corroded Reinforced Concrete Beams. *Earthquake Engineering & Structural Dynamics* **2012**, *41*, 593–604, doi:https://doi.org/10.1002/eqe.1145.

121. Ou, Y.-C.; Chen, H.-H. Cyclic Behavior of Reinforced Concrete Beams with Corroded Transverse Steel Reinforcement. *Journal of Structural Engineering* **2014**, *140*, 04014050, doi:10.1061/(ASCE)ST.1943-541X.0000932.

122. Ou, Y.-C.; Nguyen, N.D. Influences of Location of Reinforcement Corrosion on Seismic Performance of Corroded Reinforced Concrete Beams. *Engineering Structures* **2016**, *126*, 210–223, doi:https://doi.org/10.1016/j.engstruct.2016.07.048.

123. Kato, E.; Iwanami, M.; Yokota, H. Deterioration in Ductility of RC Beams with Corroded Reinforcement. In Proceedings of the Proc., 2nd FIB Int. Congress; 2006; pp. 1–8.

124. Kobayashi, K. The Seismic Behavior of RC Members Suffering from Chloride-Induced Corrosion. In Proceedings of the Proceedings of the 2nd International fib Congress; 2006.

125. Architectural Institute of Japan *Standard for Structural Calculation of Reinforced Concrete Structures-Based on Allowable Stress Concept*; 2010;

126. Architectural Institute of Japan *Design Guidelines for Earthquake Resistant Reinforced Concrete Buildings Based on Ultimate Strength Concept*; 1990;

127. Ikeda, S.; Uji, K. Studies on the Effect of Bond on the Shear Behaviour of Reinforced Concrete Beams. *Proceedings of the Japan Society of Civil Engineers* **1980**, 101–109, doi:10.2208/jscej1969.1980.101.

To my beloved mother

I would like to dedicate this thesis to my mother, ***Khadi Diagne****, who unfortunately passed away at the beginning of my PhD journey. My mother was my biggest supporter and inspiration, and her unwavering love and encouragement propelled me through some of the toughest times of my life. Even though she is no longer here, her memory continues to inspire me every day. I am grateful for the time we had together, and I hope that this thesis makes her proud.*

Acknowledgment

ACKNOWLEDGEMENTS

I would like to express my deepest gratitude to my supervisor and mentor, Professor Kanakubo Toshiyuki, for his friendly support, never-ending patience, encouragement, and constructive supervision throughout my PhD study. Professor Kanakubo Toshiyuki's exceptional supervisory skills gave me the strength and motivation to complete this research. Moreover, working with Professor Kanakubo Toshiyuki has helped me learn the values that make an outstanding researcher. I cannot think of anyone better to have as supervisor. Also, a big thanks to his wife, Kanakubo Noriko, for being a valuable advisor during my life in Japan.

I would like to convey my appreciation to my vice-supervisor, Prof. Yasojima Akira and Prof. Shoji Gaku, for showing their interest in my work and taking the time to get involved and share their valuable thoughts, comments and also having their door always open to share their vast knowledge.

I would like to acknowledge Professor Castro Juan Jose, from The University of the Ryukyus, for providing invaluable advices.

I would like to thank all my former and present colleagues at Kanakubo laboratory for creating such a pleasant working environment. Special thanks go to my co-investigators: Nagai Masato (Chapter 3), Kawamura Yoshihiro and Aburano Togo (Chapter 4), Shimokobe Hiroki , Kai Fujiwara and Aburano Togo (Chapter 6). I would also like to acknowledge Kojima Atsushi for his support during the experimental work.

Finally, I would like to express my heartfelt gratitude to my family, who supported me throughout my academic journey.. my special thanks to my lovely wife Aida and daughter Khady, who have been very understanding and patient. Their unwavering love, encouragement, and patience were crucial in enabling me to complete this thesis. For all that and much more, thank you.

PUBLICATIONS ARISING FROM THE THESIS

REVIEWED PAPERS

1) Syll, A.S., Kanakubo, T.: Residual bond strength in reinforced concrete cracked by expansion agent filled pipe simulating rebar corrosion, Case Studies in Construction Materials, Vol.17, e01565 (16pp.), 2022.10
2) Syll, A.S., Kanakubo, T.: Impact of Corrosion on the Bond Strength between Concrete and Rebar: A Systematic Review, materials, 15-19, 7016 (21pp.), 2022.10
3) Shimokobe, H.,, Fujiwara, K., Syll Amadou Sakhir, Kanakubo, T：Cyclic Bending Structural of RC Beams with Bond Deterioration due to rebar Corrosion, Japan Concrete Institute annual Ronbunnshu, Vol.44, No.2, pp.997～1002, 2022.7 (in Japanese)
4) Syll, A.S., Shimokobe, H., Kanakubo, T.: Effect of Stirrup on Bond Strength Degradation in Concrete Cracked by Expansion Agent Filled Pipes, applied sciences, 11-19, 8874 (16pp.), 2021.9
5) Syll, A.S., Aburano, T., Fujiwara, K., Kanakubo, T.: Bond Failure of RC Beams with Induced Corrosion Cracks by Aluminum Pipe Filled with an Expansion Agent, Proceedings of the 17th World Conference on Earthquake Engineering (17WCEE), 2d-0127, 9pp., 2021.9
6) Syll, A.S., Aburano, T., Kanakubo, T.: Bond strength degradation in concrete cracked by expansion agent filled pipes, Structural Concrete, 22, 3156-3172, 2021, doi:10.1002/suco.202000764
7) T. Aburano, A. S. Syll, T. Kanakubo: Structural Performance of RC Beams with Induced Corrosion Cracks by Aluminum Pipe Filled with an Expansion Agent, Proceedings of the 17th World Conference on Earthquake Engineering, Sendai, Japan, version 2020 (published in September 2020), 3b-0073, 2020.9
8) T. Aburano, T. Kanakubo, Syll Amadou Sakhir：Structural Performance of RC Beams with Induced Corrosion Cracks by Aluminum Pipe Filled with an Expansion Agent, Japan Concrete Institute annual Ronbunnshu, Vol.42, No.2, pp.181～186, 2020.7 (in Japanese)

PROCEEDINGS

1) Syll Amadou Sakhir, Toshiyuki Kanakubo： Bond Strength Degradation due to Corrosion Cracking in Concrete Specimens without Stirrups, Japan Society Civil Engineer (JSCE) Annual Meeting, Section V－371, 2022.9
2) Kai Fujiwara, Amadou Sakhir Syll, Togo Aburano, Toshiyuki Kanakubo：Shear Performance of RC Beams with Induced Corrosion Cracks by Aluminum Pipe Filled with an Expansion Agent, Summaries of Technical Papers of Annual Meeting, Architectural Institute of Japan, Structure IV, pp.497～498, 2021.9 (in Japanese)
3) Amadou Sakhir Syll, Hiroki Shimokobe, Toshiyuki Kanakubo： Effect of Stirrups on Bond Strength Degradation in Cracked Concrete by Expansion Agent Filled Pipes, Japan Society Civil Engineer (JSCE) Annual Meeting, Section V－515, 2021.9
4) Aburano, T, Syll, A. S., Kanakubo, T, Castro, J.J.: Bond Behavior in Cracked Concrete by Expansion Agent Filled Pipes, Part 1: Concrete cracks in side-split type specimens

Summaries of Technical Papers of Annual Meeting, Architectural Institute of Japan, Structure IV, pp.37～38, 2020.9

5) Syll, A. S., Aburano, T, Kanakubo, T, Castro, J.J.： Bond Behavior in Cracked Concrete by Expansion Agent Filled Pipes, Part 2: Bond strength degradation in side-split type specimens, Summaries of Technical Papers of Annual Meeting, Architectural Institute of Japan, Structure IV, pp.39～40, 2020.9
6) Togo Aburano, Syll Amadou Sakhir, Toshiyuki Kanakubo：Bending Performance of RC Beams with Induced Corrosion Cracks by Aluminum Pipe Filled with an Expansion Agent, Japan Society Civil Engineer (JSCE) Annual Meeting, Section V－348, 2020.9 (in Japanese)
7) Syll Amadou Sakhir, Togo Aburano, Toshiyuki Kanakubo： Bond Strength Degradation in Cracked Concrete by Expansion Agent Filled Pipes, Japan Society Civil Engineer (JSCE) Annual Meeting, Section V－612, 2020.9
8) Aburano, T., Juan Jose Castro, Amadou Sakhir Syll, Kanakubo, T：Tensile Performance of Aluminum Pipe Filled with an Expansion Agent Simulating Corroded rebar, Summaries of Technical Papers of Annual Meeting, Architectural Institute of Japan, Structure IV, pp.297～298, 2019.9 (in Japanese)
9) Kanakubo, T, Castro, J.J., Syll, A. S., Aburano, T.： Concrete Cracks by Expansion Agent Filled Pipes in Bond Test Specimens, Summaries of Technical Papers of Annual Meeting, Architectural Institute of Japan, Structure IV, pp.299～300, 2019.9
10) Syll, A. S., Aburano, T., Kanakubo, T., Castro, J.J.： Bond Behavior in Cracked Concrete by Expansion Agent Filled Pipes, Summaries of Technical Papers of Annual Meeting, Architectural Institute of Japan, Structure IV, pp.301～302, 2019.9
11) Syll, A. S., Kawamura, Y., Kanakubo, T.: Simulation of Concrete Cracks due to Bar Corrosion by Aluminum Pipe Filled with An Expansion Agent, Summaries of Technical Papers of Annual Meeting, Architectural Institute of Japan, Structure IV, pp.55-56, 2018.9